5-18-2007

Numerical Analysis and Applications of the Process of Nonlinear Supratransmission in Mechanical Systems of Coupled Oscillators with Damping

Diaz Jorge Macias
University of New Orleans

Numerical Analysis and Applications of the Process of Nonlinear Supratransmission in Mechanical Systems of Coupled Oscillators with Damping

A Dissertation

Submitted to the Graduate Faculty of the
University of New Orleans
in partial fulfillment of the
requirements for the degree of

Doctor of Philosophy
in
The Engineering and Applied Science

by

Jorge Eduardo Macías Díaz

B.S. Universidad Autonoma de Aguascalientes, 1994
M.S. Tulane University Of Louisiana, 1998
Ph.D. Tulane University Of Louisiana, 2001
M.S. Louisiana State University of New Orleans, 2004
Ph.D. Louisiana State University of New Orleans, 2006

May 2007

To Iliana,
Sieg, Carlos, and Néstor
with all my love

Acknowledgments

First of all I wish to express my gratitude to the University of New Orleans and its Department of Physics for giving me the chance to take graduate studies in physics and financially supporting me during my stay as a graduate student. Being part of this institution was an invaluable academic and personal experience that I will cherish for a lifetime. Academically, the University of New Orleans widen my vision toward branches of mathematics and science I had never been exposed before; personally, it offered me the chance of interacting with all the delightful people in the Department of Physics, from secretaries, to my dissertation adviser Dr. Ashok Puri, to chairmen.

Likewise, I wish to acknowledge financial support from the *Universidad Autónoma de Aguascalientes*. Particularly, I wish to thank the president of the University, Dr. Rafael Urzúa Macías, the dean of the *Centro de Ciencias Básicas*, Dr. Francisco Javier Álvarez Rodríguez, and the head of the *Dirección General de Investigación y Posgrado*, Dr. Francisco Javier Avelar González. Without their uninterested support, these last visits to New Orleans to complete the remaining requirements of my studies as well as the use of state-of-the-art computational resources to complete my dissertation paper would have been naught but a mere dream.

I also wish to thank Iliana, my wife, for her profound devotion and encouragement to complete this paper. Truly, I am eternally in debt for all her support from the beginning of my graduate studies at the University of New Orleans to the realization of this dissertation. May her support and trust translate in a better future for us both and our kids.

Last but not least, I want to thank my sons Sieg, Carlos, and Néstor for their understanding, support, and love. It is my desire to use this opportunity to let them know how much I love them and that it is my supreme desire that this love they still express for *papá* may never, ever die out in the future!

Foreword

In this thesis we label exclusively those formulas which are relevant to our study, that is those expressions that posses a relevant importance on themselves as terminal results or that will be used later on in the derivation of other expressions. These formulas will be invariantly labeled by two numbers presented in the form (n, m), the first corresponds to the chapter where they appear for the first time and the second is the number of labeled formula within that chapter.

Important statements are denominated lemmas, theorems and corollaries. We use the standard convention used throughout the mathematical sciences. So, by a lemma we mean a technical result needed to prove a more general statement. It is worth mentioning that a lemma is not important *per se*, its importance lies in its usefulness to prove further results. By a theorem or a proposition we understand a statement which is relevant to our investigation and that may answer some of the concerns in this thesis in a rather general form. In this sense, theorem and propositions are terminal results in our research that may or may not need of a lemma to be proved. A corollary is a particular case of a theorem; its importance is manifested in the fact that it answers some specific objectives of this paper. Lemmas, theorems, propositions and corollaries are numbered by a single counter within a chapter, and new chapters restart the numeration. Cross-references of lemmas, theorems and corollaries between chapters will be indicated following the same convention as for formulas. Results in Chapter 2 are used in our research, however we do not refer to them in later chapters since they are assumed to be part of the standard literature.

We have included an appendix with the numeric routines we used in our investigation as well as an alphabetic index at the end of this thesis for the sake of easiness in the reading. An index is also included to facilitate the search of concepts in this paper.

The present document was typeset using the packages LaTeX 2_ε, $\mathcal{AMS}$-LaTeX and BibTeX, and the freely-distributed typesetting system TeXnicCenter 1 beta 6.21 ('Fawkes'). $\mathcal{AMS}$-LaTeX was used to create special fonts in our formulas, while the package BibTeX was employed to generate the bibliography at the end of the present work. The graphs were generated using computer programs designed to run in Matlab Student Version 6.1.0.450 release 12.1.

Contents

List of Figures

List of Tables

Abstract

In this paper we develop a finite-difference scheme to approximate radially symmetric solutions and $(1+1)$-dimensional solutions of the initial-value problem with smooth initial conditions

$$\frac{\partial^2 w}{\partial t^2} - \nabla^2 w - \beta \frac{\partial}{\partial t}\left(\nabla^2 w\right) + \gamma \frac{\partial w}{\partial t} + m^2 w + G'(w) = 0,$$
$$\text{subject to :} \quad \begin{cases} w(\bar{x},0) = \phi(\bar{x}), & \bar{x} \in D, \\ \dfrac{\partial w}{\partial t}(\bar{x},0) = \psi(\bar{x}), & \bar{x} \in D, \end{cases}$$

in an open sphere D around the origin, where the internal and external damping coefficients β and γ, respectively, are constant. The functions ϕ and ψ are radially symmetric in D, they are small at infinity, and $r\phi(r)$ and $r\psi(r)$ are also assumed to be small at infinity. We prove that our scheme is consistent order $\mathcal{O}(\Delta t^2) + \mathcal{O}(\Delta r^2)$ for G' identically equal to zero, and provide a necessary condition for it to be stable order n. A cornerstone of our investigation will be the study of potential applications of our model to discrete versions involving nonlinear systems of coupled oscillators. More concretely, we make use of the process of nonlinear supratransmission of energy in these chain systems and our numerical techniques in order to transmit binary information. Our simulations show that, under suitable parametric conditions, the transmission of binary signals can be achieved successfully.

Chapter 1

Introduction

Modified Klein-Gordon equations appear in several branches of physics. A modified sine-Gordon equation appears for instance in the study of long Josephson junctions between superconductors when dissipative effects are taken into account [1]. A similar partial differential equation with different nonlinear term appears in the study of fluxons in Josephson tramsmission lines [2]. A modified Klein-Gordon equation appears in the statistical mechanics of nonlinear coherent structures such as solitary waves in the form of a Langevin equation [3]; here no internal damping coefficient appears, though. Finally, this differential equation describes the motion of a string with internal and external damping in a non-Hookean medium.

The classical $(1 + 1)$-dimensional linear Klein-Gordon equation has an exact soliton-like solution in the form of a traveling wave [4]. Some results concerning the analytic behavior of solutions of nonlinear Klein-Gordon equations have been established [5, 6, 7]; however, no exact method of solution is known for arbitrary initial-value problems involving this equation. From that point of view it is important to investigate numerical techniques to describe the evolution of radially symmetric solutions of our problem.

It is worth mentioning that some numerical research has been done in this direction. Strauss and Vázquez [8] developed a finite-difference scheme to approximate radially symmetric solutions of the nonlinear Klein-Gordon equation for the same nonlinear term we study in this paper; one of the most important features of their numerical method was that the discrete energy associated with the differential equation is conserved. The numerical study of the sine-Gordon model that describes the Josephson tunnel junctions has been undertaken by Lomdahl *et al.* [2]. Numerical simulations have also been performed to solve the $(1 + 1)$-dimensional Langevin equation [9].

In this paper we present a numerical analysis of the radially symmetric solutions to a modified nonlinear Klein-Gordon equation that generalizes the applications described in the previous paragraphs, as well as several other well-known physically and biologically important partial differential equations. With the purpose of providing applications of our numerical scheme, our attention will be directed to the study of the process of nonlinear supratransmission in nonlinear chains of coupled oscillators aiming at exploring the possibilities of transmitting binary information in such systems.

* * *

Chapter 2 provides a list of important second-order partial differential equations that constitute particular cases of the equation under study. We state the general form of our problem, describe the most important applications that it models, and provide analytical methods to compute solution and, particularly, soliton-like solutions to several particular cases. We close this chapter stating some important definitions and results from numerical analysis that we use in this thesis without reference.

The next chapter is devoted to the study of our modified nonlinear Klein-Gordon equation without damping. We show that the energy associated with our differential equation is constant throughout time and derive a conditionally stable finite-difference scheme consistent to the second order, which has the property that the discrete energy is conserved. We close that chapter showing numerical results that are in agreement with [8], and provide several physical applications of our method.

In the next chapter we derive a numerical method to approximate radially symmetric solutions of the modified nonlinear Klein-Gordon equation under study. As we will observe, if no external damping is present then the inclusion of an extra term in the finite-difference scheme of the previous chapter yields a second-order approximation to the exact solution of our problem. For the externally damped case we notice that the solution of the problem requires a more complicated reformulation in order to achieve consistency to the second order. We analyze the energy associated with our equation and derive a discrete expression for the rate of change of energy. We study the stability and consistency of our numerical methods in detail and show graphically that our results are in agreement with the non-dissipative case.

Chapter 6 presents a discrete space, mixed-value problem version of the model introduced in the previous chapter. The model under study in this section describes the motion of a semi-infinite chain of coupled oscillators with damping, subject to harmonic driving at the free end. In this chapter, we derive a finite-difference scheme to approximate solutions to our new problem, and derive energy properties of the system. The study of the process of nonlinear supratransmission of the chain is carried out in detail, and we obtain bifurcation diagrams to predict the occurrence of nonlinear supratransmission under the presence of the parameters of the model. Meanwhile, the last chapters of this work show how nonlinear supratransmission in nonlinear chains of coupled oscillators can be controlled in order to achieve a successful transmission of binary information.

The appendix at the end of this work contains the most basic form of the numerical routines we developed to approximate the solutions of our equation. The programs do not contain the subroutines to generate the graphs included in this thesis.

Chapter 2

Preliminaries

The nonlinear Klein-Gordon equation is one of the most important and simplest nonlinear differential equations that appear in relativistic quantum mechanics. As a second-order partial differential equation, the Klein-Gordon equation generalizes several other important problems in various branches of physics, chemistry and mathematical biology that range from the classical diffusion equation to the stochastic Fisher-KPP equation, from the classical wave equation to the Schrödinger and the telegrapher's equations.

The present chapter is devoted to introduce and evidence the importance of the differential equation under study in this thesis. We also present some important definitions and results of numerical analysis that will be used without reference in further chapters.

2.1 Basic definitions

By a **domain** we understand a closed connected subset of $\mathbb{R}^n$. A function u defined in a domain D is said to be have **compact support** if it is zero outside a compact subset of D.

A function u defined on a domain D is called **smooth** in D if it has continuous partial derivatives of all orders in D. The function u is called **small at infinity** if for every $\bar{x}_0$ in the boundary of D,

$$\lim_{\substack{\bar{x} \to \bar{x}_0 \\ \bar{x} \in D}} u(\bar{x}) = 0.$$

Let a, b, c, d and e be real numbers with at least one of a, b or c not equal to zero. A second-order partial differential equation in the variables x and y with constant coefficients is an equation of the form

$$a\frac{\partial^2 u}{\partial x^2} + b\frac{\partial^2 u}{\partial x \partial y} + c\frac{\partial^2 u}{\partial y^2} + d\frac{\partial u}{\partial x} + e\frac{\partial u}{\partial y} = F(x, y), \tag{2.1}$$

where u is a function of (x, y) usually assumed to be defined and of compact support in some domain D, that has continuous partial derivatives up to the second order in

D. The number $b^2 - 4ac$ is called the **discriminant** of Equation (2.1) and yields a criterion to classify second-order partial differential equations:

- If $b^2 - 4ac > 0$ then Equation (2.1) is called a **hyperbolic** equation. As an example of this type of equation we have the classical one-dimensional **wave equation**

$$\frac{\partial^2 u}{\partial x^2} = \frac{1}{\nu^2}\frac{\partial^2 u}{\partial t^2}.$$

  It describes the vertical disturbance of a wave with phase velocity ν as it travels on the horizontal direction. The wave equation applies to a stretched string or a plane electromagnetic wave. Given initial and boundary conditions the wave equation can be solved exactly by using a Fourier transform method or via separation of variables.

- If $b^2 - 4ac = 0$ then Equation (2.1) is called a **parabolic** equation. An example of parabolic equation is the one-dimensional **diffusion equation** (also called **heat equation**)

$$\frac{\partial u}{\partial t} = \kappa\frac{\partial^2 u}{\partial x^2}.$$

  This equation commonly arises in problems of heat conductivity. In those situations κ represents thermal diffusivity and u represents temperature. If initial and boundary conditions are given, the diffusion equation can be solved analytically by separation of variables.

- If $b^2 - 4ac < 0$ then Equation (2.1) is called an **elliptic** equation. **Laplace's equation**

$$\frac{\partial^2 u}{\partial x^2} + \frac{\partial^2 u}{\partial y^2} = 0$$

  is an example of an elliptic equation. It is satisfied by the potential of any distribution of matter which attracts according to the Newtonian Law. A solution to Laplace's equation is uniquely determined if the value of the function or the normal derivative of the function is specified on all boundaries.

We must remark that the wave equation, the heat equation and Laplace's equation have generalizations that model the corresponding physical phenomena in three dimensions. For example, the **wave equation** in three space variables reads

$$\nabla^2 u = \frac{1}{\nu^2}\frac{\partial^2 u}{\partial t^2},$$

where u is a scalar function that depends on the space coordinate (x, y, z) and time t. The symbol ∇^2 denotes the **Laplacian** differential operator, which is the divergence of the gradient of a scalar function. With this notation the three-dimensional **diffusion equation** is described by the equation

$$\frac{\partial u}{\partial t} = \frac{1}{\kappa}\nabla^2 u,$$

and the three-dimensional **Laplace's equation** by

$$\nabla^2 u = 0.$$

Let V and ρ be scalar functions depending only on space. An important variation of the three-dimensional Laplace's equation occurs in classical electromagnetic theory when relating the electric potential V of a distribution and its charge density ρ. The relation between V and ρ is described by the equation $\epsilon_0 \nabla^2 V = \rho$, which is called **Poisson's equation**. More generally, every equation of the form

$$\nabla^2 u = F(x, y, z, t),$$

where u is a scalar function depending on x, y, z and t, is called a Poisson equation.

Another useful classification of second-order partial differential equations with constant coefficients is in terms of a property called *linearity*. Differential equation (2.1) is called **linear** if for arbitrary real constants k_1, k_2 and solutions u_1, u_2 of (2.1), $k_1 u_1 + k_2 u_2$ is also a solution of (2.1).

Finally, if the variable time is one of the independent variables of the scalar function u then the term $k\partial u/\partial t$ in the differential equation modeling u is called the **external damping term** and the constant k is called the **external damping coefficient**. The differential equation is said to be **damped** if k is not equal to zero, otherwise it is called **undamped**.

2.2 Important partial differential equations

Many other three-dimensional generalizations of the wave equation, the diffusion equation and Laplace's equation happen to appear in mathematical physics and biology. For example, the manipulation of Maxwell's equations to obtain propagating waves gives rise to the so called **Helmholtz equation** [10], whose general form is

$$\nabla^2 u + k^2 u = 0,$$

where k is a real constant and u is a scalar function in the variables x, y, z, t. Obviously, Helmholtz equation is a linear second-order partial differential equation that generalizes the three-dimensional wave equation.

Another physical example appears in the field of non-relativistic quantum mechanics: Let $\hbar$ denote Planck's original constant divided by 2π. The wave function associated to a particle of mass m with potential scalar function V is a scalar function u that depends on the position vector (x, y, z) of the particle and the time t, given by the differential equation

$$i\hbar \frac{\partial u}{\partial t} = -\frac{\hbar^2}{2m} \nabla^2 u + V u.$$

This differential equation is called **Schrödinger's equation**. In this equation the scalar function u may be complex, but the square of its modulus is a real scalar function that represents the probability density function associated with the location of

the particle at any time. It is worth noticing that Schrödinger's equation provides a mathematical generalization of the three-dimensional diffusion equation. Observe that because the scalar function V does not need to be constant, Schrödinger's equation is a linear partial differential equation with not necessarily constant coefficients.

The relativistic counterpart of Schrödinger's equation is the Klein-Gordon equation. By the **linear Klein-Gordon equation** we understand the linear second-order partial differential equation

$$\nabla^2 u = \frac{1}{c^2}\frac{\partial^2 u}{\partial t^2} + m^2 u,$$

where m is a real constant and u is a scalar function of position and time. This is the equation for a relativistic quantum-mechanical scalar (spin-zero) particle of mass m. The exact solution of this equation in the form of a traveling wave is given in [4]. An important nonlinear variation of this equation that often appears in the study of the collisional properties of **solitons** [11, 12], that is solitary waves, and a number of other physical applications [7, 13, 14] is the **sine-Gordon equation**

$$\nabla^2 u = \frac{1}{c^2}\frac{\partial^2 u}{\partial t^2} + m^2 \sin u.$$

Several nonlinear variations of the Klein-Gordon equation appear in many branches of physics, chemistry and other sciences. The **Landau-Ginzburg equation** is one of those equations. Studied by Lev Landau and Vitaly Grinzburg in 1950 while studying the theory of superconductivity, this equation is used to study simple periodic oscillations and the change of their amplitude and frequency with respect to initial excitations in problems that arise in oscillating chemical reactions and atomic physics. In dimensionless form, the three-dimensional Landau-Grinzburg equation is given by

$$\frac{\partial^2 u}{\partial t^2} - \nabla^2 u - m^2 u + G'(u) = 0$$

In mathematical biology, consider a population distributed in a linear habitat with uniform density. If at any point of the habitat a mutation advantageous to survival occurs then the mutant gene increases at the expense of the allelomorphs previously occupying the same locus. Mathematically, let u be the frequency of the mutant gene and let m be a constant representing intensity of selection in favor of the mutant gene. Then u must satisfy **Fisher's equation** (also called the **Fisher-KPP equation**)

$$\frac{\partial u}{\partial t} = k\frac{\partial^2 u}{\partial x^2} + F(u),$$

where k is a diffusion coefficient and u depends on the position x in the linear habitat and time t given in generations. This parabolic equation was simultaneously and independently investigated by Fisher [15] and Kolmogoroff *et al.* [16], using $F(u) = mu(1-u)$. It is used also in describing the process of epidermal wound healing [17]. Other applications appear in the theory of superconducting electrodynamics [18] and in the study of excitons [19]. Fisher's equation is a nonlinear equation that obviously

generalizes the three-dimensional diffusion model if we rewrite Fisher's equation as

$$\frac{\partial u}{\partial t} = k\nabla^2 u + F(u).$$

The **stochastic Fisher-KPP equation** is the one-dimensional Fisher equation with $F(u) = mu(1-u) + \gamma\sqrt{u(1-u)}\eta(x,t)$, where $0 \leq u \leq 1$, γ is a real constant, and $\eta(x,t)$ is a *Gaussian white noise process* in space and time with mean equal to zero [20]. To fix ideas, we may think of a **noise** as a random signal of known statistical properties of amplitude, distribution, and spectral density. A noise is a **white noise** in space and time if it is uncorrelated in these two variables, and it is **Gaussian** if its probability density function over a given frequency band is normal. The stochastic Fisher-KPP equation is a stochastic partial differential equation that describes random walk processes that have applications in hydrodynamics and economics.

Second-order partial differential equations describing diffusion or conduction happen to appear in the area of thermodynamics [21]. Heat conduction is understood as the transfer of heat from warm areas to cooler ones, and effectively occurs by diffusion. Under the assumption of a macroscopic continuum formulation, the **Fourier equation** [22] for the heat flux $\bar{q}$ in a medium of density ρ, mass heat capacity C_P, and temperature function u, is

$$\bar{q} = -k\nabla u,$$

where both $\bar{q}$ and u depend on the three spatial coordinates and time, $k = \rho\kappa C_P$ is the thermal conductivity of the medium, and κ is the thermal diffusivity term of the classical diffusion equation.

The previously mentioned Fourier heat conduction equation is diffusive and does not account for the temperature propagation speed in transient situations. Because of certain issues argued and identified earlier, attempts to account for a finite speed of heat propagation have evolved over the years. The **Maxwell-Cattaneo model** [23], which is based on the notion of relaxing the heat flux, is given as

$$\tau\frac{\partial \bar{q}}{\partial t} = -\bar{q} - k\nabla u,$$

where τ is the relaxation time. Assuming that there are no heat sources and that k is constant, the one-dimensional version of the Maxwell-Cattaneo equation together with the energy equation

$$\rho C_P\frac{\partial u}{\partial t} + \frac{\partial q}{\partial x} = 0,$$

yield the hyperbolic equation

$$\tau\rho C_P\frac{\partial^2 u}{\partial t^2} - k\frac{\partial^2 u}{\partial x^2} + \rho C_P\frac{\partial u}{\partial t} = 0.$$

Obviously, it can be generalized to the three-dimensional case as

$$\frac{\partial^2 u}{\partial t^2} - \frac{k}{\tau\rho C_P}\nabla^2 u + \frac{1}{\tau}\frac{\partial u}{\partial t} = 0.$$

The **telegraph equation** is a hyperbolic equation that describes heat or mass transport. It models phenomena that are mixtures between diffusion and wave propagation. In this model a small section of a telegraph wire is treated to study the pulse of voltage moving along the wire. It was studied in 1876 by Heaviside in his research on coaxial marine telegraph cables [24]. The telegraph equation is the linear second-order partial differential equation

$$\frac{\partial^2 u}{\partial x^2} - \frac{1}{\nu^2}\frac{\partial^2 u}{\partial t^2} - \gamma\frac{\partial u}{\partial t} - b^2 u = 0,$$

where ν is positive, and γ and b are nonnegative constants. The one-dimensional wave equation is just a particular case of the telegraph equation with γ and b both equal to zero. The generalization of the telegraph equation to three dimensions is

$$\nabla^2 u - \frac{1}{\nu^2}\frac{\partial^2 u}{\partial t^2} - \gamma\frac{\partial u}{\partial t} - b^2 u = 0.$$

2.3 Modified Klein-Gordon equations

The objective of this paper is to study a general form of the Klein-Gordon equation that embraces the partial differential equations described in the previous section and, at the same time, takes into account a third-order term proportional to the Laplacian of the partial derivative of u in time, which physically represents the **internal damping term**. More precisely, let u be a function of the spatial variables X, Y, Z, and the time variable T. The nonlinear partial differential equation with constant coefficients that we wish to study in this thesis is

$$a\frac{\partial^2 u}{\partial T^2} - b\nabla^2 u - c\frac{\partial}{\partial T}\left(\nabla^2 u\right) + d\frac{\partial u}{\partial T} + m^2 u + G'(u) = 0,$$

Let $x = X/\sqrt{b}$, $y = Y/\sqrt{b}$, $z = Z/\sqrt{b}$, and $t = T/\sqrt{a}$ for a and b positive numbers. Let $\beta = c/(b\sqrt{a})$ and $\gamma = d/\sqrt{a}$. Our problem can be stated in dimensionless form as

$$\frac{\partial^2 u}{\partial t^2} - \nabla^2 u - \beta\frac{\partial}{\partial t}\left(\nabla^2 u\right) + \gamma\frac{\partial u}{\partial t} + m^2 u + G'(u) = 0,$$

$$\text{subject to :} \quad \begin{cases} u(\bar{x}, 0) = \phi(\bar{x}), & \bar{x} \in D, \\ \dfrac{\partial u}{\partial t}(\bar{x}, 0) = \psi(\bar{x}), & \bar{x} \in D. \end{cases} \tag{2.2}$$

This initial-value problem will be referred to as the **modified nonlinear Klein-Gordon equation** or the **dissipative nonlinear Klein-Gordon equation**, and its numerical study for the particular choice $G'(u) = u^p$, for $p > 1$ an odd number, is the topic of this paper. We identify the term containing the coefficient β as the internal damping term, while the term containing γ is easily identified as the external damping term. Needless to say that the differential equation in (2.2) generalizes the equations listed in Section 2.2 either by choosing suitable coefficients or by suppressing

terms; the classical Klein-Gordon equation, for instance, can be obtained by setting β and γ both equal to zero and G' identically zero. It is worthwhile mentioning that the undamped nonlinear Klein-Gordon equation with $G'(u) = u^3$ is called the **quasilinear Klein-Gordon equation**, and it also has physical applications [25].

The following is the major theoretic result we will use in our investigation. It is valid only for certain classical one-dimensional nonlinear Klein-Gordon equations. Here $M(t)$ represents the amplitude of a solution of (2.2) at time t, that is

$$M(t) = \max_x |u(x,t)|.$$

THEOREM 1. *Let β and γ be both equal to zero, and let $G'(u) = |u|^{p-1}u$. Suppose that ϕ and ψ are smooth and small at infinity. Then*

(1) *If $p < 5$, a unique smooth solution of* (2.2) *exists with amplitude bounded at all time* [6].

(2) *If $p \geq 5$, a weak solution exists for all time* [26].

(3) *For $p > 8/3$ and for solutions of bounded amplitude, there is a scattering theory; in particular, they decay uniformly as fast as $M(t) \leq c(1 + |t|)^{-3/2}$* [27]. □

2.3.1 Josephson transmission lines

As we stated in the introductory chapter, initial-value problem (2.2) has applications in several physical problems. In the remainder of this section we will describe some of them.

A **Josephson junction** is a type of electronic circuit capable of switching at very high speeds when operated at temperatures approaching absolute zero. Named for the British physicist who designed it, a Josephson junction exploits the phenomenon of superconductivity, that is the ability of certain materials to conduct electric current with practically zero resistance. Josephson junctions are used in certain specialized instruments such as highly-sensitive microwave detectors, magnetometers, and quantum interference devices.

A Josephson junction is made up of two superconductors, separated by a non-superconducting layer so thin that electrons can cross through the insulating barrier. The flow of current between the superconductors in the absence of an applied voltage is called a **Josephson current**, and the movement of electrons across the barrier is known as **Josephson tunneling**. Two or more junctions joined by superconducting paths form what is called a **Josephson interferometer.**

While researching superconductivity, Josephson studied the properties of a junction between two superconductors [28]. Following up on earlier work by Leo Esaki and Ivar Giaever, he demonstrated that in a situation when there is electron flow between two superconductors through an insulating layer (in the absence of an applied voltage), and a voltage is applied, the current stops flowing and oscillates at a high frequency. This phenomenon is called the **Josephson effect**, and it is

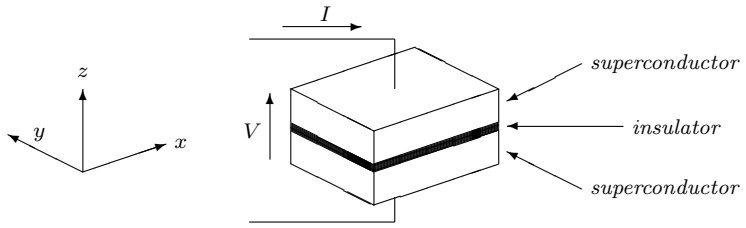

FIGURE 2.1: Schematic representation of a small Josephson junction.

influenced by magnetic fields in the vicinity, a capacity that enables the Josephson junction to be used in devices that measure extremely weak magnetic fields, such as superconducting quantum interference devices. For their efforts, Josephson, Esaki, and Giaever shared the Nobel Prize for Physics in 1973.

It is worthwhile mentioning that the theory of low temperature conductivity tells us that a superconductor is a system where a fraction of the conduction electrons form pairs called **Cooper pairs**. In these pairs the two electrons have opposite momentum and spin. These pairs are able to condense in the same quantum state so that the superconductor can be described by a single macroscopic wave function

$$\Psi = \sqrt{\rho} e^{i\phi}.$$

Here ρ represents the pair density and ϕ is the quantum phase common to all pairs.

A **small Josephson junction** consists of two small layers of superconducting metal separated by a thin dielectric barrier layer, which is small enough to permit tunneling of Cooper pairs (equivalently, coupling of the wave functions of the two superconductors).

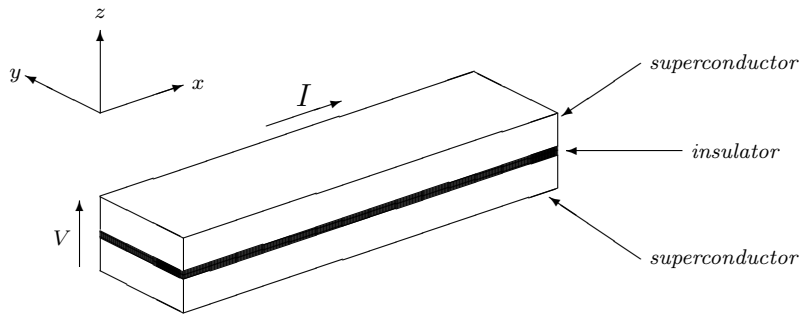

FIGURE 2.2: Schematic representation of a long Josephson junction.

A **long Josephson junction** consists of two identical superconducting long strips separated by a thin dielectric layer. This long tunneling junction can be regarded as a transmission line as far its electromagnetic behavior is concerned [7]. However, in dealing with real transmission lines for the long Josephson junction one must take into account losses, bias, and junction irregularities which influence motion [1]. When we account for all of these effects, we obtain the third-order partial

differential equation

$$\frac{\partial^2\phi}{\partial x^2} - \frac{\partial^2\phi}{\partial t^2} - \alpha\frac{\partial\phi}{\partial t} + \beta\frac{\partial^3\phi}{\partial x^2\partial t} = \sin\phi - \gamma,$$

where α, β and γ are constants.

2.3.2 The statistical mechanics of kinks

The statistical mechanics of **kinks** (that is, exact solitary waves) of nonlinear coherent structures has been studied by two approaches. In the first approach one assumes that the kinks may be treated as weakly interacting elementary excitations. Provided the kink density is low, the canonical partition function can be found by standard methods [29, 30, 31]. Alternatively, it is possible to calculate the partition function to exploit a transfer operator technique. This method was used by Krumhansl and Schrieffer in [30], and it showed that in the low temperature limit the partition function naturally factorizes into two contributions: A tunneling term which they were able to identify with the kink contribution, and the remainder which they identified as linearized phonons (by a **phonon** we mean a quantized mode of vibration occurring in a rigid crystal lattice, such as the atomic lattice of a solid).

The ideas of Krumhansl and Schrieffer were further refined and extended to a wider class of systems [31]. In particular, interactions of kinks with linearized phonons were considered, leading to substantial corrections of results.

Computer simulations based on standard methods [9] made possible to verify results on the equilibrium statistical mechanics of kinks using a dimensionless **Langevin equation** describing the $(1+1)$-dimensional theory:

$$\frac{\partial^2\phi}{\partial t^2} = \frac{\partial^2\phi}{\partial x^2} - \gamma\frac{\partial\phi}{\partial t} - \phi(1-\phi^2) + F(x,t).$$

2.3.3 The wave equation revisited

Initial-value problem (2.2) also describes the mechanical motion of strings for certain physical situations. Consider the one-dimensional motion of a string immersed in a non-Hookean medium. We represent the vertical motion of the string as a function $u(r,t)$ of horizontal position and time, and the nonlinear force of the medium by $G'(u)$. The string is assumed to posses internal damping due to its inner stiffness, which is proportional to u_{rrt}. Finally, we assume that there exists friction between the string and the medium that derives in a force which opposes the motion of the string and is proportional to the vertical velocity of the string. In these circumstances, the motion of our string will be described by (2.2).

2.4 Elementary solutions

In our study we will be often interested in studying soliton solutions. As mentioned before, solitons are solitary waves found in many nonlinear physical phenomena. They were first named by Zabusky and Kruskal in 1965 [32], and first appeared in the solution of the **Korteweg-de Vries equation**

$$\frac{\partial u}{\partial t} + \frac{\partial^3 u}{\partial x^3} - 6u\frac{\partial u}{\partial x} = 0.$$

Later on it was proved that equations such as the nonlinear Schrödinger equation, the nonlinear Klein-Gordon equation and the sine-Gordon equation also posses soliton solutions. Mathematically, **solitons** have been defined [33] as solutions of nonlinear partial differential equations which

(i) represent waves of permanent form and velocity,

(ii) decay or approach a constant at infinity, and

(iii) can interact strongly with other solitons and retain their identity.

Given a differential equation in the variables x and t, an **elementary soliton solution** is a solution of the differential equation u of the form $u(x,t) = \phi(x-vt)$ with the property that the infinite limits $\lim_{x\to-\infty} u(x,t)$ and $\lim_{x\to+\infty} u(x,t)$ are constant with respect to time.

In this section we derive the solution of the linear Klein-Gordon equation using Fourier transforms and some elementary soliton solutions for some important nonlinear partial differential equations. Throughout ξ will denote the quantity $x-vt$.

2.4.1 The linear Klein-Gordon equation

First we wish to use Fourier transform to solve an arbitrary initial value-problem involving the linear Klein-Gordon equation and provide a solution in terms of the source function. After that, we will find the traveling wave solutions of this differential equation. Thus, let m be a real constant and the consider the $(1+1)$-dimensional initial-value problem

$$\frac{\partial^2 u}{\partial t^2} - \nabla^2 u + m^2 u = 0,$$

$$\text{subject to :} \qquad \begin{cases} u(x,0) = \phi(x), & \bar{x} \in \mathbb{R}, \\ \dfrac{\partial u}{\partial t}(x,0) = \psi(x), & x \in \mathbb{R}. \end{cases}$$

Using Fourier transform, this problem in terms of the source function $S(x,t)$ can be expressed as the initial-value problem

$$\frac{\partial^2 \hat{S}}{\partial t^2} + k^2 \hat{S} + m^2 \hat{S} = 0,$$

$$\text{subject to :} \qquad \begin{cases} \hat{S}(k,0) = 0, & -\pi < k < \pi, \\ \dfrac{\partial \hat{S}}{\partial t}(k,0) = 1, & -\pi < k < \pi. \end{cases}$$

For a fixed value of k, the differential equation in the initial-value problem above is ordinary, and its solution is a linear combination of sines and cosines. It can be seen then that the particular solution to this problem is of the form $\hat{S}(k,t) = \sin(\omega t)/\omega$, where $\omega = \sqrt{k^2 + m^2}$. After applying inverse Fourier transform to $\hat{S}$ and simplifying, it is easy to obtain that

$$S(x,t) = \begin{cases} \dfrac{1}{2} J_0\left(m\sqrt{t^2 - x^2}\right), & \text{for } |x| < t, \\ 0, & \text{for } |x| \geq t, \end{cases}$$

Where J_0 is the Bessel function of the first kind of order 0 whose general definition may be found in [34]. Needless to say that the source function S of the linear Klein-Gordon equation converges to the source function corresponding to the classical wave equation when m tends to 0.

We are interested now in computing radially symmetric solutions of the three-dimensional linear Klein-Gordon equation using Fourier transforms. It is easy to verify that the expression $\hat{S}(\bar{k},t)$ of the Fourier transform of the source function in this case will be the same as that of the $(1+1)$-dimensional one. Letting r represent the Euclidean norm of $\bar{x}$ in $\mathbb{R}^3$ and computing the inverse Fourier transform of $\hat{S}$ we get

$$\begin{aligned} S(r,t) &= \frac{1}{8\pi^3} \int_0^{2\pi} \int_0^{\pi} \int_0^{\infty} \frac{\sin(\omega t)}{\omega}\ k^2 \sin\theta e^{ikr\cos\theta} dk\ d\theta\ d\phi \\ &= \frac{1}{2\pi r^2} \int_0^{\infty} \frac{\sin(t\sqrt{k^2+m^2})}{\sqrt{k^2+m^2}}\ k \sin kr\ dk \\ &= -\frac{1}{4\pi r} \frac{\delta}{\delta r} \int_{-\infty}^{\infty} \frac{\sin(t\sqrt{k^2+m^2})}{\sqrt{k^2+m^2}}\ e^{ikr} dk. \end{aligned}$$

Let H represent the Heaviside function. Computing the above derivative with respect to r and using the identities $J_0 = -J_1$ and $J_0(0) = 1$, we obtain that

$$S(r,t) = \frac{1}{2\pi}\delta(t^2 - r^2) - mH(t^2 - r^2)\frac{J_1(m\sqrt{t^2 - r^2})}{4\pi\sqrt{t^2 - r^2}}.$$

2.4.2 The sine-Gordon equation

The sine-Gordon equation has been used as a mathematical model in many different applications, including the propagation of ultra-short optical pulses in resonant laser media [35], a universal theory of elementary particles [36, 37, 38], and the prop-

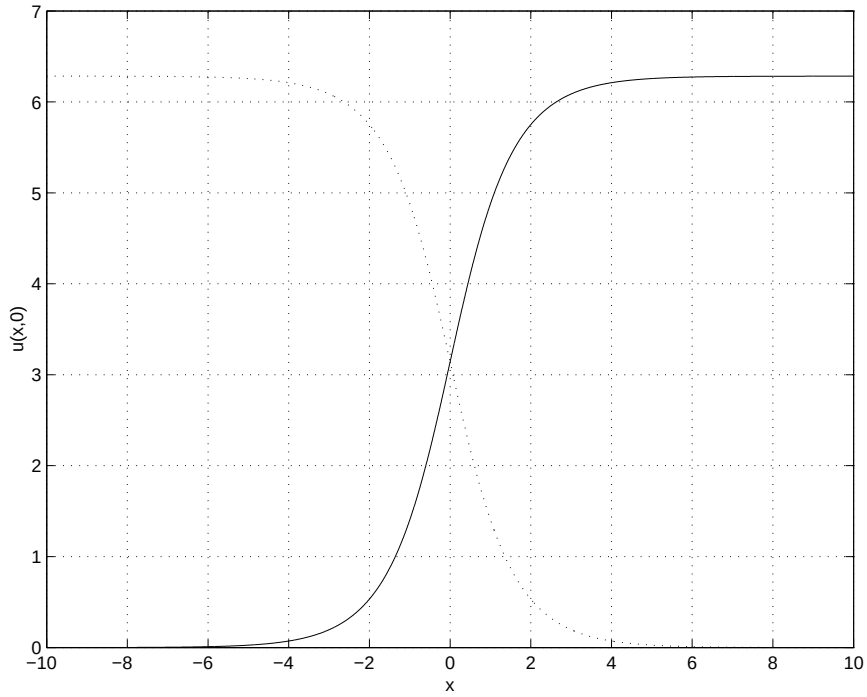

FIGURE 2.3: Soliton solution (solid line) and anti-soliton solution (dotted line) of the sine-Gordon equation at time 0, with $v = 0.1$.

agation of magnetic flux in Josephson junctions [39]. Here we consider the classical $(1+1)$-dimensional sine-Gordon equation presented in Section 2.2, with parameters $m^2 = c = 1$, and assume that $u(x,t) = \phi(x - vt) = u(\xi)$ is an elementary soliton solution. Then ϕ satisfies the ordinary differential equation $(1-v^2)\phi_{\xi\xi} - \sin\phi = 0$. Multiplying then by ϕ_x, integrating with respect to ξ and solving for ϕ_ξ, we obtain that

$$\frac{d\phi}{d\xi} = \left(2A - \frac{2\cos\phi}{1-v^2}\right)^{1/2},$$

where A is the constant of integration. Now we use separation of variables and the substitution $A(1-v^2) = 1$. Integrating both sides and noting that $1 - \cos\phi = 2\sin^2(\frac{1}{2}\phi)$ and noting that the derivative with respect to ϕ of $\ln\tan(\frac{1}{4}\phi)$ equals $\frac{1}{2}\csc(\frac{1}{2}\phi)$, we get

$$\sqrt{2}\ln\left[\frac{\tan(\frac{1}{4}\phi)}{\tan(\frac{1}{4}\phi_0)}\right] = \left[\frac{2}{1-v^2}\right]^{1/2}(\xi - \xi_0).$$

Finally, solving for ϕ and expressing the result in terms of x and t, it is possible to write the elementary soliton solution as

$$u(x,t) = 4\arctan\left[\exp\left(\frac{x-vt}{\sqrt{1-v^2}}\right)\right].$$

This solution is sometimes called a **kink**; its profile is shown in Figure 2.3. The other soliton solution that can be obtained from the sine-Gordon equation, called the **anti-kink** or **anti-soliton**, is shown in the same figure. Its analytical expression

is given by

$$u(x,t) = 4\,\mathrm{arccot}\left[\exp\left(\frac{x-vt}{\sqrt{1-v^2}}\right)\right].$$

To close this section, we must mention that the sine-Gordon equation possesses solutions built up from the superposition of solitons and/or anti-solitons. Those solutions and the elementary soliton solutions obtained above are listed in the following table for the sake of future reference (see [40]).

Type of solution	**Analytical expression**
single soliton	$u(x,t) = 4\arctan\left[\exp\left(\frac{x-vt}{\sqrt{1-v^2}}\right)\right]$
single anti-soliton	$u(x,t) = u(x,t) = 4\,\mathrm{arccot}\left[\exp\left(\frac{x-vt}{\sqrt{1-v^2}}\right)\right]$
two solitons	$u(x,t) = 4\arctan\left[\frac{v\sinh(x/\sqrt{1-v^2})}{\cosh(vt/\sqrt{1-v^2})}\right]$
soliton and anti-soliton	$4\arctan\left[\frac{\sinh(vt/\sqrt{1-v^2})}{v\cosh(x/\sqrt{1-v^2})}\right]$
"breather"	$u(x,t) = 4\arctan\left[\frac{\sqrt{1-v^2}}{v}\frac{\sin(vt)}{\cosh(x\sqrt{1-v^2})}\right]$

TABLE 2.1: Different types of soliton solutions of the sine-Gordon equation.

2.4.3 The Landau-Ginzburg equation

The $(1+1)$-dimensional Landau-Ginzburg equation is another important nonlinear partial differential equation arising in physics that possesses soliton solutions. From the mathematical point of view, the Landau-Ginzburg equation can be seen as a quasilinear Klein-Gordon equation with purely imaginary mass and nonlinear term proportional to u^3. More concretely, the Landau-Ginzburg equation with real parameters m and λ under study in this section can be written as

$$\frac{\partial^2 u}{\partial t^2} - \frac{\partial^2 u}{\partial x^2} - m^2 u + \lambda u^3 = 0.$$

Using the same technique to find elementary, solitary wave solutions, we suppose that $u(x,t) = \phi(\xi)$, where $\xi = x - vt$ for some $v \in \mathbb{R}$. Then ϕ satisfies the ordinary differential equation

$$(1-v^2)\frac{d^2\phi}{d\xi^2} = -m^2\phi + \lambda\phi^3.$$

Solving and then multiplying by $2\phi'(\xi)$, we obtain that

$$\frac{d}{d\xi}\left[\left(\frac{d\phi}{d\xi}\right)^2\right] = \frac{1}{2(1-v^2)}\,\frac{d}{d\xi}\left(\lambda\phi^4 - 2m^2\phi^2\right).$$

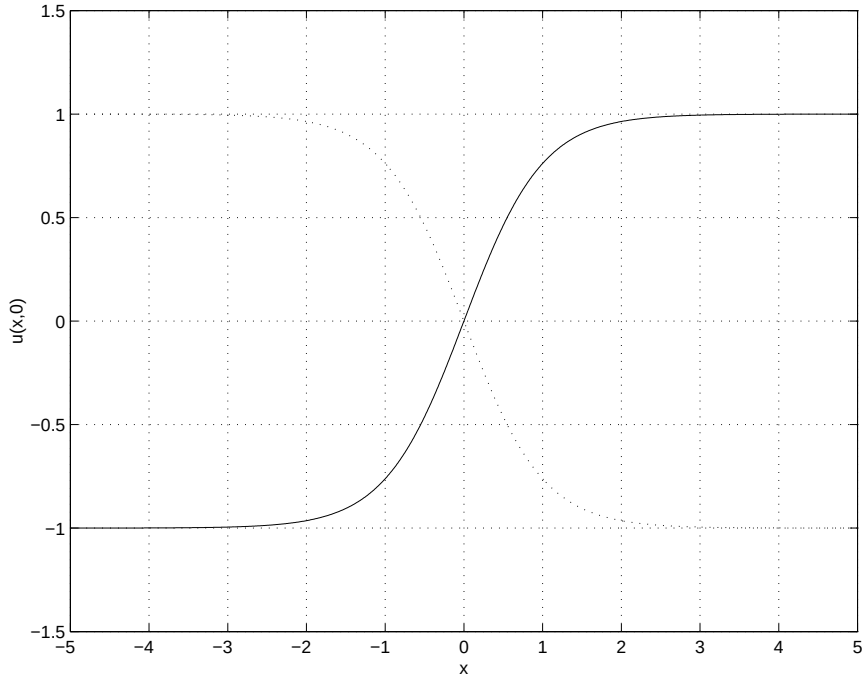

FIGURE 2.4: Soliton solution (solid line) and anti-soliton solution (dotted line) of the Landau-Ginzburg equation at time 0, with $v = 0.1$.

We integrate now with respect to ξ both sides of the equation. An integration constant will appear in the right-hand side of the resulting equality. By choosing this constant of integration equal to $m^2/(2\lambda(1-v^2))$, taking the negative square root on both sides of the equation, separating variables, and completing the square in the radical that contains ϕ, we obtain that

$$-\frac{1}{\sqrt{\lambda}}\int_{\phi_0}^{\phi}\frac{d\phi}{\phi^2 - m^2/\lambda} = \int_{\xi_0}^{\xi}\frac{d\xi}{\sqrt{2(1-v^2)}}.$$

Let ξ_0 and ϕ_0 be both equal to zero. Expressing the integrand in the left-hand side of the preceding equality, integrating, and then evaluating from ϕ_0 to ϕ, we get

$$\frac{1}{2m}\ln\left|\frac{(\phi + m/\sqrt{\lambda})(\phi_0 - m/\sqrt{\lambda})}{(\phi - m/\sqrt{\lambda})(\phi_0 + m/\sqrt{\lambda})}\right| = \frac{\xi - \xi_0}{\sqrt{2(1-v^2)}}$$

We choose ϕ_0 and ξ_0 to be equal to zero. Solving then for ϕ we obtain the following soliton (kink) solution for the Landau-Ginzburg equation

$$u(x,t) = \frac{m}{\sqrt{\lambda}} = \tanh\left[\frac{m(x-vt)}{\sqrt{2(1-v^2)}}\right]$$

The corresponding anti-soliton (anti-kink) solution to the Landau-Ginzburg equation is obtained by evaluationg the solition solution at $(-x,t)$. A graph showing the kink and anti-kink of the Landau-Ginzburg equation is shown in Figure 2.4.

2.5 Elements of numerical analysis

In our investigation, we are interested in developing finite-difference schemes to approximate radially symmetric solutions of modified nonlinear Klein-Gordon equations. In order to determine how accurate our approximations are, we need to introduce the notions of convergence, consistency and stability. To understand these concepts we must first clarify some ideas from mathematical analysis. Here we follow [41] and [42]. Throughout K denotes the fields $\mathbb{R}$ and $\mathbb{C}$.

2.5.1 Normed linear spaces

A **norm** on a vector space V over a scalar field K is a function $||\cdot||$ that associates every element of V with a real number, such that for any vectors $\bar{u}$ and $\bar{v}$, and any scalar a, the following properties are satisfied:

(i) $||\bar{v}|| \geq 0$, and $||\bar{v}|| = 0$ iff $\bar{v} = 0$,

(ii) $||a\bar{v}|| = |a|\ ||\bar{v}||$, and

(iii) $||\bar{u} + \bar{v}|| \leq ||\bar{u}|| + ||\bar{v}||$.

It is worthwhile mentioning that a vector space with a norm associated with it is called a **normed linear space** or simply **normed space**. The following are examples of normed linear spaces with the given norms.

Example 2. Denote by $|\cdot|$ the standard norm in K. The linear space K^n can be given the **p-norm** ($p \geq 1$)

$$||\bar{x}||_p = \left(\sum_{i=1}^{n} |x_i|^p \right)^{1/p}.$$

The 1-norm and the 2-norm in K^n are called the the **taxicab norm** and the **Euclidean norm** , respectively. K^n can also be normed by the so called **infinity norm** $||\bar{x}||_\infty = \max\{|x_1|, \ldots, |x_n|\}$. □

Example 3. Let Δx and p be positive numbers with $p > 1$. The space $\ell_{p,\Delta x}$ is the normed linear space of all infinite sequences $\mathbf{u} = (\ldots, u_{-1}, u_0, u_1, \ldots)$ of elements in K with vector addition and scalar multiplication given componentwise, such that $\sum_{-\infty<j<\infty} |u_j|^p < \infty$. The norm is given by

$$||\mathbf{u}||_{p,\Delta x} = \left(\sum_{k=-\infty}^{\infty} |u_k|^p \Delta x \right)^{1/p}.$$

The space ℓ_p is defined to be the space $\ell_{p,1}$. If p is equal to 2 then $\ell_{p,\Delta x}$ is called the **energy space**. □

EXAMPLE 4. Let λ represent the Lebesgue measure on $X \subseteq \mathbb{R}$. The space $L_p(X)$ for $p > 1$ is the normed linear space of all equivalence classes of functions $f\colon X \to \mathbb{R}$ under the relation of equivalence almost everywhere, together with addition and scalar multiplication defined in representatives, such that $\int_X f^p \, d\lambda < \infty$. Its norm is given by

$$||f||_p = \left(\int_X f^p \, d\lambda \right)^{1/p}. \quad \square$$

EXAMPLE 5. Let $|| \cdot ||$ be any norm in K^n. The space of all $n \times n$-matrices with coefficients in K is a normed linear space with the usual operations of addition of matrices and scalar multiplication, with **matrix norm** defined by

$$||Q|| = \sup_{||\bar{u}|| \leq 1} \{Q\bar{u}\}. \quad \square$$

2.5.2 Analysis of stability

Convergence

A difference scheme $L_k^n u_k^n = G_k^n$ approximating the partial differential equation $\mathcal{L}v = F$ is a **convergent** scheme at time t in the norm $||\cdot||$ of $\ell_{p,\Delta x}$ if, as $(n+1)\Delta t \to t$,

$$||\mathbf{u}^{n+1} - \mathbf{v}^{n+1}|| \to 0$$

as $\Delta x, \Delta t \to 0$. Here $\mathbf{u}^n = (\ldots, u_{-1}^n, u_0^n, u_1^n, \ldots)$ and $\mathbf{v}^n = (\ldots, v_{-1}^n, v_0^n, v_1^n, \ldots)$ are the sequences representing the vector of approximations to the solution of the partial differential equation and the vector of exact solutions whose k-th component is $v(k\Delta x, n\Delta t)$, respectively.

Consistency

The difference scheme $\mathbf{u}^{n+1} = Q\mathbf{u}^n + \Delta t \mathbf{G}^n$ is **consistent** with the partial differential equation $\mathcal{L}v = F$ in the norm $|| \cdot ||$ if the solution v of the differential equation satisfies

$$\mathbf{v}^{n+1} = Q\mathbf{v}^n + \Delta t \mathbf{g}^n + \Delta t \tau^n,$$

and $||\tau^n|| \to 0$ as $\Delta x, \Delta t \to 0$. Moreover, the scheme is said to be accurate with order $\mathcal{O}(\Delta x^p) + \mathcal{O}(\Delta t^q)$ if

$$||\tau^n|| = \mathcal{O}(\Delta x^p) + \mathcal{O}(\Delta t^q).$$

Stability

One interpretation of stability of a finite-difference scheme is that, for a stable scheme, small errors in the initial conditions cause small errors in the solution. As we will see, the definition does allow the errors to grow but limits them to grow no faster than exponential. More precisely, the finite-difference scheme $\mathbf{u}^{n+1} = Q\mathbf{u}^n$ is

said to be **stable** with respect to the norm $||\cdot||$ if there exist positive constants Δx_0 and Δt_0, and nonnegative constants K and β so that

$$||\mathbf{u}^{n+1}|| \leq Ke^{\beta t}||\mathbf{u}^0||,$$

for $0 \leq t = (n+1)\Delta t$, $0 < \Delta x \leq \Delta x_0$ and $0 < \Delta t \leq \Delta t_0$. If further restrictions on the relationship between Δt and Δx are needed in order to guarantee stability of the finite-difference scheme, we say that the scheme is **conditionally stable**.

One characterization of stability that is often useful comes from the inequality in the definition above. We state this in the following result.

THEOREM 6. *The scheme $\mathbf{u}^{n+1} = Q\mathbf{u}^n$ is stable with respect to the norm $||\cdot||$ if and only if there exist positive constants Δx_0 and Δt_0, and nonnegative constants K and β so that*

$$||Q^{n+1}|| \leq Ke^{\beta t},$$

for $0 \leq t = (n+1)\Delta t$, $0 < \Delta x \leq \Delta x_0$ and $0 < \Delta t \leq \Delta t_0$. □

The difference scheme $\mathbf{u}^{n+1} = Q\mathbf{u}^n$ is said to be **stable order** n with respect to the norm $||\cdot||$ if there exist positive constants Δx_0 and Δt_0, and nonnegative constants K_1, K_2 and β such that

$$||\mathbf{u}^{n+1}|| \leq (K_1 + nK_2)e^{\beta t}||\mathbf{u}^0||,$$

for $0 \leq t = (n+1)\Delta t$, $0 < \Delta x \leq \Delta x_0$ and $0 < \Delta t \leq \Delta t_0$. Obviously, if a finite-difference scheme is stable then it will be stable order n. We also realize that the above definition is equivalent to requiring that Q satisfy $||Q^n|| \leq (K_1 + nK_2)e^{\beta t}$.

The use of the discrete Fourier transform is a useful tool in the analysis of stability of finite-difference schemes for initial-value problems. We define the **discrete Fourier transform** of $\mathbf{u} \in \ell_2$ as the function $\hat{u} \in L_2([-\pi, \pi])$ given by

$$\hat{u}(\xi) = \frac{1}{\sqrt{2\pi}} \sum_{m=-\infty}^{\infty} e^{-im\xi} u_m,$$

for $\xi \in [-\pi, \pi]$. The ℓ_2 vectors that we will be using later will be the $\ell_{2,\Delta x}$ vectors that are the solutions to our finite-difference schemes at time step n.

EXAMPLE 7. The **central second-order difference** is the linear operator δ^2 that associates with each infinite sequence $\mathbf{u} = (\dots, u_{-1}, u_0, u_1, \dots)$ of real numbers the infinite sequence $\delta^2\mathbf{u}$ whose m-th component is given by $u_{m+1} - 2u_m + u_{m-1}$. It is easy to check that the Fourier transform of $\delta^2\mathbf{u}$ is given by $-4\sin^2\frac{\xi}{2}\hat{u}$. □

It is important to remark that if $\mathbf{u} \in \ell_2$ has discrete Fourier transform $\hat{u}$ then $||\hat{u}||_2 = ||\mathbf{u}||_2$, where the first norm is the L_2-norm on $[-\pi, \pi]$ and the second norm is the ℓ_2-norm. This fact constitutes a bridge between the spaces ℓ_2 and $L_2([-\pi, \pi])$ that provides us with the following important result for stability.

THEOREM 8. *The sequence $\{\mathbf{u}^n\}$ is stable in $\ell_{2,\Delta x}$ if and only if the sequence $\{\hat{u}^n\}$ is stable in $L_2([-\pi, \pi])$.* □

Let $\mathbf{u}^{n+1} = Q\mathbf{u}^n$ be a finite difference scheme. Taking discrete Fourier transform in both sides we obtain an equation of the form $\hat{u}^{n+1} = A(\xi)\hat{u}^n$. The matrix $A(\xi)$ is called the **amplification matrix** of the difference scheme. By virtue of Theorem 8, the stability of the scheme depends on the growth of the amplification matrix raised to the n-th power.

THEOREM 9 (Lax Theorem). *If a two-level difference scheme* $\mathbf{u}^{n+1} = Q\mathbf{u}^n + \Delta t\mathbf{G}^n$ *is consistent in the norm* $||\cdot||$ *to an initial-value problem and is stable with respect to* $||\cdot||$*, the it is convergent with respect to* $||\cdot||$*.* □

Chapter 3

The undamped, nonlinear Klein-Gordon equation

In the present chapter we describe a numerical method to approximate radially symmetric solutions, and one-dimensional not necessarily radially symmetric solutions of the nonlinear Klein-Gordon equation. The energy analysis of this equation shows that the total energy is conserved. We propose a discrete scheme for the energy of this equation and prove that it is conserved at every time step. Finally, we show that our results are in general agreement with Strauss and Vázquez [8] and give applications application to solitonlike solutions for a Higgs scalar field and the analysis of non-dissipative long Josephson junctions.

3.1 Finite-difference scheme

Let u be a function of position $\bar{x}$ and time t, and suppose that ϕ and ψ are smooth functions of $\bar{x}$ of compact support in a domain D of $\mathbb{R}^3$. The problem under study in this chapter can be rewritten in dimensionless form as the initial-value problem

$$\begin{aligned} &\frac{\partial^2 u}{\partial t^2} - \nabla^2 u \pm m^2 u + G'(u) = 0, \\ \text{subject to :} \quad &\begin{cases} u(\bar{x},0) = \phi(\bar{x}), & \bar{x} \in D, \\ \dfrac{\partial u}{\partial t}(\bar{x},0) = \psi(\bar{x}), & \bar{x} \in D. \end{cases} \end{aligned} \tag{3.1}$$

Radially symmetric solutions

We are interested now in computing radially symmetric solutions of (3.1), that is solutions of the form $u = u(r,t)$ with $r = ||\bar{x}||$, where $||\cdot||$ denotes the usual Euclidean norm in $\mathbb{R}^3$. For the sake of simplicity we may assume that D represents the open sphere with center in the origin and radius L, that ϕ and ψ are radially symmetric in D, and that ϕ, ψ, $r\phi$ and $r\psi$ are small at infinity in D.

In spherical coordinates

$$r\nabla^2 u = r\frac{\partial^2 u}{\partial r^2} + 2\frac{\partial u}{\partial r},$$

so that our nonlinear Klein-Gordon equation reads

$$\frac{\partial^2 u}{\partial t^2} - \frac{\partial^2 u}{\partial r^2} - \frac{2}{r}\frac{\partial u}{\partial r} \pm m^2 u + G'(u) = 0, \qquad \text{for } 0 < r < L.$$

In order to simplify this equation we let $v(r,t) = ru(r,t)$. Obviously v satisfies $v(0,t) = 0$, for every $t \geq 0$. Moveover, for every $0 < r < L$

$$\begin{aligned} \frac{1}{r}\frac{\partial^2 v}{\partial t^2} &= \frac{\partial^2 u}{\partial t^2}, \qquad \text{and} \\ \frac{1}{r}\frac{\partial^2 v}{\partial r^2} &= \frac{\partial^2 u}{\partial r^2} + \frac{2}{r}\frac{\partial u}{\partial r}. \end{aligned} \tag{3.2}$$

These equations together with the initial conditions in (3.1) and the boundary condition stated in the previous paragraph yield the mixed-value problem

$$\begin{aligned} &\frac{\partial^2 v}{\partial t^2} - \frac{\partial^2 v}{\partial r^2} \pm m^2 v + rG'(v/r) = 0, \qquad \text{for } 0 < r < L, \\ &\text{subject to :} \quad \begin{cases} v(r,0) = r\phi(r), & 0 \leq r < L, \\ \dfrac{\partial v}{\partial t}(r,0) = r\psi(r), & 0 \leq r < L, \\ v(0,t) = 0, & t \geq 0. \end{cases} \end{aligned} \tag{3.3}$$

Suppose that $a < L$ and T are positive numbers, and that a is approximately equal to L. To discretize the differential equation in (3.3) we approximate solutions for values of r and t in the intervals $[0,a]$ and $[0,T]$, respectively. We construct partitions $0 = r_0 < r_1 < \cdots < r_M = a$ and $0 = t_0 < t_1 < \cdots < t_N = T$ of $[0,a]$ and $[0,T]$ consisting of M and N regular subintervals of lengths $\Delta r = a/M$ and $\Delta t = T/N$, respectively.

Denote the approximate value of $v(r_j, t_n)$ by v_j^n, for $j = 0, 1, \ldots, M$ and $n = 0, 1, \ldots, N$. For the first time step the first initial condition gives $v_j^0 = r_j\phi(r_j)$, for each $j = 0, 1, \ldots, M$. Using second-order approximation the second initial condition yields

$$v_j^1 = v_j^0 + \frac{v_{j-1}^0 - 2v_j^0 + v_{j+1}^0}{2}\left(\frac{\Delta t}{\Delta r}\right)^2 + r_j\psi(r_j)\Delta t,$$

for every $j = 1, \ldots, M-1$. The boundary condition in problem (3.3) states that v_0^n is zero for every $n = 0, 1, \ldots, N$. Moreover, we impose the constraint that every v_m^n is also equal to zero in our scheme since we expect solutions to be small at infinity.

Assuming that the solution of (3.3) has been approximated up to the n-th time step, we proceed to approximate the solution of the $(n+1)$-st time step by induction, using central second-differences to estimate the second-order partial derivatives of v with respect to t and r. The term $v(r_j, t_n)$ is approximated using the average of v_j^{n+1} and v_j^{n-1}, and $G'(v(r_j,t_n)/r_j)$ is estimated using the average rate of change of G between v_j^{n+1}/r_j and v_j^{n-1}/r_j. Our finite-difference scheme is thus

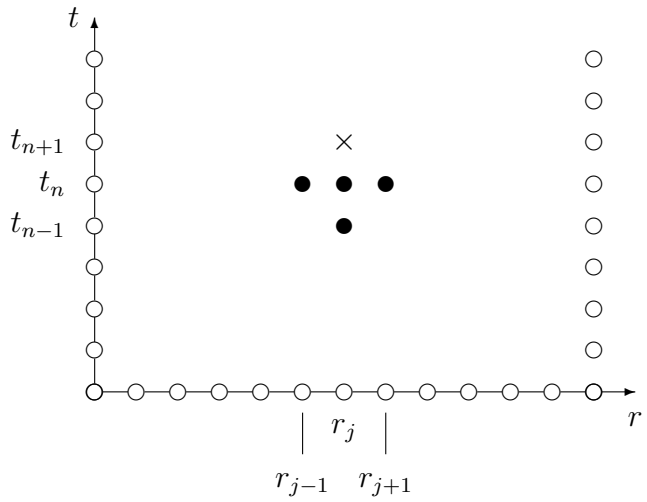

FIGURE 3.1: Forward-difference scheme for the nonlinear Klein-Gordon equation.

$$\frac{v_j^{n+1} - 2v_j^n + v_j^{n-1}}{(\Delta t)^2} - \frac{v_{j+1}^n - 2v_j^n + v_{j-1}^n}{(\Delta r)^2} \pm \frac{m^2}{2}\left[v_j^{n+1} + v_j^{n-1}\right] + r_j^2 \frac{G(v_j^{n+1}/r_j) - G(v_j^{n-1}/r_j)}{v_j^{n+1} - v_j^{n-1}} = 0.$$

The method is explicit if G is constant. If G is not constant the approximation v_j^{n+1} can be obtained from Newton's method, keeping all other terms constant. More precisely, let y_0 be an estimate of the true value of v_j^n. Define

$$F(y) = \frac{y - 2v_j^n + v_j^{n-1}}{(\Delta t)^2} - \frac{v_{j+1}^n - 2v_j^n + v_{j-1}^n}{(\Delta r)^2} \pm \frac{m^2}{2}\left[y + v_j^{n-1}\right] + r_j^2 \frac{G(y/r_j) - G(v_j^{n-1}/r_j)}{y - v_j^{n-1}}.$$

Then

$$F'(y) = \frac{1}{(\Delta t)^2} \pm \frac{m^2}{2} + r_j^2 \frac{G(v_j^{n-1}/r_j) - G(y/r_j) + (y - v_j^{n-1})G'(y/r_j)}{\left(y - v_j^{n-1}\right)^2}.$$

For initial approximations sufficiently close, Newton's method guarantees that the true value of v_j^{n+1} is the limit at which the recursive sequence $y_{n+1} = y_n - F(y_n)/F'(y_n)$ converges. The order of convergence is quadratic in such circumstances.

As mentioned earlier in Chapter 4, it is physically interesting to approximate radially symmetric solutions of the nonlinear Klein-Gordon equation when $G'(u) = u^p$, for $p > 1$ an odd number. For this choice of G', our finite-difference scheme has the simpler expression

$$\frac{v_j^{n+1}-2v_j^n+v_j^{n-1}}{(\Delta t)^2}-\frac{v_{j+1}^n-2v_j^n+v_{j-1}^n}{(\Delta r)^2}\pm\frac{m^2}{2}\left[v_j^{n+1}+v_j^{n-1}\right]+ \frac{1}{(j\Delta r)^{p-1}}\frac{G(v_j^{n+1})-G(v_j^{n-1})}{v_j^{n+1}-v_j^{n-1}} = 0. \quad (3.4)$$

We state the most important numerical properties of our scheme in the following theorem, whose proof will be given in a more general context in Chapter 6. For a proof of consistency and stability in case that G' and m are both equal to zero, refer to [42].

THEOREM 1. *Let G' be identically equal to zero. Then scheme* (3.4) *is consistent $\mathcal{O}(\Delta t^2)+\mathcal{O}(\Delta r^2)$. Moreover, it is stable (and thus convergent) if*

$$\left(\frac{\Delta t}{\Delta r}\right)^2 < 1+\frac{1}{4}(m\Delta t)^2. \quad \square$$

The $(1+1)$-dimensional solutions

We consider not the case where u is a function of a one-dimensional space variable and time. Then (3.1) becomes the initial-value problem

$$\frac{\partial^2 u}{\partial t^2}-\frac{\partial^2 u}{\partial x^2}\pm m^2u+G'(u)=0,$$
$$\text{subject to :} \quad \begin{cases} u(x,0)=\phi(x), & a\le x\le b, \\ \dfrac{\partial u}{\partial t}(x,0)=\psi(x), & a\le x\le b. \end{cases} \quad (3.5)$$

Let $a=x_0<x_1<\cdots<x_M=b$ and $0=t_0<t_1<\cdots<t_N=T$ be partitions of $[a,b]$ and $[0,T]$ consisting of M and N regular subintervals of lengths $\Delta x=(b-a)/M$ and $\Delta t=T/N$, respectively. Let $u(x_j,t_n)$ be represented by u_j^n, for $j=0,1,\ldots,M$ and $n=0,1,\ldots,N$. A finite-difference scheme to approximate solutions to this problem is given by

$$\frac{u_j^{n+1}-2u_j^n+u_j^{n-1}}{(\Delta t)^2}-\frac{u_{j+1}^n-2u_j^n+u_{j-1}^n}{(\Delta x)^2}\pm\frac{m^2}{2}\left[u_j^{n+1}+u_j^{n-1}\right]+ \frac{G(u_j^{n+1})-G(u_j^{n-1})}{u_j^{n+1}-u_j^{n-1}} = 0, \quad (3.6)$$

where $u_j^0=\phi(x_j)$ for $j=0,\ldots,M$, and

$$u_j^1=u_j^0+\frac{u_{j-1}^0-2u_j^0+u_{j+1}^0}{2}\left(\frac{\Delta t}{\Delta x}\right)^2+\psi(x_j)\Delta t$$

for $j=1,\ldots,M-1$. In order for the method to be completely defined, the boundary values u_0^{n+1} and u_M^{n+1} must be somehow specified. This is typically done by either one

of two ways:

- using Dirichlet boundary conditions $u(a,t) = g(t)$ and $u(b,t) = h(t)$, with g and h continuous functions; in which case $u_0^n = g(n\Delta x)$ and $u_M^n = h(n\Delta x)$ for every $n = 0, 1, \ldots, N$, or
- using a combination of Dirichlet and Neumann boundary conditions, say $u_x(a,t) = g(t)$ and $u(b,t) = h(t)$, where g and h are continuous functions. In this case u_0^n can be obtained by using first a second-order difference to estimate $u_x(a,t_n)$, and then estimating u_0^{n+1} using (3.6) with $j = 0$. The estimation of $u_x(a,t_n)$ would require the introduction of a dummy approximation u_{-1}^n of $u(a-\Delta x, t_n)$, whence $u_{-1} = u_1 - 2\Delta x g(t_n)$ holds.

As (3.4), this method is consistent to the second order and conditionally stable (thus conditionally convergent). Likewise, its implementation requires an application of Newton's method.

3.2 Energy analysis

The present section is primarily devoted to compute an expression for the total energy of the three-dimensional nonlinear Klein-Gordon equation. We prove that the energy is conserved throughout time and develop a numeric scheme for the discrete energy that has the same conservative property.

3.2.1 Derivation of the energy equation

In order to derive the energy expression of the three-dimensional nonlinear Klein-Gordon equation, it is necessary to compute the Lagrangian and the Hamiltonian of the differential equation in (3.1). Throughout we will use equations from the Lagrangian and Hamiltonian formulations of mechanics. We refer the reader to [43] for more details.

LEMMA 2. *The Lagrangian of the nonlinear Klein-Gordon equation is given by*

$$\mathcal{L} = \frac{1}{2}\left\{\left(\frac{\partial u}{\partial t}\right)^2 - |\nabla u|^2 \mp m^2 u^2\right\} - G(u).$$

Proof. Let $x_0 = t$, $x_1 = x$, $x_2 = y$, and $x_3 = z$. To simplify notation, we define

$$\dot{u}_i = \frac{\partial u}{\partial x_i}, \qquad \text{for } i = 0, 1, 2, 3.$$

To prove our lemma, we must verify that the *Euler-Lagrange equation* associated with $\mathcal{L}$ yields the nonlinear Klein-Gordon equation. The **canonical Euler-Lagrange equation** in this case reads

$$\sum_{i=0}^{4} \frac{\partial}{\partial x_i}\left(\frac{\partial \mathcal{L}}{\partial \dot{u}_i}\right) - \frac{\partial \mathcal{L}}{\partial u} = 0.$$

Notice that

$$\begin{aligned} \frac{\partial \mathcal{L}}{\partial u} &= \mp m^2 u - G'(u), \qquad \text{and} \\ \frac{\partial}{\partial x_i}\left(\frac{\partial \mathcal{L}}{\partial \dot{u}_i}\right) &= \begin{cases} \dfrac{\partial^2 u}{\partial t^2}, & \text{if } i = 0, \\ -\dfrac{\partial^2 u}{\partial x_i^2}, & \text{if } i = 1, 2, 3. \end{cases} \end{aligned}$$

The result is now evident. □

THEOREM 3. *The Hamiltonian of the nonlinear Klein-Gordon equation is given by*

$$\mathcal{H} = \frac{1}{2}\left\{\left(\frac{\partial u}{\partial t}\right)^2 + |\nabla u|^2 \pm m^2 u^2\right\} + G(u). \quad \square$$

COROLLARY 4. *The total energy associated with the nonlinear Klein-Gordon equation at time t is given by*

$$E(t) = \iiint_D \left\{\frac{1}{2}\left(\frac{\partial u}{\partial t}\right)^2 + \frac{1}{2}|\nabla u|^2 \pm \frac{m^2}{2}u^2 + G(u)\right\} d\bar{x}. \quad \square$$

Suppose that the solution u of the nonlinear Klein-Gordon equation has radial symmetry at every time t and that D represents the open sphere with center in the origin and radius L. Recall that the general expression of the **gradient in spherical coordinates** is given by

$$\nabla u = \frac{\partial u}{\partial r}\hat{\mathbf{r}} + \frac{1}{r}\frac{\partial u}{\partial \theta}\hat{\theta} + \frac{1}{r\sin\theta}\frac{\partial u}{\partial \phi}\hat{\phi}.$$

Using this fact, the total energy can be rewritten as

$$E(t) = 4\pi \int_0^L \left\{\frac{1}{2}\left(\frac{\partial u}{\partial t}\right)^2 + \frac{1}{2}\left(\frac{\partial u}{\partial r}\right)^2 \pm \frac{m^2}{2}u^2 + G(u)\right\} r^2 dr, \tag{3.7}$$

and using the change of variable $v(r,t) = ru(r,t)$, the energy expression for radially symmetric solutions of the nonlinear Klein-Gordon equation adopts the following form.

COROLLARY 5. *The energy expression at time t of a radially symmetric solution u of the nonlinear Klein-Gordon equation has the form $E(t) = 4\pi E_0(t)$, where*

$$E_0(t) = \int_0^L \left\{\frac{1}{2}\left(\frac{\partial v}{\partial t}\right)^2 + \frac{1}{2}\left(\frac{\partial v}{\partial r}\right)^2 \pm \frac{m^2}{2}v^2 + r^2 G(v/r)\right\} dr$$

and $u(r,t) = rv(r,t)$. □

COROLLARY 6. *The energy expression at time t of a radially symmetric solution u of the nonlinear Klein-Gordon equation with $G'(u) = u^p$ has the form $E(t) = 4\pi E_0(t)$, where*

$$E_0(t) = \int_0^L \left\{ \frac{1}{2}\left(\frac{\partial v}{\partial t}\right)^2 + \frac{1}{2}\left(\frac{\partial v}{\partial r}\right)^2 \pm \frac{m^2}{2}v^2 + r^{1-p}G(v) \right\} dr$$

and $v(r,t) = ru(r,t)$. □

Before we proceed to do the continuous energy analysis, it is important to point out that a similar analysis can be carried out for the expression of the continuous energy in the $(1+1)$-dimensional case. In fact, the total energy associated with the $(1+1)$-dimensional nonlinear Klein-Gordon equation at time t is given by

$$E(t) = \int_a^b \left\{ \frac{1}{2}\left(\frac{\partial u}{\partial t}\right)^2 + \frac{1}{2}\left(\frac{\partial u}{\partial x}\right)^2 \pm \frac{m^2}{2}u^2 + G(u) \right\} dx.$$

3.2.2 Continuous energy

One of the most interesting properties of the energy expression in Corollary 4 is that it is unchanged in time under certain analytical conditions. This statement is proved in Theorem 8 and requires the following result whose proof can be found in [44].

LEMMA 7. *Let ϕ and ψ scalar functions on a domain D of $\mathbb{R}^3$ with continuous partial derivatives in D. Then for every closed simple domain $R \subseteq D$ with boundary ∂R,*

$$\iint_{\partial R} \psi \nabla\phi \cdot \hat{\mathrm{n}}\, d\sigma = \iiint_R \left(\psi\nabla^2\phi + \nabla\psi\cdot\nabla\phi\right) d\bar{x},$$

where $\hat{\mathrm{n}}$ represents the unit vector normal to the surface ∂R . □

It is worthwhile noticing that if D is a domain of $\mathbb{R}^3$ and if u is a function of $\bar{x}$ and t with continuous partial derivatives in $D \times \mathbb{R}$ up to the second order then

$$\frac{\partial}{\partial t}|\nabla u|^2 = 2\nabla u \cdot \nabla\left(\frac{\partial u}{\partial t}\right).$$

By virtue of Lemma 7, for every closed simple domain R contained in D we have that **Green's first identity** is satisfied:

$$\iint_{\partial R} \frac{\partial u}{\partial t}\nabla u \cdot \hat{\mathrm{n}}\, d\sigma = \iiint_R \left(\frac{\partial u}{\partial t}\nabla^2 u + \frac{1}{2}\frac{\partial}{\partial t}|\nabla u|^2\right) d\bar{x}.$$

Equivalently

$$\frac{1}{2}\iiint_R \frac{\partial}{\partial t}|\nabla u|^2\, d\bar{x} = \iint_{\partial R} \frac{\partial u}{\partial t}\nabla u\cdot\hat{\mathrm{n}}\, d\sigma - \iiint_R \frac{\partial u}{\partial t}\nabla^2 u\, d\bar{x}. \tag{3.8}$$

THEOREM 8. *Let D be a domain in $\mathbb{R}^3$, and suppose that $\nabla u \cdot \hat{\mathrm{n}} = 0$ on the boundary of D at all times. Then the energy of the nonlinear Klein-Gordon equation is conserved.*

Proof. Differentiating the expression of the total energy in Corollary 4 and applying successively Equations (3.8) and (3.1), we obtain

$$\begin{aligned}\frac{dE}{dt}(t) &= \iiint_D \frac{\partial u}{\partial t}\left\{\frac{\partial^2 u}{\partial t^2} \pm m^2 u + G'(u)\right\} d\bar{x} + \frac{1}{2}\iiint_D \frac{\partial}{\partial t}|\nabla u|^2 d\bar{x} \\ &= \iiint_D \frac{\partial u}{\partial t}\left\{\frac{\partial^2 u}{\partial t^2} - \nabla^2 u \pm m^2 u + G'(u)\right\} d\bar{x} + \iint_{\partial D} \frac{\partial u}{\partial t}\nabla u \cdot \hat{\mathrm{n}}\, d\sigma \;=\; 0.\end{aligned}$$

□

If ϕ and ψ are supposed to be small at infinity then the solution of the nonlinear Klein-Gordon equation will be likewise small at infinity. This implies in particular that $\nabla u = 0$ on the boundary of D, whence the following result follows.

COROLLARY 9. *Let D be a domain in $\mathbb{R}^3$, and suppose that ϕ and ψ are smooth functions of compact support in D which are small at infinity. Then the energy of the nonlinear Klein-Gordon equation is conserved.* □

Our next result implies in particular that radial solutions of the nonlinear Klein-Gordon equation are bounded outside of every open neighborhood of the origin.

THEOREM 10. *Let u be a radially symmetric solution of initial-value problem (2.2) in a sphere with center in the origin and radius L, with smooth initial conditions which are small at infinity and total energy $E = 4\pi E_0$. Then for every $r > 0$ and t,*

$$|u(r,t)| \leq \frac{(2E_0)^{1/2}}{r}.$$

Proof. First observe that for every differentiable function $v(r,t)$,

$$0 \leq \left(\frac{\partial v}{\partial r} - v\right)^2 = \left(\frac{\partial v}{\partial r}\right)^2 - \frac{\partial (v^2)}{\partial r} + v^2.$$

Let u be a radially symmetric solution of initial-value problem (2.2), and set $v(r,t) = ru(r,t)$. The expression of the total energy of the nonlinear Klein-Gordon equation in Corollary 5 and the fact that $v(0,t) = 0$ for every t imply that

$$v^2(r,t) = \int_0^r \frac{\partial (v^2)}{\partial r}\, dr \leq \int_0^r \left\{\left(\frac{\partial v}{\partial r}\right)^2 + v^2\right\} dr \leq 2E_0.$$

for every r and t, whence the result follows. □

Needless to say that the continuous energy analysis of radially symmetric solutions of the nonlinear Klein-Gordon equation carries over to the $(1+1)$-dimensional case. Indeed, it is easy to check that the energy associated to the solutions of the

$(1+1)$-dimensional nonlinear Klein-Gordon equation is preserved throughout time. The only difference between the radially symmetric and the linear cases lies then in the fact that solutions in the former case are bounded by $(2E_0)^{1/2}/r$. In particular, this mean that the radially symmetric nonlinear Klein-Gordon equation lacks of soliton solutions for which the amplitude is preserved.

3.2.3 Discrete energy

It becomes now necessary to posses a discrete expression to compute the total energy of the system. In view of the fact that the energy of the nonlinear Klein-Gordon equation is conserved throughout time, it is highly desirable to posses a discrete expression to approximate the total energy E_n of the system in the n-th time step, such that $E_n = E_{n-1}$ for each $n \in \mathbb{N}$.

Radially symmetric solutions

For the sake of precision, let $0 = r_0 < r_1 < \cdots < r_M = a$ and $0 = t_0 < t_1 < \cdots < t_N = T$ be regular partitions of $[0, a]$ and $[0, T]$ into M and N subintervals of lengths $\Delta r = a/N$ and $\Delta t = T/M$, respectively. Let v_j^n be the value of the function v—defined in Corollary 5—at (r_j, t_n). Strauss and Vázquez [8] propose the scheme

$$\begin{aligned}\frac{E_n^0}{\Delta r} &= \frac{1}{2}\sum_{j=0}^{M-1}\left(\frac{v_j^{n+1}-v_j^n}{\Delta t}\right)^2 + \frac{1}{2}\sum_{j=0}^{M-1}\left(\frac{v_{j+1}^{n+1}-v_j^{n+1}}{\Delta r}\right)\left(\frac{v_{j+1}^n - v_j^n}{\Delta r}\right) \\ &\quad + \frac{m^2}{2}\sum_{j=0}^{M-1}\frac{(v_j^{n+1})^2 + (v_j^n)^2}{2} + \sum_{j=1}^{M-1}\frac{G(v_j^{n+1}) + G(v_j^n)}{2(j\Delta r)^{p-1}}\end{aligned}$$

to approximate the true value of E_0 in Corollary 5. We claim that this scheme has the property that energy is conserved throughout time. To prove this statement, let n and j be positive integers such that $j < M$ and $n < N$. Notice first of all that

$$\begin{aligned}(v_{j+1}^n - 2v_j^n + v_{j-1}^n)(v_j^{n+1} - v_j^{n-1}) &= -(v_{j+1}^{n+1} - v_j^{n+1})(v_{j+1}^n - v_j^n) \\ &\quad +(v_{j+1}^n - v_j^n)(v_{j+1}^{n-1} - v_j^{n-1}) \\ &\quad +(v_{j+1}^{n+1} - v_{j+1}^{n-1})(v_{j+1}^n - v_j^n) \\ &\quad -(v_j^{n+1} - v_j^{n-1})(v_j^n - v_{j-1}^n).\end{aligned} \tag{3.9}$$

Taking the sum over j from 1 to $M-1$ we notice that the last two terms in the right-hand side of Equation (3.9) form a telescoping series. Using the fact that for every nonnegative integer n the quantities v_m^n and v_0^n are both equal to zero, this telescoping series becomes

$$\sum_{j=1}^{M-1}\left[(v_{j+1}^{n+1} - v_{j+1}^{n-1})(v_{j+1}^n - v_j^n) - (v_j^{n+1} - v_j^{n-1})(v_j^n - v_{j-1}^n)\right] = -v_1^n(v_1^{n+1} - v_1^{n-1}).$$

Multiplying finite-difference equation (3.4) by $(v_j^{n+1} - v_j^{n-1})$ and simplifying,

$$\frac{(v_j^{n+1})^2 - 2v_j^n v_j^{n+1} + 2v_j^n v_j^{n-1} - (v_j^{n-1})^2}{(\Delta t)^2} - \frac{(v_{j+1}^n - 2v_j^n + v_{j-1}^n)(v_j^{n+1} - v_j^{n-1})}{(\Delta r)^2}$$
$$+\frac{m^2}{2}[(v_j^{n+1})^2 - (v_j^{n-1})^2] + \frac{1}{(j\Delta r)^{p-1}}\left[G(v_j^{n+1}) - G(v_j^{n-1})\right] = 0.$$

Next we add the terms $(v_j^n)^2$ to the numerators of the first and second terms, and $G(v_j^n)$ to the numerator of the last term in the left-hand side of this last equation. By regrouping and using Equation (3.9) we obtain

$$\begin{aligned} 0 = & \left\{ \left(\frac{v_j^{n+1} - v_j^n}{\Delta t} \right)^2 + \left(\frac{v_{j+1}^{n+1} - v_j^{n+1}}{\Delta r} \right) \left(\frac{v_{j+1}^n - v_j^n}{\Delta r} \right) + \frac{m^2}{2}\left[(v_j^{n+1})^2 + (v_j^n)^2\right] \right. \\ & \left. + \frac{G(v_j^{n+1}) + G(v_j^n)}{(j\Delta r)^{p-1}} \right\} - \left\{ \left(\frac{v_j^n - v_j^{n-1}}{\Delta t} \right)^2 + \left(\frac{v_{j+1}^n - v_j^n}{\Delta r} \right) \left(\frac{v_{j+1}^{n-1} - v_j^{n-1}}{\Delta r} \right) \right. \\ & \left. + \frac{m^2}{2}\left[(v_j^n)^2 + (v_j^{n-1})^2\right] + \frac{G(v_j^n) + G(v_j^{n-1})}{(j\Delta r)^{p-1}} \right\} \\ & - \left[\frac{(v_{j+1}^{n+1} - v_{j+1}^{n-1})(v_{j+1}^n - v_j^n)}{(\Delta r)^2} - \frac{(v_j^{n+1} - v_j^{n-1})(v_j^n - v_{j-1}^n)}{(\Delta r)^2} \right]. \end{aligned}$$

Finally, we take half of the sum over j from 1 to $M-1$ in both sides of this equation. Observe that the sum of the first four terms differs from twice the total discrete energy in the n-th time step by $v_1^n v_1^{n+1}/(\Delta r)^2$. Similarly, the sum of the next four terms differs from twice the total discrete energy in the $(n-1)$-st time step by $v_1^{n-1} v_1^n/(\Delta r)^2$. Thus it follows that

$$\left[E_n^0 - \frac{v_1^n v_1^{n+1}}{2(\Delta r)^2} \right] - \left[E_{n-1}^0 - \frac{v_1^{n-1} v_1^n}{2(\Delta r)^2} \right] + \frac{v_1^n (v_1^{n+1} - v_1^{n-1})}{2(\Delta r)^2} = 0.$$

We conclude that $E_n^0 = E_{n-1}^0$ for every $n \in \mathbb{N}$ and, in particular, $E_n^0 = E_0^0$.

The $(1+1)$-dimensional solutions

Let $a = x_0 < x_1 < \cdots < x_M = b$ and $0 = t_0 < t_1 < \cdots < t_N = T$ be regular partitions of $[0, a]$ and $[0, T]$ into M and N subintervals of lengths $\Delta x = (b-a)/N$ and $\Delta t = T/M$, respectively. Let u_j^n be the value of the solution u of (3.5) at (r_j, t_n).

The discrete energy is given by

$$\begin{aligned}\frac{E_n}{\Delta x} &= \frac{1}{2}\sum_{j=0}^{M-1}\left(\frac{u_j^{n+1}-u_j^n}{\Delta t}\right)^2+\frac{1}{2}\sum_{j=0}^{M-1}\left(\frac{u_{j+1}^{n+1}-u_j^{n+1}}{\Delta x}\right)\left(\frac{u_{j+1}^n-u_j^n}{\Delta x}\right)\\ &\pm\frac{m^2}{2}\sum_{j=0}^{M-1}\frac{(u_j^{n+1})^2+(u_j^n)^2}{2}+\sum_{j=1}^{M-1}\frac{G(u_j^{n+1})+G(u_j^n)}{2}\end{aligned}$$

This numeric scheme is consistent with the one-dimensional energy equation in Corollary 4, and has the property that energy is conserved throughout time.

3.3 Numerical computations

Throughout this section we approximate radially symmetric solutions of the nonlinear Klein-Gordon equation with $m^2 = 1$ and $G'(u) = u^p$, for $p > 1$ and odd number.

3.3.1 Results

Let $p = 7$ and let the space and time steps be $\Delta r = \Delta t = 0.002$. As initial data we choose $\phi(r) = h(r)$ and $\psi(r) = h'(r) + h(r)/r$, where

$$h(r) = \begin{cases} 5\exp\left\{100\left[1-\dfrac{1}{1-(10r-1)^2}\right]\right\}, & \text{if } 0 \le r < 0.2\\ 0, & \text{if } 0.2 \le r \le 0.4.\end{cases}$$

The results at successive time intervals $t = 0, 0.04, 0.08, 0.12, 0.16, 0.2$—depicted in Figure 3.2—are in agreement with Strauss and Vázquez [8]. The total energy is effectively conserved and equal to 67.85. Graphically, the initial data immediately break up into an incoming part (moving toward the origin) and an outgoing part (moving away from the origin). The incoming part resolves into oscillations. By time $t = 0.16$, the incoming part does not produce new oscillations and all the existing ones have already been reflected away from the origin; all the oscillations from this time on move at the same speed (which appears to be equal to one). We notice that the solutions are bounded at all time, which is in agreement with [6]. Moreover, it appears that $\max_{r\in[0,0.4]} |u(r,t)|$ is a decreasing function of time for values of $t > 0.16$.

	$G'(u)$					
	0	u^3	u^5	u^7	u^9	$\sinh(5u)-5u$
$\max_{(r,t)} \lvert u(r,t)\rvert$	49.98	47.59	19.09	9.74	6.56	3.72

TABLE 3.1: Maximum amplitudes over space and time of solutions of the nonlinear Klein-Gordon equation for six nonlinear terms $G'(u)$.

We wish to study now the effect of the nonlinear term. We approximated solutions at time $t = 0.2$ for the initial data $\phi(r) = 0$ and $\psi(r) = 100h(r)$, and

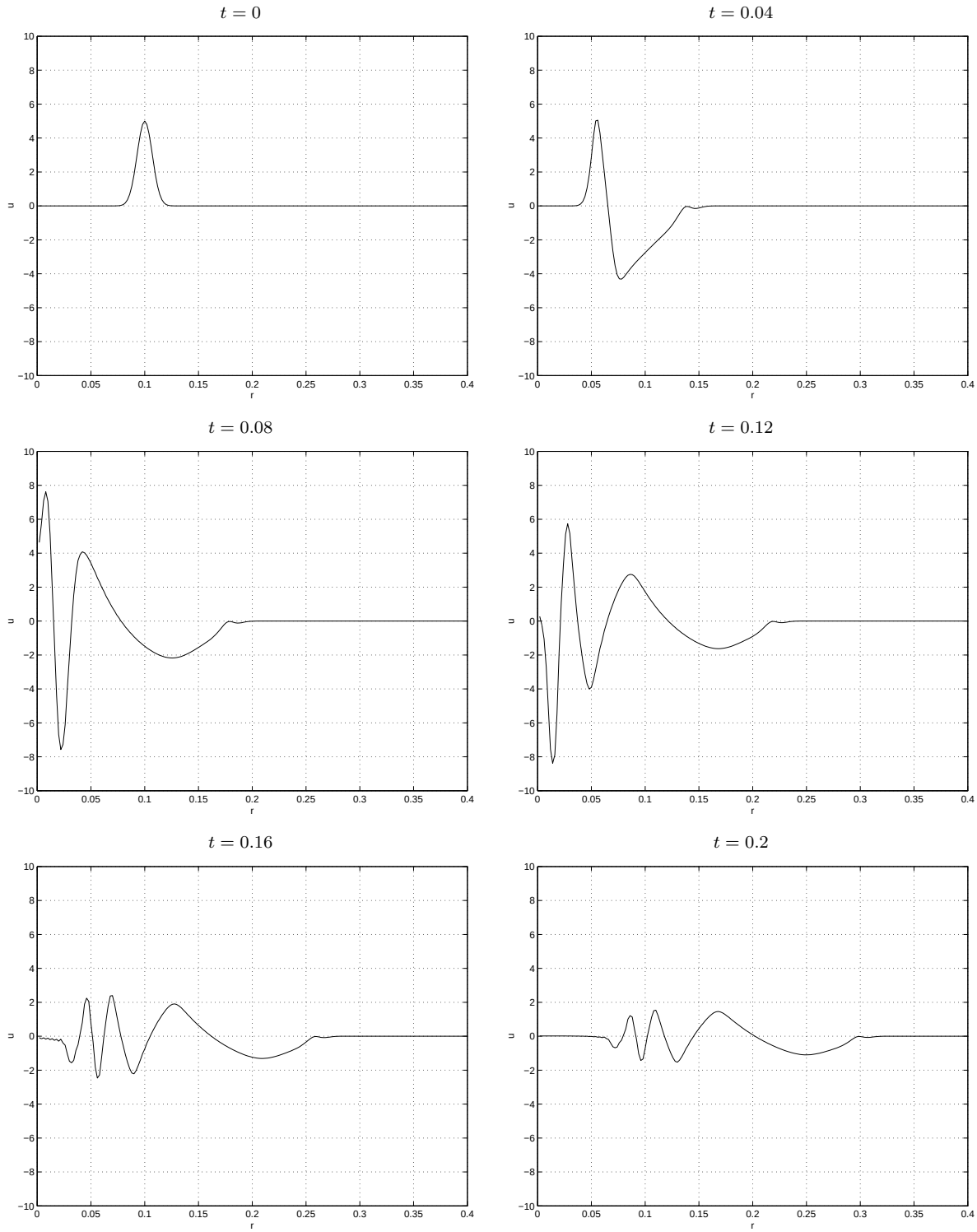

FIGURE 3.2: Approximate radial solutions at successive times of the nonlinear Klein-Gordon equation with $G'(u) = u^7$, initial data $\phi(r) = h(r)$, $\psi(r) = h'(r) + h(r)/r$, and boundary condition $u(0.4, t) = 0$.

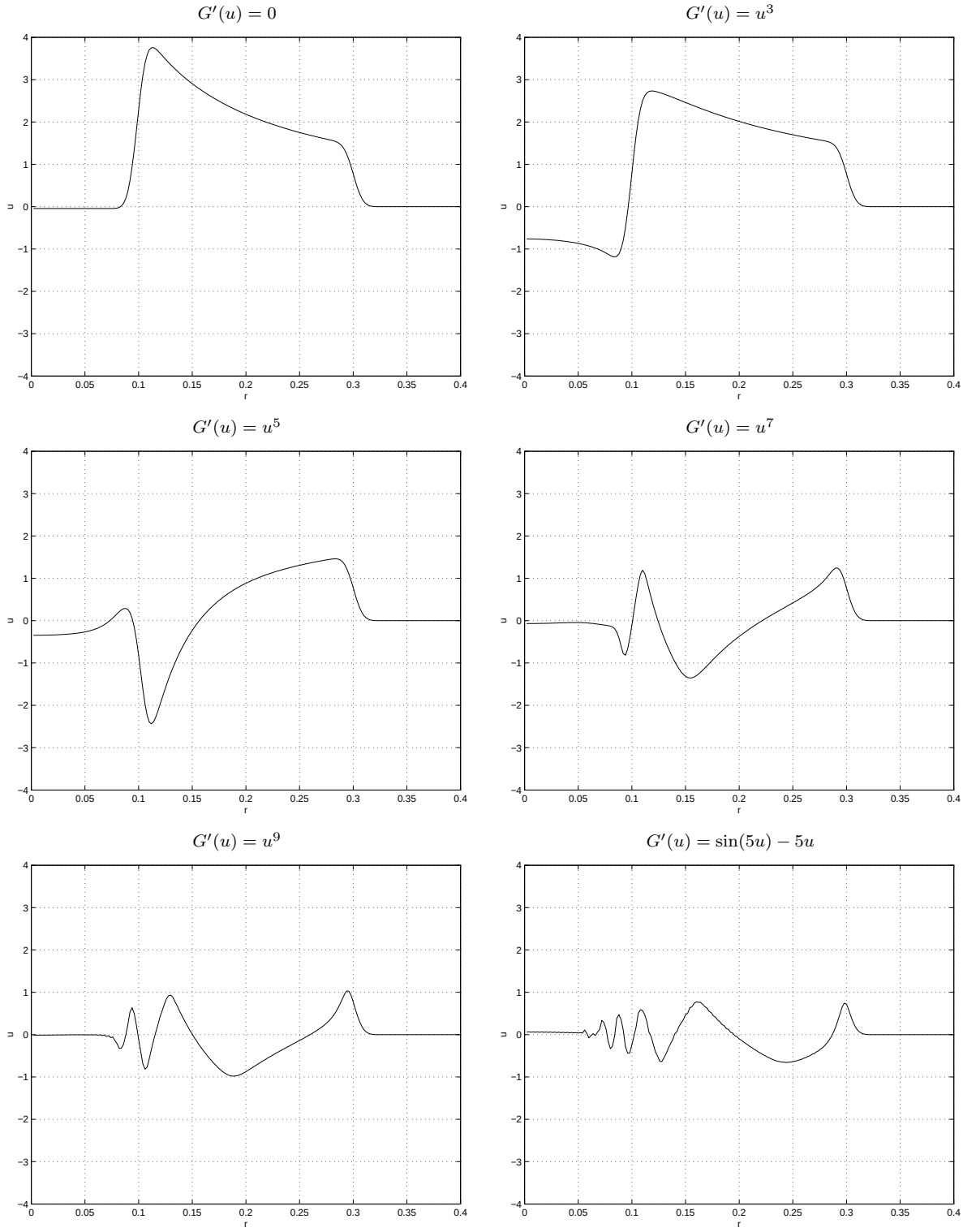

FIGURE 3.3: Approximate radial solutions for the given function $G'(u)$ at time $t = 0.2$ for initial data $\phi(r) = 0$ and $\psi(r) = 100h(r)$, and boundary condition $u(0.4, t) = 0$.

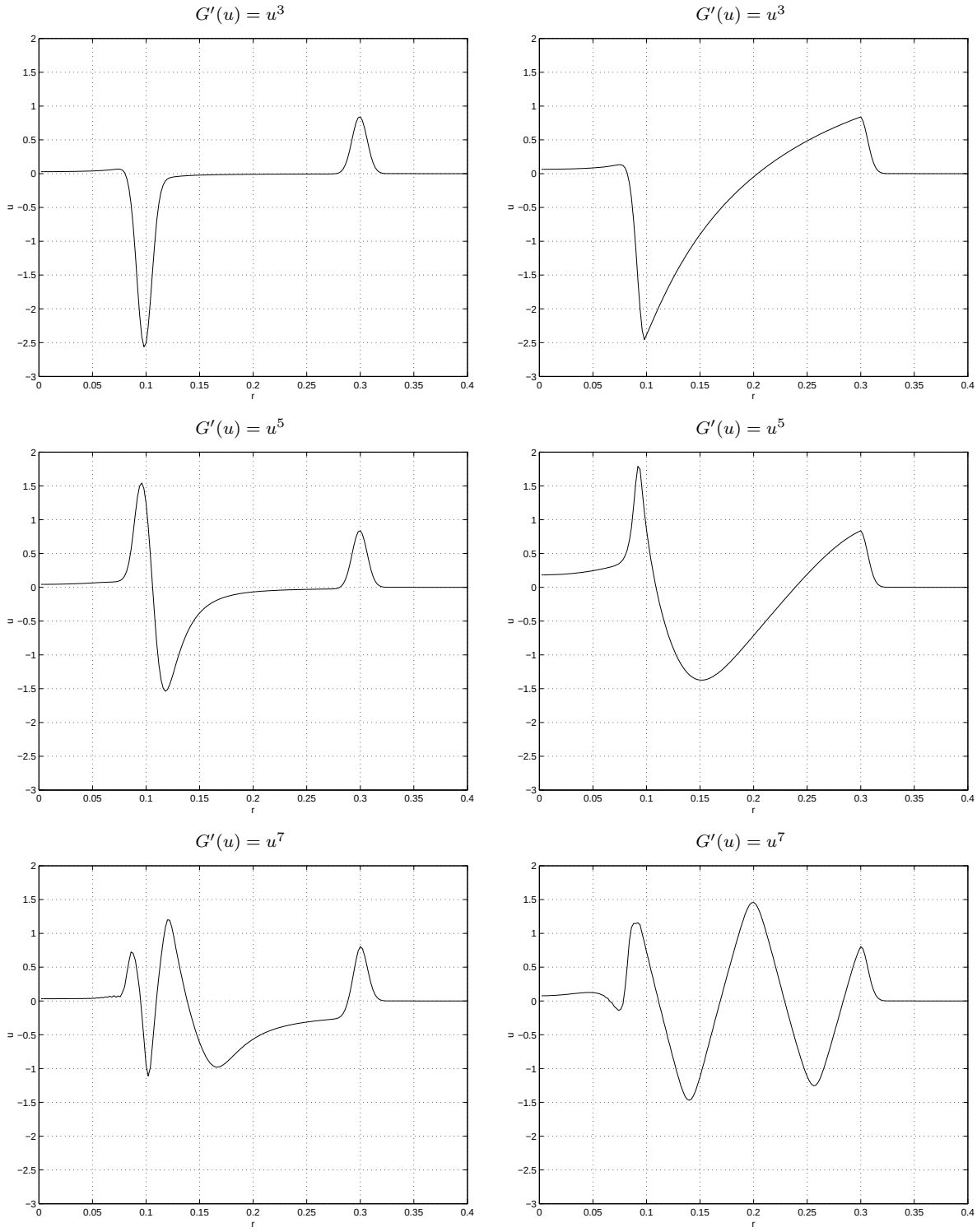

FIGURE 3.4: Approximate radial solutions for the given function $G'(u)$ at time $t = 0.2$ for initial data $\phi(r) = h(r)$, $\psi(r) = 0$ on the left column, and initial conditions (3.10) on the right column.

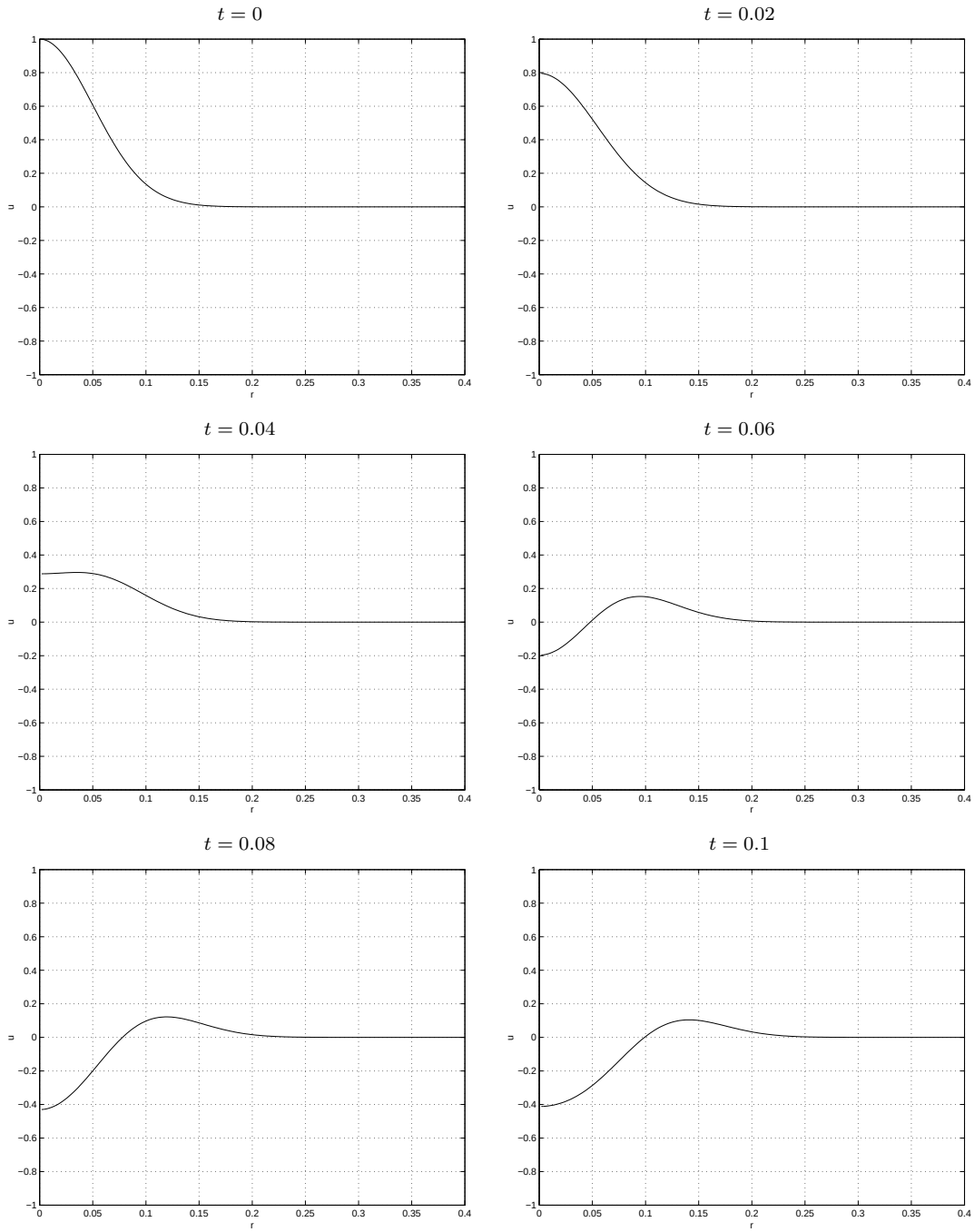

FIGURE 3.5: Approximate radial solutions for the nonlinear term $G'(u) = u^3$ at successive times, for $\beta = 0$, $\gamma = 0$, and initial data $\phi(r) = e^{-200r^2}$ and $\psi(r) = 0$.

six different equations: $G'(u) = 0, u^3, u^5, u^7, u^9$, and $\sinh(5u) - 5u$. The results are shown in Figure 3.3 for $\Delta r = \Delta t = 0.002$. We observe that the amplitude of the curves seems to decrease as the degree of $G'(u)$ increases. Indeed, our computations show that the maximum amplitude decreases with respect to the exponent as Table 3.1 shows. The energy for all powers is equal to 31.294; for the last case the energy equals 31.317.

Next we computed solutions to the nonlinear Klein-Gordon equation at time $t = 0.2$ for the initial data $\phi(r) = h(r)$ and $\psi(r) = 0$, and for $p = 3, 5, 7$. The results are printed in the left column of Figure 3.4; the right column shows the solutions of the nonlinear Klein-Gordon equation at the same time and nonlinear term similar to the corresponding graph to the left, for initial data

$$\phi(r) = \begin{cases} 5, & \text{for } 0 \leq r \leq 0.1 \\ h(r), & \text{for } 0.1 < r \leq 0.4 \end{cases} \qquad \text{and} \qquad \psi(r) = 0. \tag{3.10}$$

As before, we verify that the number of oscillations increases with the exponent p of the nonlinear term. Similarly, the amplitude over space and time decreases as the degree of the nonlinear term increases. For each case the energy is conserved; however, the values of the total energy are different for the six cases presented in Figure 3.4.

Next we wish to verify that our method runs for a bump-like initial condition in the origin. We have computed approximate radially symmetric solutions for the initial data $\phi(r) = e^{-200r^2}$ and $\psi(r) = 0$, $G'(w) = w^3$, and parameters $\Delta t = \Delta r = 0.002$. The solutions (depicted in Figure 3.5) show that the derivative with respect to r at the origin is approximately equal to 0. This will be in agreement with that property of our more general numerical method for non-zero internal and external damping that solutions at the origin will be smooth throughout time provided that the initial conditions grant smooth initial approximations at the origin.

We finally wish to mention that we have computed solutions of the nonlinear Klein-Gordon equation with nonlinear term given by $G'(u) = u^2, u^4, u^6$ and we found out that their graphs blow out in finite time. This is in agreement with [5].

3.3.2 Discussion

Our numerical analysis of the nonlinear Klein-Gordon equation induces us to conclude that for a fixed nonlinear term and initial data, the total energy is conserved throughout time. Moreover, for any initial data the equation immediately breaks up into an *incoming part* and an *outgoing part*. The incoming part moves toward the origin while the outgoing moves away from it. The incoming part resolves in oscillations and is reflected away at the origin. From certain time on (about $t = 0.16$ in our experiments) the incoming part does not produce new oscillations and all the oscillations move away from the origin at the same speed.

The number of final oscillations in the solutions increases with the exponent p of the nonlinear term, and the amplitude of the curves over space and time seems to decrease as p increases. Similarly, for a fixed value of p the amplitude of the solution decreases as time increases.

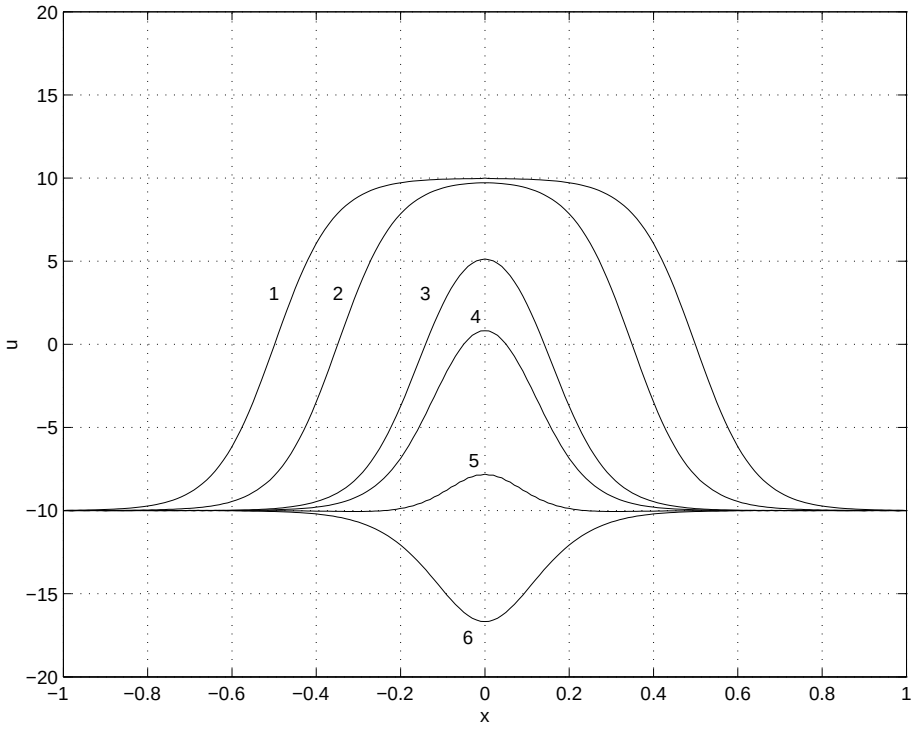

FIGURE 3.6: Approximate solutions of the Landau-Grinzburg equation at successive times.

3.4 Applications

In this section we present previously reported applications of our numerical method to solutions of differential equations that appear in nuclear physics, superstring theory, substring theory, and Josephson junctions. More applications can be found in areas such as stochastic resonances [45] and hydrodynamics.

3.4.1 Nuclear physics

The Landau-Ginzburg equation is used for the construction of the theory of Ψ bosons on the basis of coherent field states [46], in the study of magnetic properties of ferromagnets [47], and even in the study of brain dynamics [48]. In its nondimensional $(1+1)$-dimensional version, the Landau-Ginzburg equation with real parameters m, λ and $G'(u) = u^3$ has a soliton solution of the form

$$u(x,t) = \frac{m}{\sqrt{\lambda}} \tanh\left(\frac{m(x - x_0 - vt)}{\sqrt{2(1-v^2)}}\right)$$

for every x_0 and $|v| < 1$. We examine the interaction of two soliton solutions of this type when the initial velocity v at which the solitons approach each other is assumed to be equal to 0.1 (much smaller than the speed of light $c = 1$). We take the boundary conditions equal to the vacuum value $u_- = -m/\sqrt{\lambda}$, and initial condition

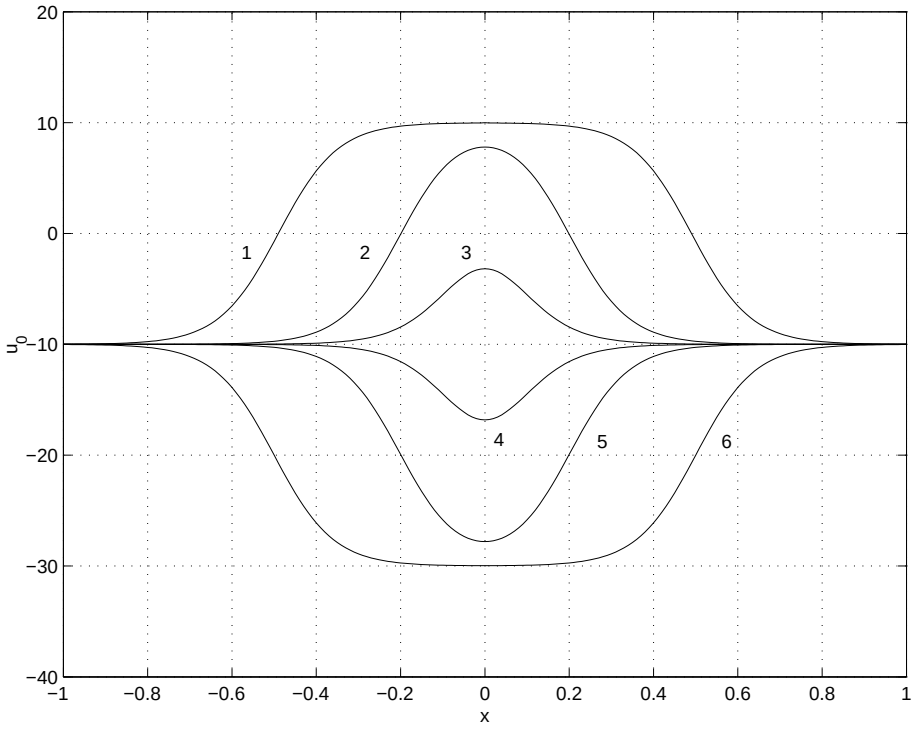

FIGURE 3.7: Exact value of the superposition $u_0(x,t)$ of two soliton solution of the Landau-Grinzburg equation and the vacuum value u_- versus x at six consecutive times.

$$u(x,0) = \frac{m}{\sqrt{\lambda}}\left[\tanh\left(\frac{m(x+x_0)}{\sqrt{2(1-v^2)}}\right) + \tanh\left(\frac{m(-x+x_0)}{\sqrt{2(1-v^2)}}\right) - 1\right]. \tag{3.11}$$

Figure 3.6 shows solutions of the Landau-Ginzburg equation at successive times for the given initial condition, and values $m = 10$, $v = 0.1$, $x_0 = 0.5$, $\lambda = 1$. After the solitons come closer together large oscillations take place in the neighborhood of the origin; the numbers indicate the time-ordered solutions $u(x,t_i)$ for $i = 1,\ldots,6$, after which the plot 5, 4, 3, 4, 5, 6 are repeated again and again. Figure 3.8 shows the time dependence of the value of the solution u at the origin. Both graphs are in agreement with [46].

The fusion of the two solitons in this mixed-value problem can be explained in the following way: Suppose that the exact solution at any time has the form $u(x,t) = u_0(x,t) + w(x,t)$, where u_0 represents the superposition of the two solitons and the vacuum value, and $w(x,t) \ll u_0(x,t)$ for every x and t (this assumption is justified by virtue of Figure 3.9). Then v and g satisfy

$$\frac{\partial^2 w}{\partial t^2} - \frac{\partial^2 w}{\partial x^2} - m^2 w + \lambda\left[3v^2 w + 3vw^2 + w^3\right] = -\frac{\partial^2 u_0}{\partial t^2} + \frac{\partial^2 u_0}{\partial x^2} + m^2 u_0 - \lambda u_0^3.$$

The right-hand side of this equation—which we will denote by $Q(x,t)$—represents the source of the field. Doing now a linear approximation for the function f we obtain

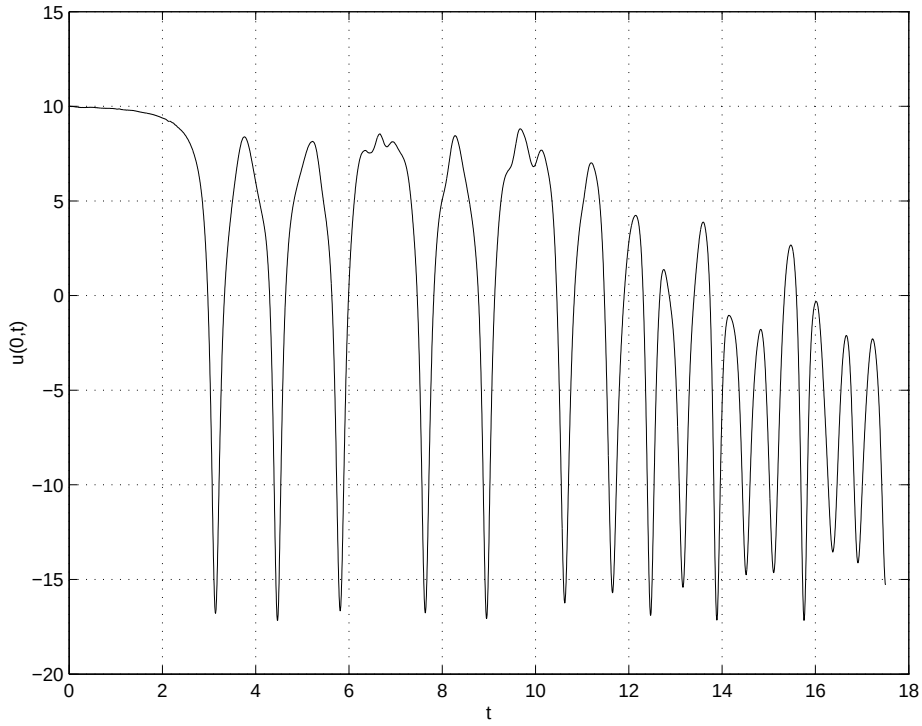

FIGURE 3.8: Graph of the value of the solution u of the Landau-Grinzburg equation at the origin at time t vs. time.

$$\frac{\partial^2 w}{\partial t^2} - \frac{\partial^2 w}{\partial x^2} + \left(3\lambda v^2 - m^2\right) w = Q(x,t).$$

It is a tedious but simple calculus task to prove that the source function $Q(x,t)$ attains an absolute maximum at $x = 0$, for each real number t. In order to compute the actual value of the source of the field at the origin observe that the function u_0 can be expressed then as

$$u_0(x,t) = \frac{m}{\sqrt{\lambda}} \left[\tanh \left[\frac{m(x + x_0 - vt)}{\sqrt{2(1-v^2)}} \right] + \tanh \left[\frac{m(-x + x_0 - vt)}{\sqrt{2(1-v^2)}} \right] - 1 \right]$$

It is easy to verify then that the following relations hold:

$$\begin{aligned}
\frac{\partial^2 u_0}{\partial t^2}(0,t) &= \frac{2m^3v^2}{\sqrt{\lambda}(1-v^2)}\ \operatorname{sech}^2\left[\frac{m(x_0-vt)}{\sqrt{2(1-v^2)}}\right]\tanh\left[\frac{m(x_0-vt)}{\sqrt{2(1-v^2)}}\right], \\
\frac{\partial^2 u_0}{\partial x^2}(0,t) &= \frac{2m^3}{\sqrt{\lambda}(1-v^2)}\ \operatorname{sech}^2\left[\frac{m(x_0-vt)}{\sqrt{2(1-v^2)}}\right]\tanh\left[\frac{m(x_0-vt)}{\sqrt{2(1-v^2)}}\right], \\
m^2u_0(0,t) &= \frac{m^3}{\sqrt{\lambda}}\left\{2\tanh\left[\frac{m(x_0-vt)}{\sqrt{2(1-v^2)}}\right]-1\right\}, \qquad \text{and} \\
\lambda u_0^3(0,t) &= \frac{m^3}{\sqrt{\lambda}}\left\{8\tanh^3\left[\frac{m(x_0-vt)}{\sqrt{2(1-v^2)}}\right]-12\tanh^2\left[\frac{m(x_0-vt)}{\sqrt{2(1-v^2)}}\right]\right. \\
&\qquad \left.+6\tanh\left[\frac{m(x_0-vt)}{\sqrt{2(1-v^2)}}\right]-1\right\}
\end{aligned}$$

For any time t, the value of the source at the origin is given by

$$Q(0,t) = -\frac{6m^3}{\sqrt{\lambda}}y(1-y)^2,$$

where $y = \tanh[(x_0 - vt)/\sqrt{2(1-v^2)}]$. The radiation at the origin vanishes when the distance between the solitons is large (in which case y is close to 1), and also when it is zero (in which case y needs to be equal to 0). The value of $Q(0,t)$ increases as the solitons come closer together. So the amplitude f of the waves increases with time.

Let us now consider the energy analysis of the approximate solution $u_0(x,t)$. Using the assumption that $f(x,t)$ is comparatively much smaller that $u_0(x,t)$ and in view of the fact that the Hamiltonian $\mathcal{H}$ associated with a solution u of the Landau-Ginzburg equation is conserved, then $\mathcal{H}$ of u_0 is also approximately conserved and the expression for the potential energy is

$$V(x_0) = \int_{-\infty}^{+\infty}\left\{\frac{1}{2}\left(\frac{\partial^2 u_0}{\partial x^2}\right) - \frac{m^2}{2}u_0^2 + \frac{\lambda}{4}u_0^4\right\}\ dx$$

A graph depicting the approximate value of the potential energy with respect to that of the vacuum value u_- of two solitons satisfying the Landau-Ginzburg equation and separated a distance $2x_0$ is shown in Figure 3.9, for values of $m = 10$, $v = 0.1$ and $\lambda = 1$. Here M_c represents the mass of each soliton, that is $(M_c = 2\sqrt{2}/3)m^3/\lambda)$. Notice that for large distances between the solitons—that is, when there is small interaction between the solitons—, the value of the potential energy is asymptotically equal to the sum of the masses of the solitons. When the solitons touch the potential energy is equal to zero; in other words, the value $V(0)$ coincides with the potential energy of the vacuum. Finally, for negative values of x_0, the function $V(x_0)$ is linear.

It is clear from this that there are two kind of motions when radiation is neglected: Infinite for energies exceeding $2M_c$, and finite in a well at lower energies. However, if radiation is permitted then the associated with u_0 is not conserved any

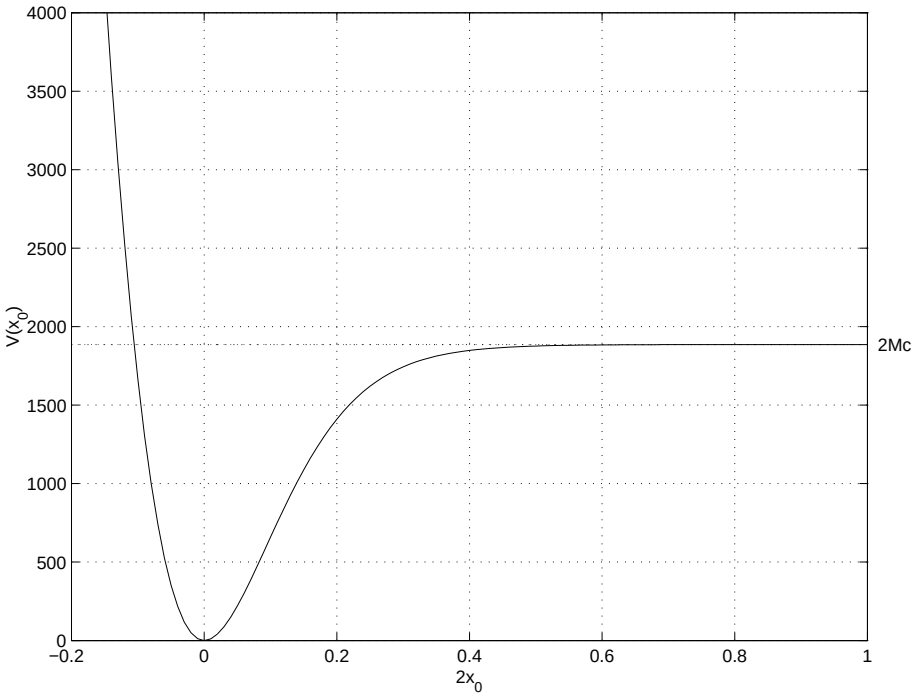

FIGURE 3.9: Potential energy of two solitons satisfying the Landau-Ginzburg equation, separated by a distance $2x_0$ (solid line) and the sum of its masses $2M_c$.

more; instead it decreases slowly and the solitons fuse as they interact with each other.

The coalescence of solitons associated to the Landau-Ginzburg equations is observable at low initial energies. For high initial velocities of the solitons the fusion process does not take place. In fact, we have observed that the solitons repel each other after interacting, loosing part of their energy due to radiation. It is worthwhile to remark once more that all our results are in agreement with [46].

Finally, in view of the apparent even symmetry of the approximate solutions to the Landau-Ginzburg equation shown in Figure 3.6, we have approximated radially symmetric solutions of the $(2 + 1)$-dimensional Landau-Ginzburg equation on the interval $[0, 1]$ at six succesive times, using $m = 10$, $v = 0.1$, $r_0 = 0.5$, $\lambda = 1$, the initial condition

$$u(r, \theta, 0) = \frac{m}{\sqrt{\lambda}} \left[\tanh\left(\frac{m(r + r_0)}{\sqrt{2(1 - v^2)}} \right) + \tanh\left(\frac{m(-r + r_0)}{\sqrt{2(1 - v^2)}} \right) - 1 \right], \quad \text{for } 0 \leq r \leq 1$$

and boundary conditions $u_r(0, t) = 0$ and $u(1, t) = 0$ for every t. The solition and its antisoliton are set to approaches the origin with an initial speed of 0.1. Needles to say that, as we expected, the oscillating behavior of solutions at the origin is observed also in the $(2 + 1)$-dimensional case (see Figure 3.10).

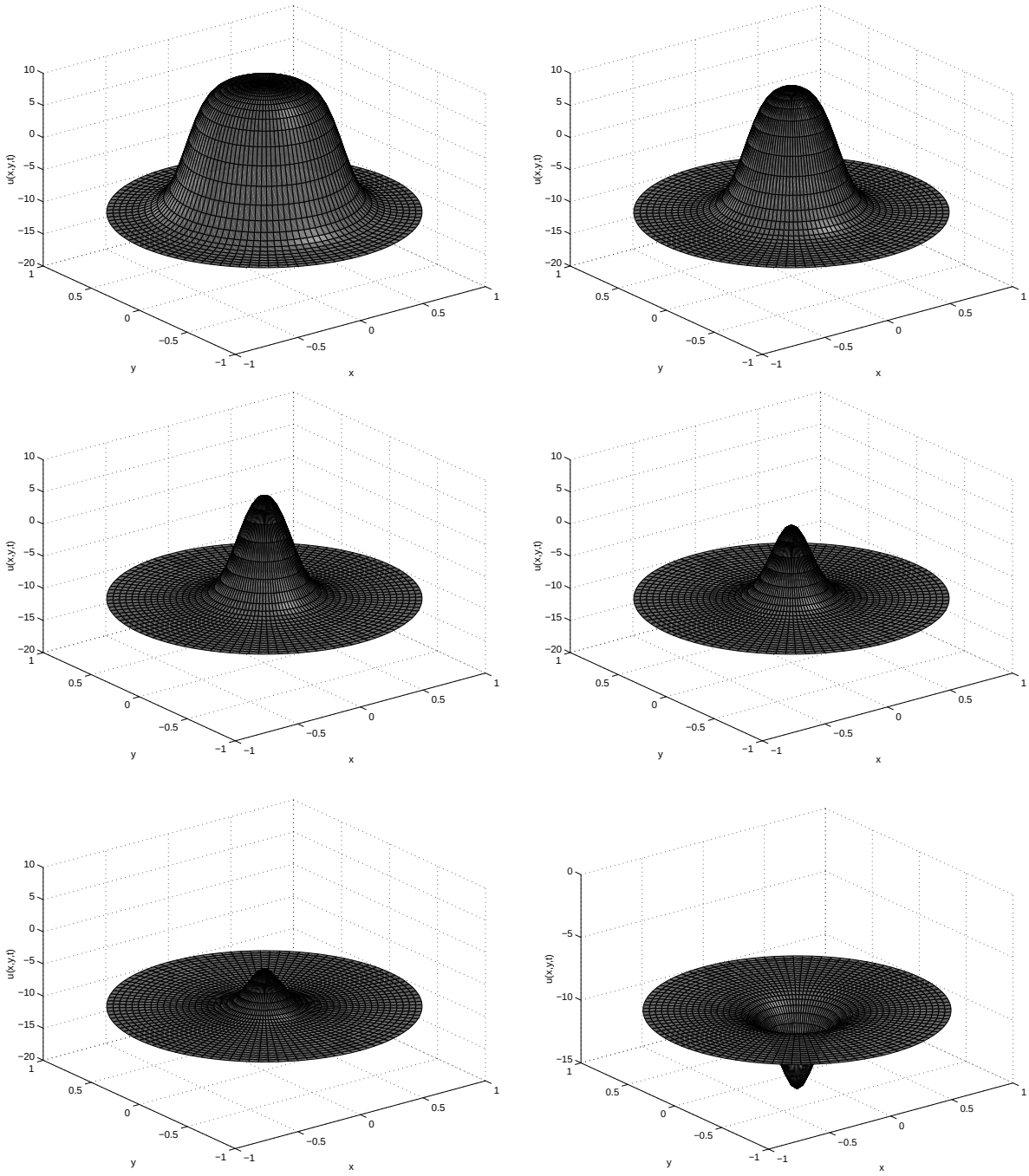

FIGURE 3.10: Approximate solutions of the $(2+1)$-dimensional Landau-Ginzburg at six succesive times.

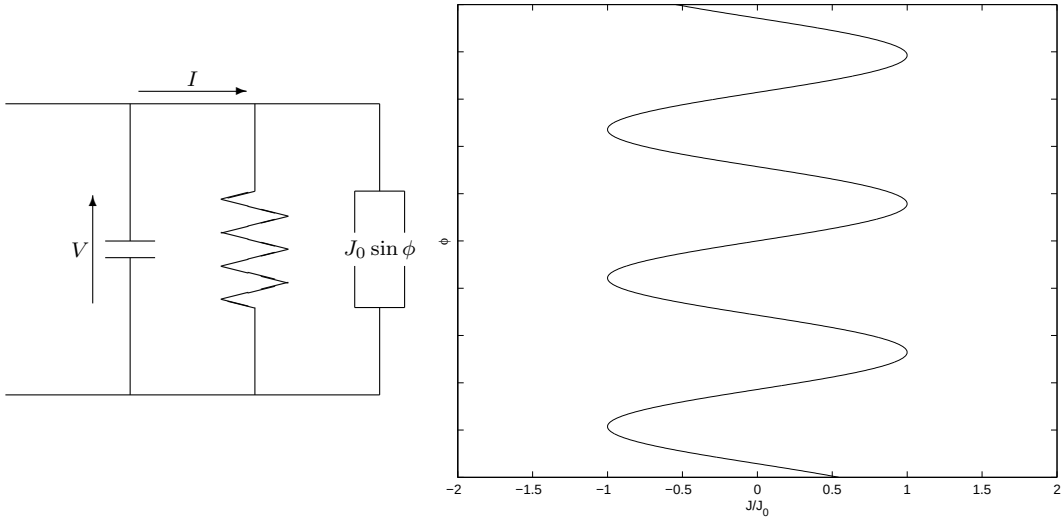

FIGURE 3.11: (a) Schematic representation of the electrical equivalent of a short Josephson junction, and (b) Representation of the nonlinear relationship between ϕ and J/J_0.

3.4.2 Superconductivity

The sine-Gordon equation appears in the study of superconductivity of long Josephson junctions where no dissipative processes take place. To understand how the sine-Gordon equation appears in the study of Josephson junctions, we use Feynman's approach to understand the phenomenon [49].

Small Josephson junction

Let J be the superconducting current in a small Josephson junction, and let V denote its voltage. We readily observe that the electrical behavior of the junction has the one of a nonlinear inductor in parallel with a capacitance and a resistance (see Figure 3.11a). The magnetic flux is then defined by the equation

$$\frac{\partial \Phi}{\partial t}(x,t) = V(x,t),$$

and the quantum phase common to all Cooper pairs is given by $\phi = 2\pi\Phi/\Phi_0$, where $\Phi_0 = 2.064 \times 10^{-15}$Wb is the quantum flux. One finds out that $J = J_0 \sin\phi$ and that $\phi_t = V/\Phi_0$, whence it follows that

$$\Phi = \frac{\Phi_0}{2\pi} \arcsin\left(\frac{J}{J_0}\right).$$

It is worthwhile noticing that if a constant voltage V_0 is applied, then the quantum phase common to all the Cooper pairs is given by $\phi = \phi_0 + V_0 t/\Phi_0$. The phase varies with time and an alternating current appears in the junction with with density $J = J_0 \sin(\phi_0 + V_0 t/\Phi_0)$. This phenomenon is called the **ac Josephson effect**.

Long Josephson junction

As we mentioned in Chapter 4, a long Josephson junction consists of two long and identical superconducting strips of small width a, separated by a thin dielectric of thickness d. When we regard this junction as a transmission line, its capacitance and inductance will be given by $C = \epsilon_r \epsilon_0 a/d$ and $\ell = \mu_0(2\lambda_L + d)/a$. Here λ_L denotes the London penetration depth, which gives a measure of the field penetration into the superconducting electrodes.

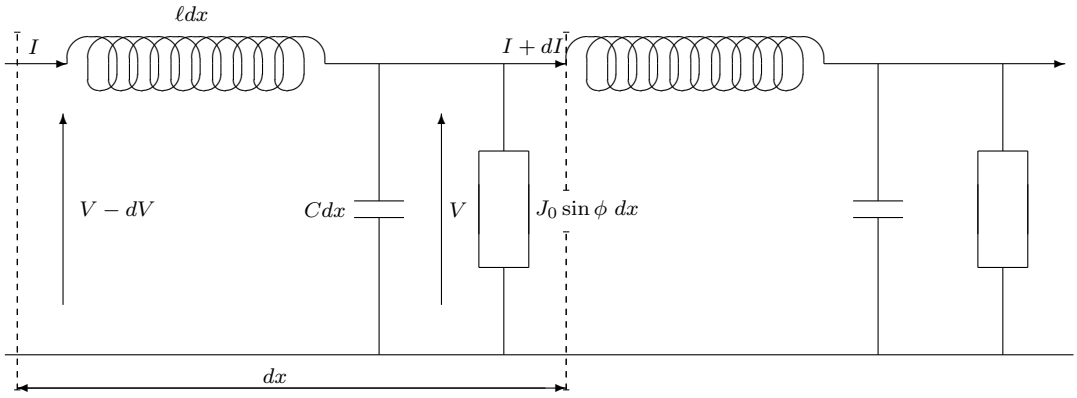

FIGURE 3.12: Schematic representation of the electrical equivalent of the non-dissipative Josephson transmission line.

Ignoring the dissipative effects, the electrical transmission line corresponding to the long Josephson junction is sketched in Figure 3.12. The differential equations governing the electrodynamics of this system are $V_x = -\ell I_t$ and $\Phi_t = V$, where I is the series current. Combining these two equations, we obtain the following expression for the flux

$$\frac{\partial^2 \Phi}{\partial x^2} - \ell C \frac{\partial^2 \Phi}{\partial t^2} = \ell J_0 \sin\left(\frac{2\pi\Phi}{\Phi_0}\right).$$

We introduce the **Swihart velocity** [50] and the **Josephson plasma frequency**, $c_J = (\ell C)^{-1/2}$ and $\omega_J = (2\pi J_0 \Phi_0^{-1} C^{-1})^{1/2}$, respectively. In terms of the quantum phase and the dimensionless variables $X = \omega_J x/c_J$ and $T = \omega_J t$, the differential equation governing the system is

$$\frac{\partial^2 \phi}{\partial T^2} - \frac{\partial^2 \phi}{\partial X^2} + \sin\phi = 0,$$

which possesses exact solutions of soliton form. In fact, for $|v| < 1$

$$\begin{aligned}
\phi(X,T) &= 4\arctan\left[\exp\left(\frac{X - X_0 - vT}{\sqrt{1-v^2}}\right)\right], \\
V(X,T) &= -\frac{2v}{\sqrt{1-v^2}}\ \mathrm{sech}\left(\frac{X - X_0 - vT}{\sqrt{1-v^2}}\right), \qquad \text{and} \\
I(X,T) &= -\frac{2}{\ell\sqrt{1-v^2}}\ \mathrm{sech}\left(\frac{X - X_0 - vT}{\sqrt{1-v^2}}\right).
\end{aligned}$$

Figure 3.13 shows the approximate time-evolution of solutions to and voltage of the sine-Gordon equation in normalized variables (dimensionless form), with initial

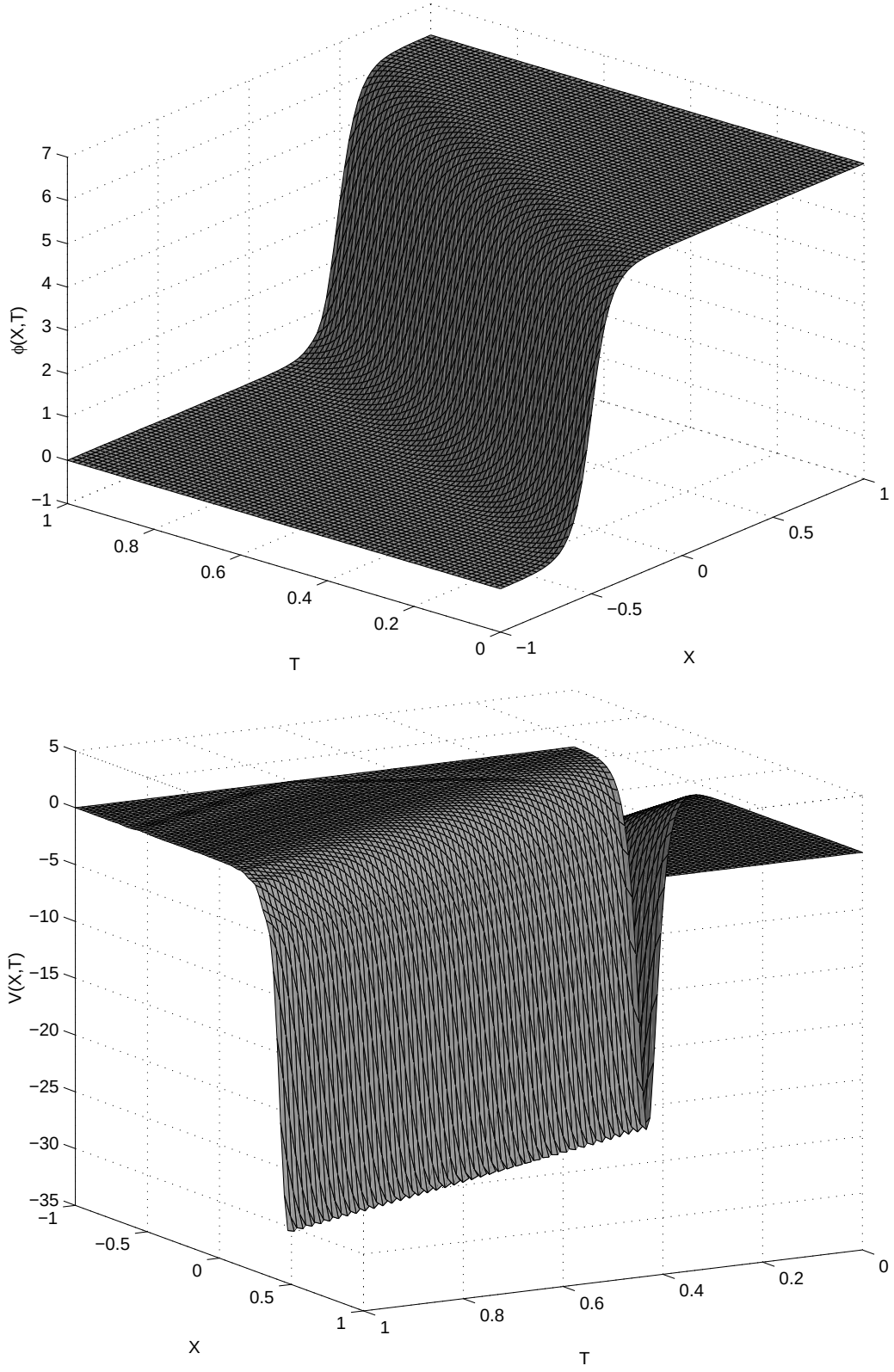

FIGURE 3.13: Quantum phase ϕ and the corresponding voltage V of a fluxon satisfying the sine-Gordon equation in dimensionless coordinates.

velocity $v = 0.998$, $X_0 = -0.5$, initial condition given by $\phi(X, 0)$, and solutions kept constant at infinity. Needless to say that the approximate solutions practically coincide with the exact solution $\phi(X, T)$.

Chapter 4

A numerical method for computing radially symmetric solutions of a dissipative nonlinear modified Klein-Gordon equation

In this paper we develop a finite-difference scheme to approximate radially symmetric solutions of the initial-value problem with smooth initial conditions

$$\frac{\partial^2 w}{\partial t^2} - \nabla^2 w - \beta \frac{\partial}{\partial t}\left(\nabla^2 w\right) + \gamma \frac{\partial w}{\partial t} + m^2 w + G'(w) = 0$$
$$\text{subject to :} \quad \begin{cases} w(\bar{x},0) = \phi(\bar{x}), & \bar{x} \in D \\ \dfrac{\partial w}{\partial t}(\bar{x},0) = \psi(\bar{x}), & \bar{x} \in D \end{cases} \tag{4.1}$$

in an open sphere D around the origin, where the internal and external damping coefficients—β and γ, respectively—are constant, and the nonlinear term has the form $G'(w) = w^p$, with $p > 1$ an odd number. The functions ϕ and ψ are radially symmetric in D, and ϕ, ψ, $r\phi$ and $r\psi$ are assumed to be small at infinity. We prove that our scheme is consistent order $\mathcal{O}(\Delta t^2) + \mathcal{O}(\Delta r^2)$ for G' identically equal to zero, and provide a necessary condition for it to be stable order n. Part of our study will be devoted to compare the physical effects of β and γ.

4.1 Introduction

Klein-Gordon-like equations appear in several branches of modern physics. A modified sine-Gordon equation appears for instance in the study of long Josephson junctions between superconductors when dissipative effects are taken into account [1]. A similar partial differential equation with different nonlinear term appears in the study of fluxons in Josephson tramsmission lines [2]. A modified Klein-Gordon equation appears in the statistical mechanics of nonlinear coherent structures such as solitary waves in the form of a Langevin equation (see [3] pp. 298–309); here no internal damping coefficient appears, though. Finally, our differential equation describes the motion of a damped string in a non-Hookean medium.

The classical $(1+1)$-dimensional linear Klein-Gordon equation has an exact soliton-like solution in the form of a traveling wave [4]. Some results concerning the analytic behavior of solutions of nonlinear Klein-Gordon equations have been established [5, 6, 7]; however, no exact method of solution is known for arbitrary initial-value problems involving this equation. From that point of view it is important to investigate numerical techniques to describe the evolution of radially symmetric solutions of (4.1).

It is worth mentioning that some numerical research has been done in this direction. Strauss and Vázquez [8] developed a finite-difference scheme to approximate radially symmetric solutions of the nonlinear Klein-Gordon equation for the same nonlinear term we study in this paper; one of the most important features of their numerical method was that the discrete energy associated with the differential equation is conserved. The numerical study of the sine-Gordon model that describes the Josephson tunnel junctions has been undertaken by Lomdahl *et al.* [2]. Numerical simulations have also been performed to solve the $(1+1)$-dimensional Langevin equation [9].

In this paper we extend Strauss and Vázquez's technique to include the effects of both internal and external damping, and validate our results against those in [8]. Section 4.2 is devoted to setting up the finite-difference scheme; the energy analysis of our problem is also carried out. Numerical results are presented in Section 4.3, followed by a brief discussion.

4.2 Analysis

4.2.1 Analytical results

The following is the major theoretic result we will use in our investigation. Here $M(t)$ represents the amplitude of a solution of (4.1) at time t, that is

$$M(t) = \max_x |w(x,t)|.$$

THEOREM 1. *Let β and γ be both equal to zero, and let $G'(w) = |w|^{p-1}w$. Suppose that ϕ and ψ are smooth and small at infinity. Then*

(1) *If $p < 5$, a unique smooth solution of* (4.1) *exists with amplitude bounded at all time* [6].

(2) *If $p \geq 5$, a weak solution exists for all time* [26].

(3) *For $p > 8/3$ and for solutions of bounded amplitude, there is a scattering theory; in particular, they decay uniformly as fast as $M(t) \leq c(1+|t|)^{-3/2}$* [27]. □

4.2.2 Finite-difference scheme

Throughout this section we will assume that the functions $\phi(\bar{x})$ and $\psi(\bar{x})$ are smooth, of compact support, radially symmetric in the open sphere D with center

in the origin and radius L, and that ϕ, ψ, $r\phi$ and $r\psi$ are small at infinity in D. Moreover, we will suppose that $w(\bar{x},t)$ is a radially symmetric solution of (4.1).

Let $r = ||\bar{x}||$ be the Euclidean norm of $\bar{x}$ and let $G'(w) = w^p$, for $p > 1$ an odd number. Setting $v(r,t) = rw(r,t)$ for every $0 < r < L$ and $t \in \mathbb{R}$, it is evident that v must satisfy the mixed-value problem

$$\begin{aligned} \frac{\partial^2 v}{\partial t^2} - \frac{\partial^2 v}{\partial r^2} + \gamma\frac{\partial v}{\partial t} - \beta\frac{\partial^3 v}{\partial t\,\partial r^2} + m^2 v + rG'\left(\frac{v}{r}\right) &= 0, \\ \text{subject to : } \begin{cases} v(r,0) = r\phi(r), & 0 < r < L, \\ \dfrac{\partial v}{\partial t}(r,0) = r\psi(r), & 0 < r < L, \\ v(0,t) = 0, & t \geq 0. \end{cases} \end{aligned} \tag{4.2}$$

Proceeding now to discretize our problem, let $a < L$ be a positive number with the property that ϕ and ψ vanish outside of the sphere with center in the origin and radius $a - \epsilon$, for some $\epsilon > 0$. Let $0 = r_0 < r_1 < \cdots < r_M = a$ and $0 = t_0 < t_1 < \cdots < t_N = T$ be partitions of $[0,a]$ and $[0,T]$, respectively, into M and N subintervals of lengths $\Delta r = a/M$ and $\Delta t = T/N$, respectively. Denote the approximate value of $v(r_j, t_n)$ by v_j^n. The finite-difference scheme associated with (4.2) is

$$\begin{aligned} &\frac{v_j^{n+1} - 2v_j^n + v_j^{n-1}}{(\Delta t)^2} - \frac{v_{j+1}^n - 2v_j^n + v_{j-1}^n}{(\Delta r)^2} + \gamma\frac{v_j^{n+1} - v_j^{n-1}}{2\Delta t} - \\ &\beta\frac{v_{j+1}^{n+1} - 2v_j^{n+1} + v_{j-1}^{n+1}}{2\Delta t\,(\Delta r)^2} + \beta\frac{v_{j+1}^{n-1} - 2v_j^{n-1} + v_{j-1}^{n-1}}{2\Delta t\,(\Delta r)^2} + \frac{m^2}{2}\left[v_j^{n+1} + v_j^{n-1}\right] + \\ &\frac{1}{(j\Delta r)^{p-1}}\frac{G(v_j^{n+1}) - G(v_j^{n-1})}{v_j^{n+1} - v_j^{n-1}} = 0, \end{aligned} \tag{4.3}$$

where $G(v) = v^{p+1}/(p+1)$.

Computationally, our method requires an application of Newton's method for systems of nonlinear equations along with Crout's reduction technique for tridiogonal linear systems.

An interesting property of this scheme is that, for initial approximations $\{w_j^0\}$ and $\{w_j^1\}$ with zero centered-difference first spatial derivatives at the origin, the successive approximations provided by the method have likewise centered-difference first spatial derivative equal to zero at the origin. This claim follows by induction using the facts that

$$v_1^k + v_{-1}^k + \beta\frac{(v_1^{k+1} + v_{-1}^{k+1}) - (v_1^{k-1} + v_{-1}^{k-1})}{2\Delta t} = 0,$$

that $w_1^n = w_{-1}^n$ iff $v_1^n + v_{-1}^n = 0$, and the substitution $v_j^n = jw_j^n\Delta r$. The induction hypothesis implies that $v_1^n + v_{-1}^n = 0$ for every $n \leq k$, whence the claim follows.

Our last statement implies that for a smooth initial profile at the origin, the subsequent approximations yielded by our method will be likewise smooth. As a test case, it is worthwhile mentioning that we have successfully obtained numerical results to verify this claim using a Gaussian initial profile centered at the origin.

4.2.3 Stability analysis

It is clear that (4.3) is consistent order $\mathcal{O}(\Delta t^2) + \mathcal{O}(\Delta r^2)$ with (4.2) whenever G' is identically equal to zero. Moreover, in order for the finite-difference scheme to be stable order n it is necessary that

$$\left(\frac{\Delta t}{\Delta r}\right)^2 \;<\; 1 + \gamma\frac{\Delta t}{4} + \beta\frac{\Delta t}{(\Delta r)^2} + m^2\frac{(\Delta t)^2}{4}.$$

To verify this claim, notice first that (4.3) can be rewritten as

$$\frac{v_j^{n+1} - 2v_j^n + v_j^{n-1}}{(\Delta t)^2} - \frac{\delta_0^2 v_j^n}{(\Delta r)^2} + \gamma\frac{v_j^{n+1} - v_j^{n-1}}{2\Delta t} - \beta\frac{\delta_0^2 v_j^{n+1} - \delta_0^2 v_j^{n-1}}{2\Delta t\,(\Delta r)^2} + \frac{m^2}{2}\left[v_j^{n+1} + v_j^{n-1}\right] \;=\; 0.$$

Define $R = \Delta t/\Delta r$. Let $V_{1j}^{n+1} = v_j^{n+1}$ and $V_{2j}^{n+1} = v_j^n$ for each $j = 0, 1, \ldots, M$ and $n = 0, 1, \ldots, N-1$. For every $j = 0, 1, \ldots, M$ and $n = 1, 2, \ldots, N$ let $\bar{V}_j^n$ be the column vector whose components are V_{1j}^n and V_{2j}^n. Our problem can be written then in matricial form as

$$\begin{pmatrix} k & 0 \\ 0 & 1 \end{pmatrix} \bar{V}_j^{n+1} \;=\; \begin{pmatrix} 2 + R^2\delta_0^2 & -h \\ 1 & 0 \end{pmatrix} \bar{V}_j^n,$$

where

$$\begin{aligned} k &= 1 + \gamma\frac{\Delta t}{2} - \frac{\beta\Delta t\delta_0^2}{2\,(\Delta r)^2} + m^2\frac{(\Delta t)^2}{2} \qquad \text{and} \\ h &= 1 - \gamma\frac{\Delta t}{2} + \frac{\beta\Delta t\delta_0^2}{2\,(\Delta r)^2} + m^2\frac{(\Delta t)^2}{2}. \end{aligned}$$

Denoting the Fourier transform of each $\bar{V}_j^n$ by $\hat{V}_j^n$, we obtain that

$$\hat{V}_j^{n+1} = \begin{pmatrix} \frac{2}{\hat{k}(\xi)}\left(1 - 2R^2\sin^2\frac{\xi}{2}\right) & -\frac{\hat{h}(\xi)}{\hat{k}(\xi)} \\ 1 & 0 \end{pmatrix} \hat{V}_j^n,$$

where

$$\begin{aligned} \hat{k}(\xi) &= 1 + \gamma\frac{\Delta t}{2} + 2\frac{\beta\Delta t}{(\Delta r)^2}\sin^2\frac{\xi}{2} + m^2\frac{(\Delta t)^2}{2} \qquad \text{and} \\ \hat{h}(\xi) &= 1 - \gamma\frac{\Delta t}{2} - 2\frac{\beta\Delta t}{(\Delta r)^2}\sin^2\frac{\xi}{2} + m^2\frac{(\Delta t)^2}{2}. \end{aligned}$$

The matrix $A(\xi)$ multiplying $\hat{V}_j^n$ in the last vector equation is the amplification

matrix of the problem, which has eigenvalues given by

$$\lambda_{\pm} = \frac{1 - 2R^2 \sin^2 \frac{\xi}{2} \pm \sqrt{\left(1 - 2R^2 \sin^2 \frac{\xi}{2}\right) - \hat{h}(\xi)\hat{k}(\xi)}}{\hat{k}(\xi)}.$$

In particular, for $\xi = \pi$ the eigenvalues of A are

$$\lambda_{\pm} = \frac{1 - 2R^2 \pm \sqrt{(1 - 2R^2)^2 - \hat{h}(\pi)\hat{k}(\pi)}}{\hat{k}(\pi)}.$$

Suppose for a moment that $1 - 2R^2 < -\hat{k}(\pi)$. If the radical in the expression for the eigenvalues of $A(\pi)$ is a pure real number then $|\lambda_-| > 1$. So for every $n \in \mathbb{N}$, $||A^n|| \geq |\lambda_-|^n$ grows faster than $K_1 + nK_2$ for any constants K_1 and K_2. A similar situation happens when the radical is a pure imaginary number, except that in this case $|\cdot|$ represents the usual Euclidean norm in the field of complex numbers.

Summarizing, if $1 - 2R^2 < -\hat{k}(\pi)$ then scheme (4.3) is unstable. Therefore in order for our numeric method to be stable order n it is necessary that $1-2R^2 > -\hat{k}(\pi)$, which is what we needed to establish.

4.2.4 Energy analysis

Assume that $G\colon \mathbb{R} \to \mathbb{R}$ is continuously differentiable, and that $w(\bar{x}, t)$ is a solution of (4.1) in a domain D of $\mathbb{R}^3$. Moreover, we assume that $\nabla w \cdot \hat{\mathrm{n}}$ is zero near the boundary of D at all time, where $\hat{\mathrm{n}}$ denotes the unit vector normal to the boundary of D. The Lagrangian associated with our nonlinear modified Klein-Gordon equation is given by

$$\mathcal{L} = \frac{1}{2}\left\{\left(\frac{\partial w}{\partial t}\right)^2 - |\nabla w|^2 - m^2 w^2\right\} - G(w).$$

It is easy to derive the following expression for the total energy associated with our nonlinear dissipative Klein-Gordon-like equation:

$$E(t) = \iiint_D \left\{\frac{1}{2}\left(\frac{\partial w}{\partial t}\right)^2 + \frac{1}{2}|\nabla w|^2 + \frac{m^2}{2}w^2 + G(w)\right\} d\bar{x}. \tag{4.4}$$

Proposition 2. *The instantaneous rate of change with respect to time of the total energy associated with the PDE in* (4.1) *is given by*

$$E'(t) = -\iiint_D \left\{\beta \left\|\nabla\left(\frac{\partial w}{\partial t}\right)\right\|^2 + \gamma\left(\frac{\partial w}{\partial t}\right)^2\right\} d\bar{x}.$$

Proof. Taking derivative on both sides of Equation (4.4), we obtain that

$$\begin{aligned}\frac{dE}{dt} &= \iiint_D \frac{\partial w}{\partial t}\left\{\frac{\partial^2 w}{\partial t^2} + m^2 w + G'(w)\right\} d\bar{x} + \frac{1}{2}\iiint_D \frac{\partial}{\partial t}|\nabla w|^2 d\bar{x} \\ &= \iiint_D \frac{\partial w}{\partial t}\left\{\frac{\partial^2 w}{\partial t^2} - \nabla^2 w + m^2 w + G'(w)\right\} d\bar{x} + \iint_{\partial D} \frac{\partial w}{\partial t}\nabla w \cdot \hat{\mathrm{n}}\ d\sigma \\ &= \beta \iiint_D \frac{\partial w}{\partial t}\nabla^2\left(\frac{\partial w}{\partial t}\right)\ d\bar{x} - \gamma \iiint_D \left(\frac{\partial w}{\partial t}\right)^2 d\bar{x} + \iint_{\partial D} \frac{\partial w}{\partial t}\nabla w \cdot \hat{\mathrm{n}}\ d\sigma.\end{aligned}$$

On the other hand, from Green's first identity we see that

$$\iiint_D \frac{\partial w}{\partial t}\nabla^2\left(\frac{\partial w}{\partial t}\right)\ d\bar{x} = \iint_{\partial D} \frac{\partial w}{\partial t}\frac{\partial}{\partial t}\left(\nabla w \cdot \hat{\mathrm{n}}\right)\ d\sigma \iiint_D \left\|\nabla\left(\frac{\partial w}{\partial t}\right)\right\|^2\ d\bar{x}.$$

The surface integrals in these last two equations are equal to zero, whence the result follows. □

It is worthwhile noticing that if β and γ are positive then the total energy is decreasing in time. Also, if β and γ are both equal to zero then the energy is conserved. Finally, if β is zero then the expression of $E'(t)$ coincides with the one derived in [51].

Let us assume now that G is nonnegative. The total energy in this case is likewise nonnegative and the integral of every term in (4.4) is bounded by $\sqrt{2E(t)}/m$. In particular, this last statement implies that the integral of w^2 at time t is bounded by $E(t)$. For those times t for which $E(t)$ is finite (and particularly for the case when β and γ are both equal to zero), this means that w is a square-integrable function in the first variable at time t.

Let $G'(w) = w^p$ with $p > 1$. Assuming that w is a radially symmetric solution of the damped nonlinear Klein-Gordon equation in a sphere D with center in the origin and radius L, and using the transformation $v(r,t) = rw(r,t)$ the energy expression adopts the form $E(t) = 4\pi E_0(t)$, with

$$E_0(t) = \int_0^L \left\{\frac{1}{2}\left(\frac{\partial v}{\partial t}\right)^2 + \frac{1}{2}\left(\frac{\partial v}{\partial r}\right)^2 + \frac{m^2}{2}v^2 + \frac{G(v)}{r^{p-1}}\right\} dr. \tag{4.5}$$

The instantaneous rate of change of energy is given by $E'(t) = 4\pi E_0'(t)$, where

$$E_0'(t) = -\int_0^L \left\{\beta\left(\frac{\partial^2 v}{\partial r \partial t} - \frac{1}{r}\frac{\partial v}{\partial t}\right)^2 + \gamma\left(\frac{\partial v}{\partial t}\right)^2\right\} dr.$$

It is possible to reproduce now the argument in [8] to show that for every t and nonzero r, $|w(r,t)| \leq \sqrt{2E_0(t)}/r$. This means in particular that if a solution were unbounded, it would have to be unbounded at the origin.

The discrete energy is given by

$$\begin{aligned}\frac{E_0^n}{\Delta r} &= \frac{1}{2}\sum_{j=0}^{m-1}\left(\frac{v_j^{n+1}-v_j^n}{\Delta t}\right)^2+\frac{1}{2}\sum_{j=0}^{m-1}\left(\frac{v_{j+1}^{n+1}-v_j^{n+1}}{\Delta r}\right)\left(\frac{v_{j+1}^n-v_j^n}{\Delta r}\right)\\ &\quad+\frac{1}{2}\sum_{j=0}^{m-1}\frac{(v_j^{n+1})^2+(v_j^n)^2}{2}+\sum_{j=1}^{m-1}\frac{G(v_j^{n+1})+G(v_j^n)}{2(j\Delta r)^{p-1}}.\end{aligned}$$

This expression is obviously consistent with (4.5). Moreover, taking the difference between $E_0^n/\Delta r$ and $E_0^{n-1}/\Delta r$ and simplifying after using (4.3), it can be shown that

$$\begin{aligned}\frac{E_0^n-E_0^{n-1}}{\Delta t} &= \Delta r\left[-\gamma\sum_{j=1}^{m-1}\left(\frac{v_j^{n+1}-v_j^{n-1}}{2\Delta t}\right)^2-\beta\sum_{j=1}^{m-1}\left(\frac{v_j^{n+1}-v_j^{n-1}}{2\Delta t}\right)\cdot\right.\\ &\quad\left.\left(\frac{(v_j^{n+1}-v_j^{n-1})-(v_{j-1}^{n+1}-v_{j-1}^{n-1})}{\Delta t(\Delta r)^2}\right)\right].\end{aligned}$$

For $\beta=0$ this expression provides us with a consistent approximation to the instantaneous rate of change of energy. Numerical results demonstrate that energy decreases as a function of time for $\beta>0$, which is in agreement with the corresponding instantaneous change of energy as a function of time.

4.3 Numerical results

The numerical results presented in this section correspond to approximate solutions of the dissipative, nonlinear, modified Klein-Gordon equation

$$\frac{\partial^2 u}{\partial t^2}-\nabla^2 u-\beta\frac{\partial}{\partial t}\left(\nabla^2 u\right)+\gamma\frac{\partial u}{\partial t}+u+G'(u)=0,$$

obtained using a tolerance of 10^{-5} and a maximum number of 20 iterations on every application of Newton's method. The space and time steps are always fixed as $\Delta r=\Delta t=0.002$.

4.3.1 External damping

Throughout this section we fix $\beta=0$.

Let us start considering the problem of approximating radially symmetric solutions of (4.1) with $G'(u)=u^7$, and initial data $\phi(r)=h(r)$ and $\psi(r)=h'(r)+h(r)/r$, where

$$h(r)=\begin{cases}5e^{100\left[1-\frac{1}{1-(10r-1)^2}\right]}, & \text{if } 0\le r<0.2,\\ 0, & \text{if } 0.2\le r\le 0.4.\end{cases}$$

We have plotted numerical solutions of this problem for several values of γ. The graphical results are presented in Figure 4.1 for $\gamma=0,5,10$. We observe first of all that the solutions of the damped nonlinear Klein-Gordon-like equation corresponding to small values of γ are consistently similar to those of the undamped case. To verify

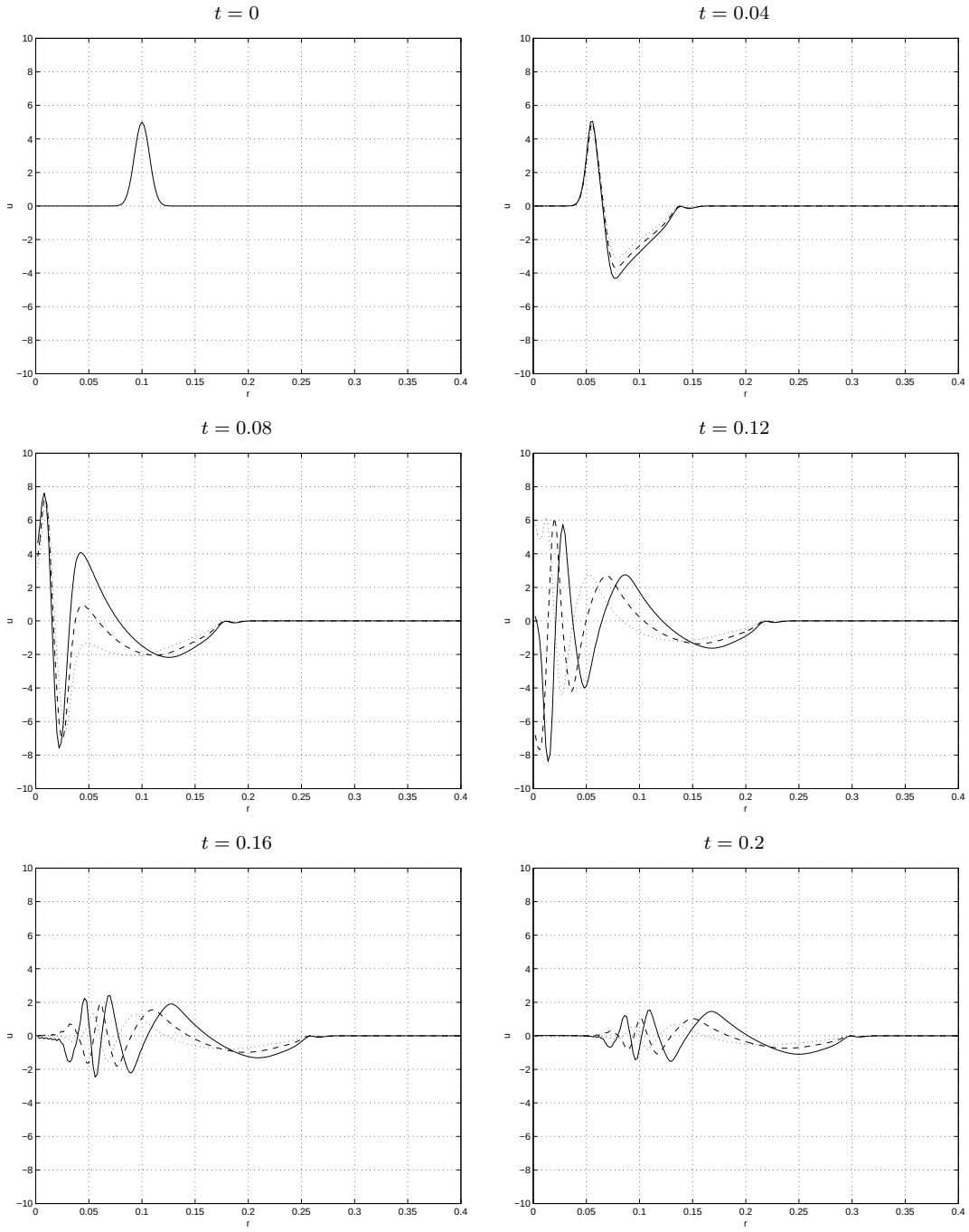

FIGURE 4.1: Approximate radial solutions of (4.1) at successive times for $\beta = 0$ and values of $\gamma = 0$ (solid), $\gamma = 5$ (dashed) and $\gamma = 10$ (dotted), $G'(u) = u^7$, and initial data $\phi(r) = h(r)$, $\psi(r) = h'(r) + h(r)/r$.

Time step	**Relative differences**				
	Values of γ				
n	0.1	0.5	1	5	10
0	0.0000	0.0000	0.0000	0.0000	0.0000
20	0.0028	0.0142	0.0283	0.1395	0.2693
40	0.0103	0.0509	0.1006	0.4491	0.7706
60	0.0167	0.0821	0.1611	0.6579	0.9573
80	0.0192	0.0942	0.1836	0.6954	0.9387
100	0.0200	0.0977	0.1896	0.6994	0.9308

TABLE 4.1: Relative differences of externally damped solutions to (4.1) with respect to the corresponding undamped solution at different time steps.

this claim quantitatively, we consider the approximations $\bar{v}_0^n$ and $\bar{v}_\gamma^n$ to the undamped and damped cases, respectively, and compute the relative difference in the $\ell_{2,\Delta x}$-norm via

$$\delta(\bar{v}_\gamma^n, \bar{v}_0^n) = \frac{||\bar{v}_\gamma^n - \bar{v}_0^n||_{2,\Delta x}}{||\bar{v}_0^n||_{2,\Delta x}}$$

(here we follow [42]). The relative differences for several values of γ at consecutive time steps are shown in Table 4.1. We observe that the difference between the solutions of the nonlinear Klein-Gordon-like equation with damping coefficient γ and the corresponding undamped equation can be made arbitrarily small by taking γ sufficiently close to 0.

We wish to corroborate this pattern for different nonlinear terms and a different set of initial conditions. With this objective in mind, Figure 4.2 depicts numerical solutions of (4.1) with $\gamma = 0, 5, 10$, nonlinear terms $G'(u) = 0, u^3, u^5, u^7, u^9$, and $\sinh(5u) - 5u$, initial conditions $\phi(r) = 0$ and $\psi(r) = 100h(r)$, and values of $\gamma = 0, 5, 10$. More accurately, Table 4.2 provides relative differences of these solutions at $t = 0.2$ (for the nonlinear functions listed above and varying values of γ) with respect to the corresponding undamped solution, for a wider selection of values of the parameter γ.

It must be mentioned that, as it was expected, the total energy was invariably decreasing for positive values of γ, and increasing for negative values. For the value

Nonlinearity	**Relative differences**				
	Values of γ				
$G'(u)$	0.1	0.5	1	5	10
0	0.0098	0.0478	0.0923	0.3642	0.5631
u^3	0.0097	0.0477	0.0929	0.3528	0.5554
u^5	0.0137	0.0665	0.1287	0.4024	0.6418
u^7	0.0171	0.0833	0.1618	0.5068	0.7819
u^9	0.0204	0.0999	0.1728	0.5736	0.8488
$\sinh(5u) - 5u$	0.0263	0.1377	0.2518	0.6284	0.8813

TABLE 4.2: Table of relative differences of externally damped solutions of (4.1) with respect to the corresponding undamped solution at $t = 0.2$.

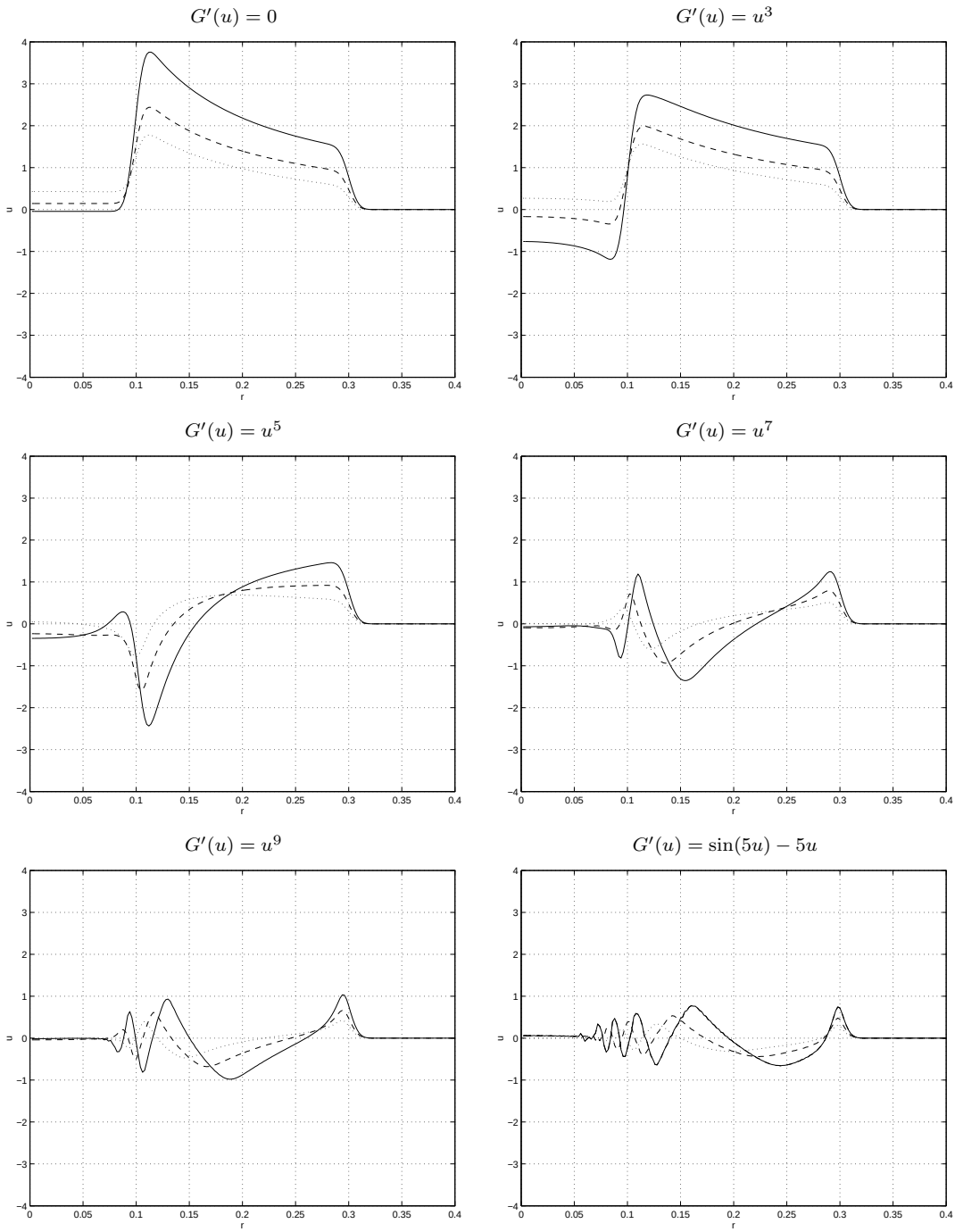

FIGURE 4.2: Approximate radial solutions of (4.1) with $G'(u)$ at $t = 0.2$, for initial data $\phi(r) = 0$ and $\psi(r) = 100h(r)$, $\beta = 0$ and $\gamma = 0$ (solid), $\gamma = 5$ (dashed) and $\gamma = 10$ (dotted).

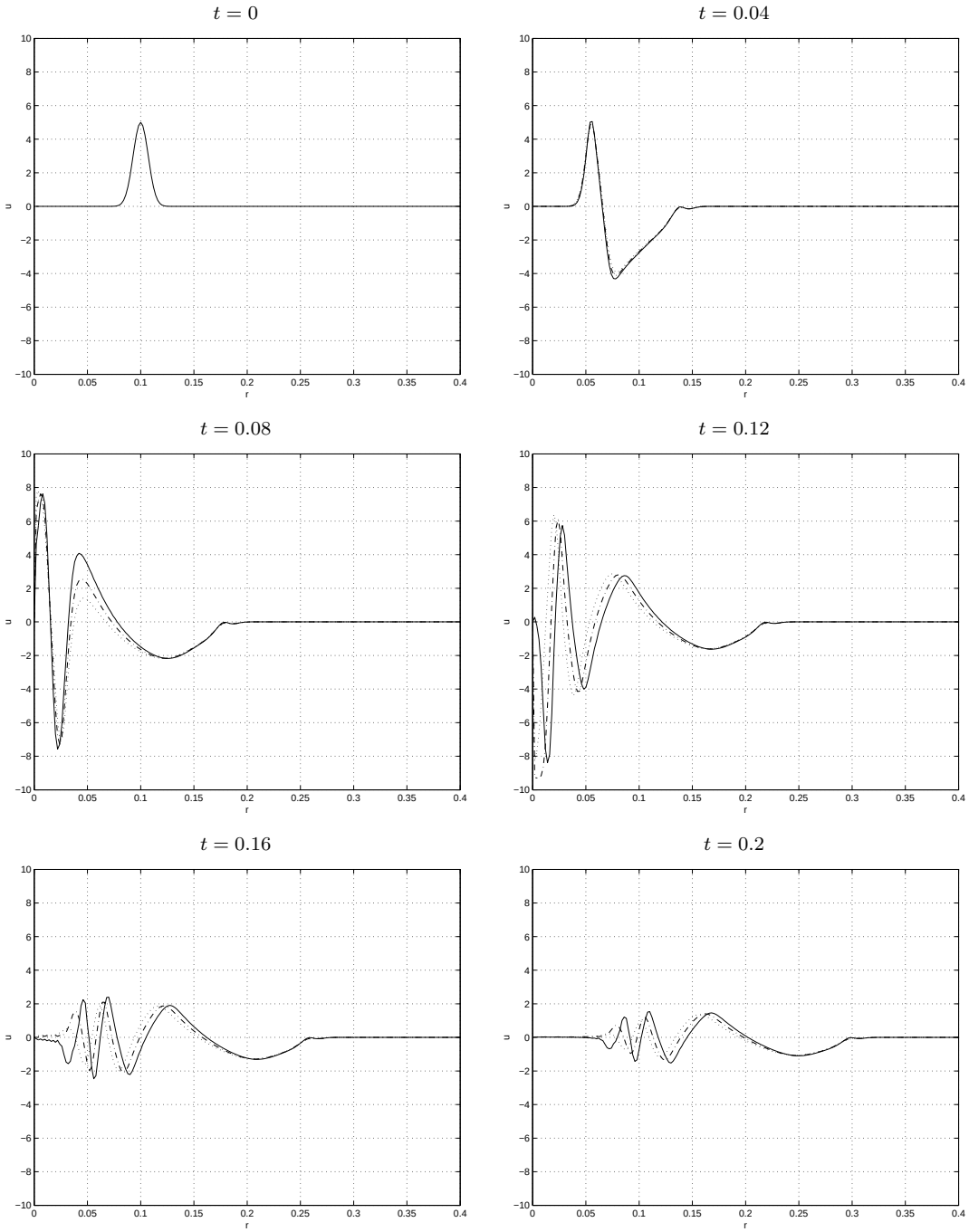

FIGURE 4.3: Approximate radial solutions at successive times of the undamped (solid) and the damped nonlinear Klein-Gordon equation with $\gamma = 0$ and $\beta = 0$ (dashed), $\beta = 0.0001$ (dash-dotted) and $\beta = 0.0002$, nonlinear term $G'(u) = u^7$, and initial data $\phi(r) = h(r)$ and $\psi(r) = h'(r) + h(r)/r$.

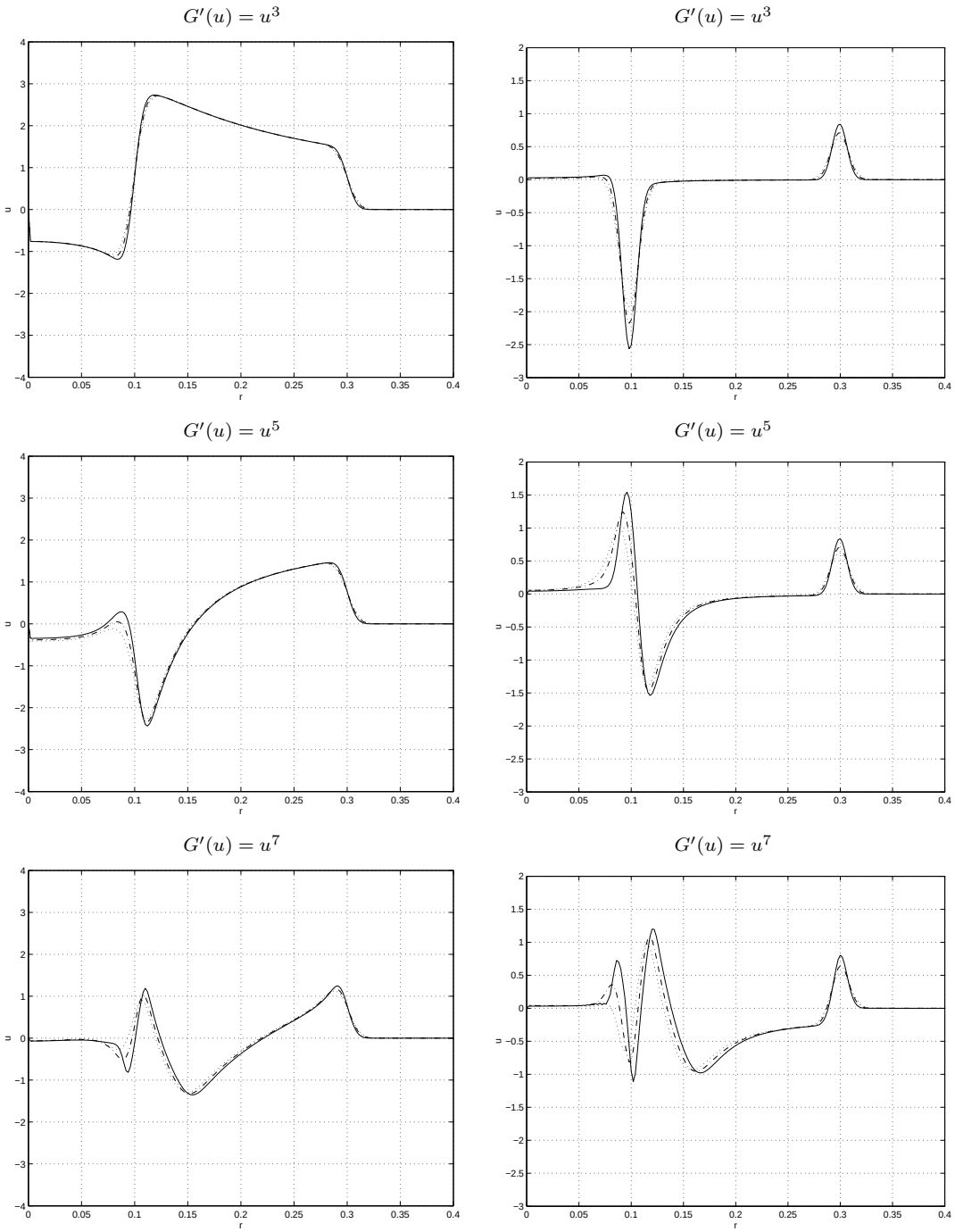

FIGURE 4.4: Approximate radial solutions of (4.1) with $G'(u)$ at $t = 0.2$, for initial data $\phi(r) = 0$, $\psi(r) = 100h(r)$ (left column) and $\phi(r) = h(r)$, $\psi(r) = 0$ (right column), $\gamma = 0$ and $\beta = 0$ (solid), $\beta = 0.0001$ (dashed) and $\beta = 0.0002$ (dotted).

Time step	Relative differences				
	Values of β				
n	10^{-6}	10^{-5}	10^{-4}	0.0005	0.001
0	0.0000	0.0000	0.0000	0.0000	0.0000
20	0.0005	0.0054	0.0517	0.2188	0.3682
40	0.0030	0.0300	0.2640	0.8281	1.1457
60	0.0156	0.0996	0.1493	1.6536	1.1460
80	0.0102	0.0970	0.7242	1.1530	1.2138
100	0.0080	0.0772	0.5751	1.0406	1.1435

TABLE 4.3: Relative differences of internally damped solutions to (4.1) with respect to the corresponding undamped solution at different time steps.

$\gamma = 0$, the rate of change of energy is equal to zero and our numeric results agree with [8]. Experimental results show that small values of γ correspond with small values of the discrete rate of change of the energy. This last observation corroborates stability of our method.

We also observe that the amplitude of solutions corresponding to positive values of γ tend to decrease as time or γ increases. Figure 4.2 partially corroborates that behavior. We have computed solutions corresponding to negative values of γ (graphs not included in this paper) and have verified that the amplitude of solutions increases with time and with $|\gamma|$.

Finally, we have obtained graphs of the energy E_0 vs. time for $G'(u) = u^3, u^5, u^7$, initial data $\phi(r) = 0$ and $\psi(r) = 100h(r)$, and values of $\gamma = 1, 5, 10$. The results (depicted in the left column of Figure 4.7) show a loss in the total energy as a function of time.

4.3.2 Internal damping

Consider first the case when γ equals zero. Figure 4.3 shows numerical solutions of (4.1) at consecutive times, for initial data $\phi(r) = h(r)$ and $\psi(r) = h'(r) + h(r)/r$, with nonlinear term $G'(u) = u^7$, and values of $\beta = 0, 0.001, 0.003$. We observe that small values of β produce results similar to those of the corresponding undamped case. To corroborate this claim, we appeal once more to the relative differences in the $\ell_{2,\Delta x}$-norm of dissipative solutions with respect to the non-dissipative one. The results are shown in Table 4.3. The results evidence the continuity of solutions with respect to the parameter β for this particular choice of nonlinearity, providing thus numerical support in favor of the stability of our method.

We want to establish now the continuity of our method for several nonlinear terms at a fixed large time. In order to do it, Figure 4.4 shows the numerical solutions of (4.1) at time $t = 0.2$, for the nonlinear terms $G'(u) = u^3, u^5, u^7$, for two different sets of initial conditions: $\phi(r) = 0$ and $\psi(r) = 100(h)$, and $\phi(r) = h(r)$ and $\psi(r) = 0$, and values of $\beta = 0, 0.0001, 0.0002$. The graphs in this figure, together with the analysis of relative differences in the $\ell_{2,\Delta x}$-norm supplied in Table 4.4 for the first set of initial conditions, evidence the continuity of the numerical solution given by our method with respect to the parameter β for different nonlinearities.

We now consider the case when γ is nonzero. We use $G'(u) = 0$, u^3, u^5, u^7,

Nonlinearity $G'(u)$	**Relative differences**				
	Values of β				
	10^{-6}	10^{-5}	10^{-4}	0.0005	0.001
0	0.0003	0.0027	0.0242	0.0859	0.1326
u^3	0.0003	0.0032	0.0289	0.1040	0.1621
u^5	0.0011	0.0105	0.0948	0.3374	0.5043
u^7	0.0023	0.0224	0.1825	0.5663	0.7327
u^9	0.0041	0.0397	0.3133	0.7318	0.9256
$\sinh(5u) - 5u$	0.0063	0.0577	0.4717	0.9403	1.1007

TABLE 4.4: Table of relative differences of internally damped solutions of (4.1) with respect to the corresponding undamped solution at $t = 0.2$.

u^9, and $\sinh(5u) - 5u$, initial data $\phi(r) = 0$ and $\psi(r) = 100h(r)$, and time $t = 0.2$. Figure 4.5 shows numerical solutions of (4.1) for values of $\beta = 0$, 0.0005, 0.005. The solutions for smaller nonzero values of β are indeed closer to the corresponding internally undamped solution, while the larger values of β spread out the internally undamped solution at the same time that the maximum amplitude is decreased.

In order to study the time behavior of the solutions near the origin we have included Figure 4.6, using initial data $\phi(r) = 0$ and $\psi(r) = 100h(r)$, the nonlinear terms $G'(u) = u^3$, u^5 and u^7, different choices of values for β and γ, and $\Delta r = \Delta t = 0.002$. The left column shows the time-dependence of solutions at the origin for $\beta = 0$ and three positive values of γ, whereas the right column shows similar results for $\gamma = 0$ and three positive values of β. We observe that the value of solutions at the origin for large times is always approximately equal to zero for $\beta = 0$, which is in agreement with our experience of the $(1 + 1)$-dimensional case.

Finally, Figure 4.7 shows the graphs of the energy E_0 vs. time for $G'(u) = u^3, u^5, u^7$, initial data $\phi(r) = 0$ and $\psi(r) = 100h(r)$, and values of $\beta = 0.0005$, 0.001, 0.005. The results (depicted in the right column) show a loss in the total energy as a function of time. It is clear that the rate at which the total energy is lost due to internal damping is greater than the corresponding rate due to external damping.

4.4 Discussion

A numerical method has been designed to approximate radially symmetric solutions of some dissipative, nonlinear, modified Klein-Gordon equations with constant internal and external damping coefficients β and γ, respectively. Our finite-difference scheme is in general agreement with the non-dissipative results presented in [8]. The method is consistent $\mathcal{O}(\Delta t^2) + \mathcal{O}(\Delta r^2)$, conditionally stable, and continuous with respect to the parameters β and γ; as expected, the total energy decays in time for positive choices of the parameters. The corresponding scheme to approximate the total energy of the system is consistent and has the property that the discrete rate of change of the discrete energy with respect to time approximates the corresponding continuous rate of change for $\beta = 0$.

Several conclusions can be drawn from our numerical computations. First of all, we have seen that both internal and external damping tend to decrease the magni-

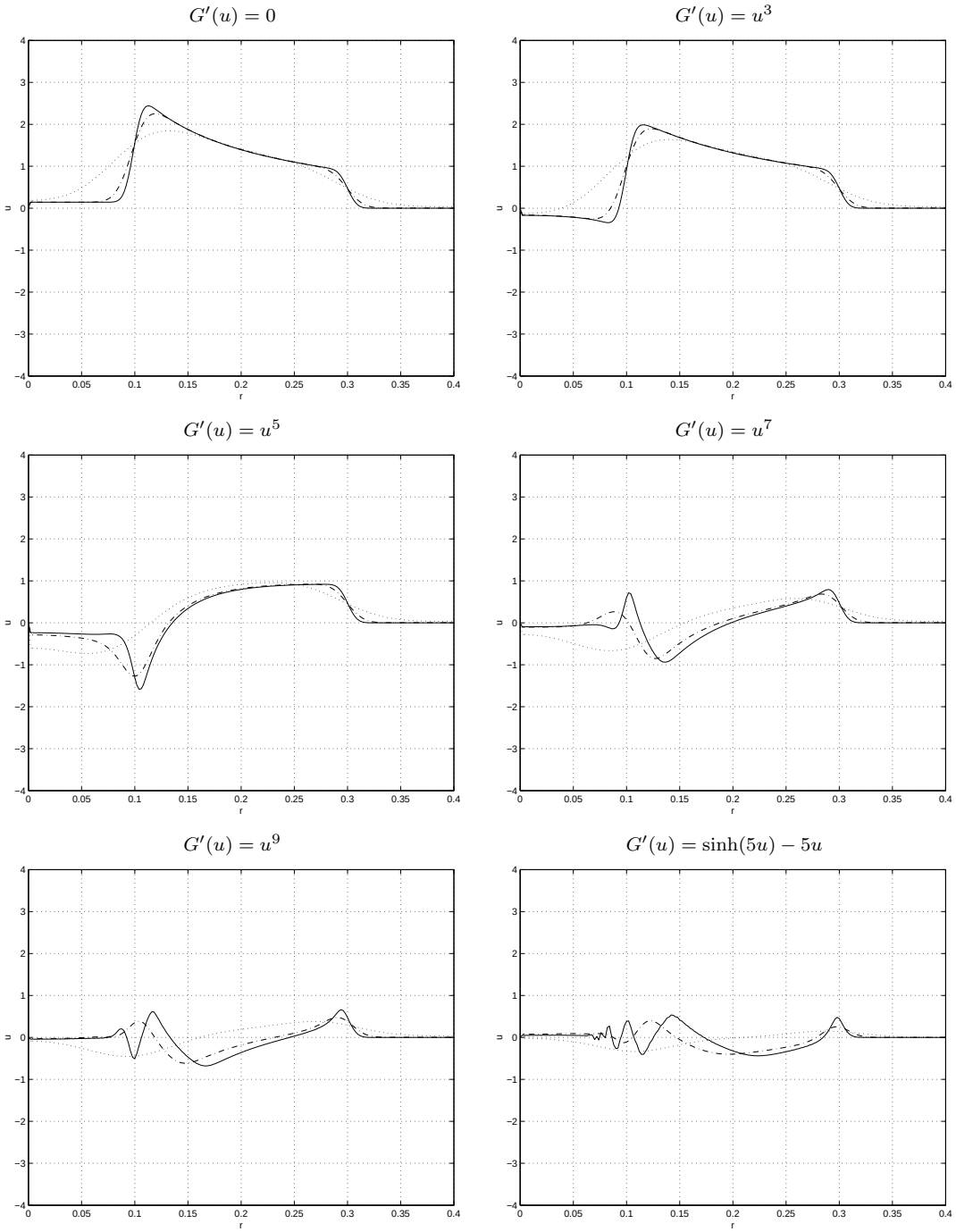

FIGURE 4.5: Approximate radial solutions of (4.1) at $t = 0.2$, for $\gamma = 5$, initial data $\phi(r) = 0$ and $\psi(r) = 100h(r)$, and $\beta = 0$ (solid), $\beta = 0.0005$ (dashed) and $\beta = 0.005$ (dotted).

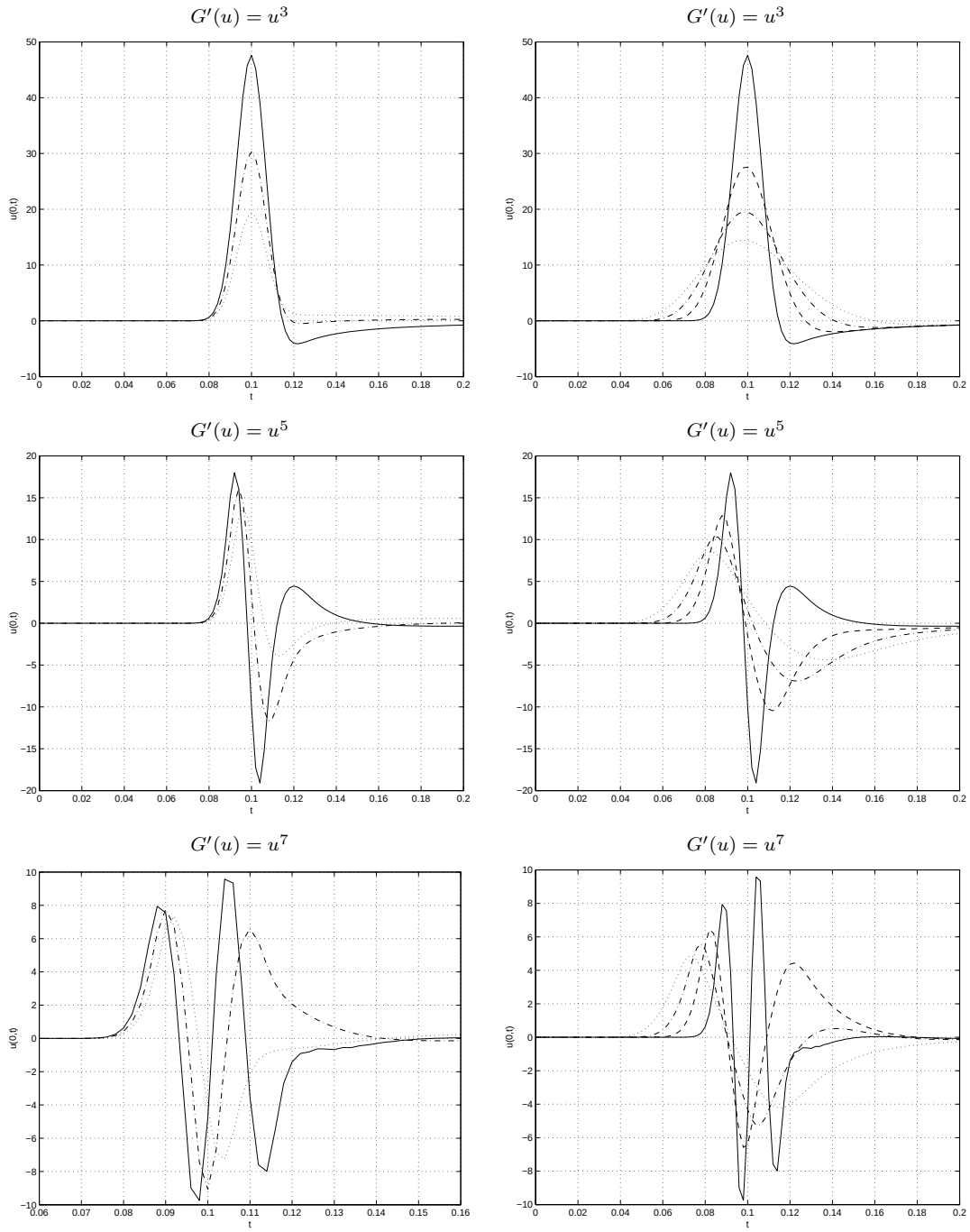

FIGURE 4.6: Approximate value of solutions to (4.1) near the origin vs. time for different nonlinear terms, and initial conditions $\phi(r) = 0$ and $\psi(r) = 100h(r)$. Left column: $\beta = 0$ and $\gamma = 0$ (solid), $\gamma = 10$ (dashed) and $\gamma = 20$ (dotted); right column: $\gamma = 0$ and $\beta = 0$ (solid), $\beta = 0.001$ (dashed), $\beta = 0.0025$ (dashed-dotted) and $\beta = 0.005$ (dotted).

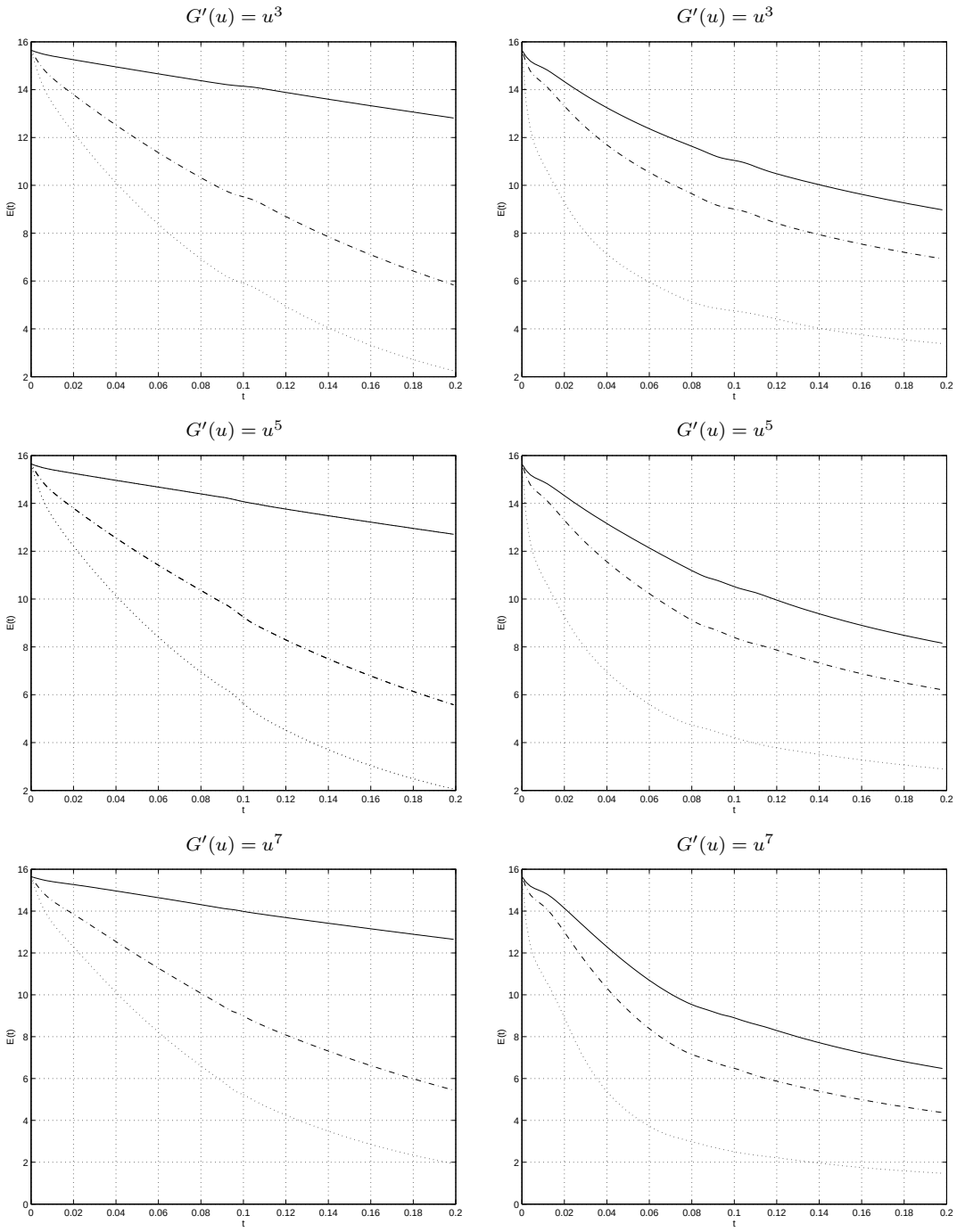

FIGURE 4.7: Total energy vs. time for initial data $\phi(r) = 0$ and $\psi(r) = 100h(r)$. Left column: $\beta = 0$ and $\gamma = 1$ (solid), 5 (dashed), 10 (dotted). Right column: $\gamma = 0$ and $\beta = 0.0005$ (solid), 0.001 (dashed), 0.005 (dotted).

tude of solutions, as it was expected. Our results clearly exhibit the dispersive effects of the parameter β and the dissipative effects of γ. Our energy computations evidence the fact that the rate at which the energy is dissipated by the internal damping is faster than the corresponding rate of external damping. Finally, we observe that the effect of the nonlinear term in the temporal behavior near the origin is to increase the number of oscillations as the degree of the nonlinearity is increased. Invariably, the solutions of the dissipative modified Klein-Gordon equation converge in time to the trivial solution.

Chapter 5

An energy-based computational method in the analysis of the transmission of energy in a chain of coupled oscillators

In this paper we study the phenomenon of nonlinear supratransmission in a semi-infinite discrete chain of coupled oscillators described by modified sine-Gordon equations with constant external and internal damping, and subject to harmonic external driving at the end. We develop a consistent and conditionally stable finite-difference scheme in order to analyze the effect of damping in the amount of energy injected in the chain of oscillators; numerical bifurcation analyses to determine the dependence of the amplitude at which supratransmission first occurs with respect to the frequency of the driving oscillator are carried out in order to show the consequences of damping on harmonic phonon quenching and the delay of appearance of critical amplitude.

5.1 Introduction

The study of nonlinear continuous media described by modified Klein-Gordon equations subject to initial conditions is a topic of interest in several branches of the physical sciences [1, 2, 3, 7]. Here the analytical study on features of solutions of Klein-Gordon-like equations as well as the development of new and more powerful computational techniques to approximate them have been the most transited highways in the mathematical research of the area.

The behavior of nonlinear continuous media described by modified Klein-Gordon equations subject to boundary conditions is also an interesting topic of study in mathematical physics. This type of mathematical models have proved to be useful when applied, for instance, to the description of the project of data transmission in optical fibers in nonlinear Kerr regimes [52, 53] or in the study of the property of self-induced transparency of a two-level system submitted to a high-energy incident (resonant) laser pulse [54, 55]. More concretely, the behavior of a continuous medium submitted to a continuous wave radiation constitutes a fundamental problem that

has not been studied in-depth, yet it has shown to have potential applications as a model in the study of Josephson transmission lines [56, 57, 58].

Numerical studies on discrete versions of these models [59] followed by experimental results [60] have shown that there exists a bifurcation of wave transmission within a forbidden band gap in certain semi-infinite undamped Klein-Gordon-like chains of coupled oscillators which are periodically forced at the end. This bifurcation is a consequence of the generation of nonlinear modes by the periodic forcing at the end of the chain, and allows energy to flow into the medium via a nonlinear process called *nonlinear supratransmission*, which has been proved numerically not to depend on integrability as long as the model possesses a natural forbidden band gap.

The process of nonlinear supratransmission has been studied numerically by means of computational algorithms already built in standard mathematical packages. Most particularly, the numerical results obtained in [59], for instance, rely on the use of a Runge-Kutta method of high order, which has the advantage of possessing high accuracy and efficiency in the computations, but lacks the consistency in the numerical estimation of the energy flowing into the medium which is desired in the study of supratransmission. With this shortcoming in mind, we present in this paper an alternate numerical formulation to study the process of supratransmission in a nonlinear system of differential equations, that has the advantage of being consistent in the approximation of the solutions to the problem and in the estimation of the continuous energy. More concretely, in the present work we study the process of nonlinear supratransmission in a semi-infinite nonlinear discrete system of coupled oscillators governed by modified sine-Gordon and Klein-Gordon equations with constant internal and external damping. We exploiting some numerical results for dissipative nonlinear modified Klein-Gordon equations that generalize a method proposed by Stauss and Vázquez [8], and validate our conclusions against [59]. Our study — rigorous in numerical nature — will soon be succeeded by future applications in forthcoming papers.

In Section II of this paper we introduce the mathematical problem under study and derive the expression of the instantaneous rate of change of the energy transmitted to the system through the boundary. Section III is devoted to introducing the finite-difference scheme; here we present the discrete energy analysis associated with the problem under study and establish in detail the numerical properties of our method. Numerical results are presented in the next section, followed by a brief discussion.

5.2 Analytical results

5.2.1 Mathematical model

In this article we study the effects of the nonnegative constant parameters β and γ, and the real constant m^2 on the behavior of solutions to the mixed-value problem with mass m,

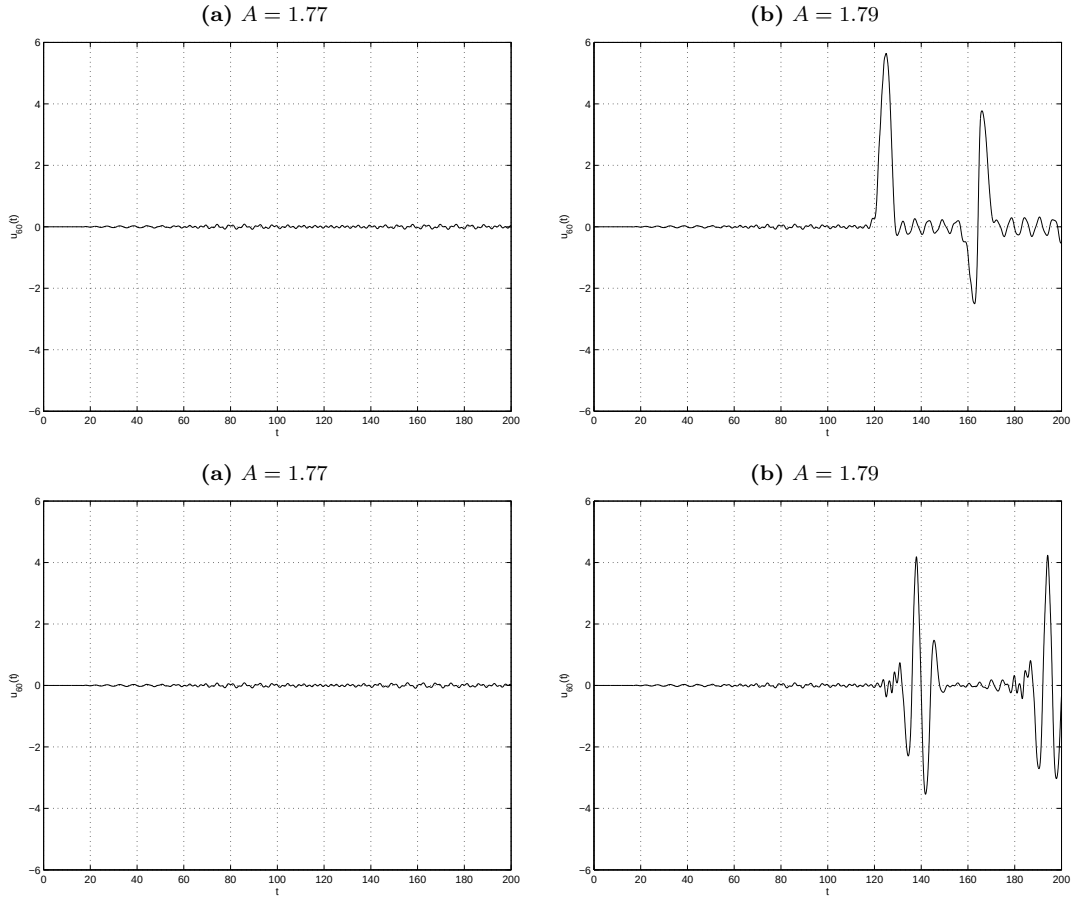

FIGURE 5.1: Approximate solution $u_{60}(t)$ of a sine-Gordon system in the first row and a Klein-Gordon system in the second, for a driving frequency of 0.9 and two different amplitude values A: (a) before and (b) after the bifurcation threshold.

$$\begin{aligned} \frac{d^2u_n}{dt^2} - \left(c^2 + \beta\frac{d}{dt}\right)\Delta_x^2 u_n + \gamma\frac{du_n}{dt} + m^2u_n + V'(u_n) &= 0, \\ \text{subject to : } \begin{cases} u_n(0) = \phi(n), & n \in \mathbb{Z}^+, \\ \dfrac{du_n}{dt}(0) = \varphi(n), & n \in \mathbb{Z}^+, \\ u_0(t) = \psi(t), & t \geq 0, \end{cases} \end{aligned} \tag{5.1}$$

which describes a system of coupled oscillators with coupling coefficient $c \gg 1$, and where β and γ clearly play the roles of internal and external damping coefficients, respectively. The number $\Delta_x^2 u_n$ is used to represent the spatial second-difference $u_{n+1} - 2u_n + u_{n-1}$ for every $n \in \mathbb{Z}^+$, and the boundary-driving function ψ is assumed continuously differentiable on $(0, +\infty)$. In our study, we will let $V(u) = 1 - \cos u$ for a chain of coupled *sine-Gordon* equations, and $V(u_n) = \frac{1}{2!}u_n^2 - \frac{1}{4!}u_n^4 + \frac{1}{6!}u_n^6$ for zero mass in the case of a *Klein-Gordon* chain.

It is worth recalling that the differential equation under study has multiple applications in the continuous limit. For instance, a similar equation appears in

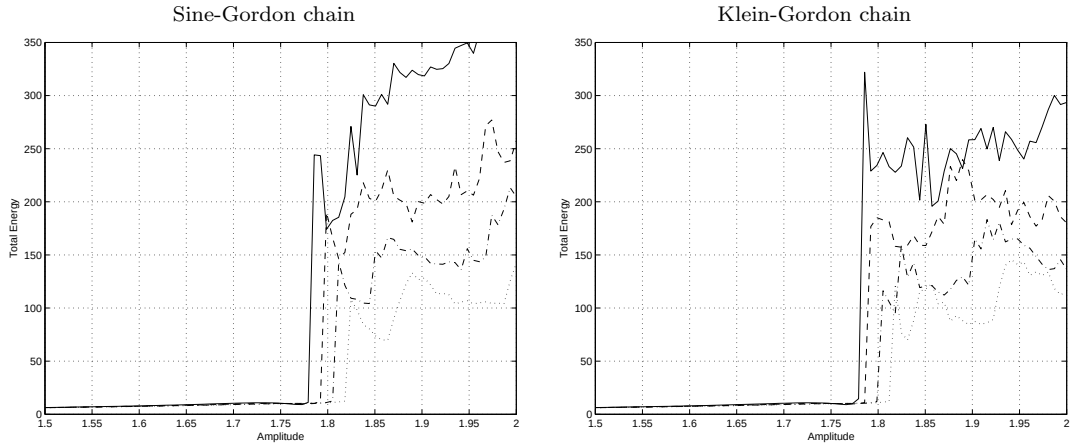

FIGURE 5.2: Graphs of total energy transmitted into the massless sine-Gordon and Klein-Gordon systems vs. driving amplitude for a driving frequency of 0.9, with $\beta = 0$ and $\gamma = 0$ (solid), 0.01 (dashed), 0.02 (dash-dotted), 0.03 (dotted).

the study of Josephson junctions between superconductors when dissipative effects are taken into account [1]. A modification of this equation is used in the study of fluxons in Josephson transmission lines [2], and a version in the form of a modified Klein-Gordon equation appears in the statistical mechanics of nonlinear coherent structures such as solitary waves (see [3] pp. 298–309) when no internal damping is present. Besides, our equation clearly describes the motion of a damped string in a non-Hookean medium.

For purposes of this paper, we will consider a system of coupled oscillators initially at rest at the origin of the system of reference, subject to an external harmonic forcing described by $\psi(t) = A \sin \Omega t$, and pure-imaginary or real mass satisfying $|m| \ll 1$. Analysis of the undamped linearized system of differential equations in (5.1) shows that the linear dispersion relation reads $\omega^2(k) = m^2 + 1 + 2c^2(1 - \cos k)$. in any case. The driving frequency will take on values in the forbidden band gap region $\Omega < \sqrt{m^2 + 1}$, in which case the linear analysis yields the exact solutions $u_n(t) = A \sin(\Omega t) e^{-\lambda n}$, where

$$\lambda = \operatorname{arccosh}\left(1 + \frac{m^2 + 1 - \Omega^2}{2c^2}\right).$$

Meanwhile, the massless undamped nonlinear case possesses an exact solution in the continuous limit which happens to work well for high values of the coupling coefficient. It has been shown numerically that, for each frequency Ω in the forbidden band gap, the massless medium starts to transmit energy by means of nonlinear mode generation for amplitudes greater than the threshold value $A_s = 4 \arctan(\lambda c/\Omega)$.

5.2.2 Energy analysis

In this section we derive the expression of the instantaneous rate of change of total energy in system (5.1). Here, by a *square-summable* sequence we understand a real sequence $(a_n)_{n=0}^{\infty}$ for which $\sum a_n^2$ is convergent.

LEMMA 1 (Discrete Green's First Identity). *If $(a_n)_{n=0}^{\infty}$ is a square-summable sequence*

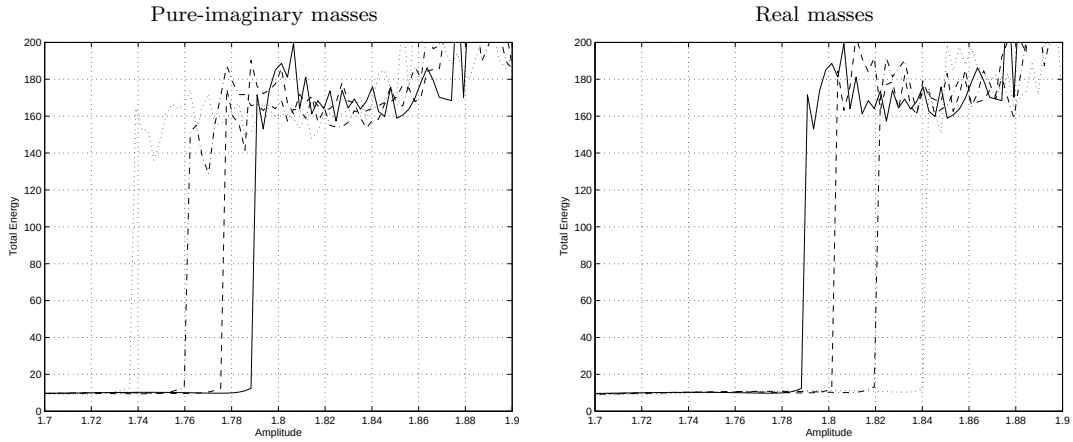

FIGURE 5.3: Total energy transmitted into the sine-Gordon system vs. driving amplitude for a driving frequency of 0.9, with $\beta = 0$, $\gamma = 0.01$, and pure-imaginary and real masses of magnitude 0 (solid), 0.05 (dashed), 0.075 (dash-dotted) and 0.1 (dotted).

then

$$\sum_{n=1}^{\infty}(a_{n+1} - 2a_n + a_{n-1})a_n = a_0(a_0 - a_1) - \sum_{n=1}^{\infty}(a_n - a_{n-1})^2.$$

Proof. Hölder's inequality implies that both series in the formula of the lemma converge. Moreover, the sequence defined by $t_n = a_n a_{n-1} - (a_{n-1})^2$ for every positive integer n converges to zero and the result follows now from the identities

$$\begin{aligned}\sum_{n=1}^{\infty}(a_{n+1} - 2a_n + a_{n-1})a_n &= \sum_{n=1}^{\infty}(t_{n+1} - t_n) - \sum_{n=1}^{\infty}(a_n - a_{n-1})^2 \\ &= -t_1 - \sum_{n=1}^{\infty}(a_n - a_{n-1})^2.\end{aligned}$$

□

PROPOSITION 2. *Let $(u_n(t))_{n=0}^{\infty}$ be solutions to* (5.1) *such that $(\dot{u}_n(t))_{n=0}^{\infty}$ is square-summable at any fixed time t. The instantaneous rate of change of the total energy in the system is given by*

$$\frac{dE}{dt} = c^2(u_0 - u_1)\dot{u}_0 - \gamma\sum_{n=1}^{\infty}(\dot{u}_n)^2 - \beta\left[\sum_{n=1}^{\infty}(\dot{u}_n - \dot{u}_{n-1})^2 + (\dot{u}_1 - \dot{u}_0)\dot{u}_0\right].$$

Proof. The energy density of the undamped system of coupled equations with a potential energy $V(u_n)$ in the n-th oscillator is given by $H_n = \frac{1}{2}[\dot{u}_n^2 + c^2(u_{n+1} - u_n)^2 + m^2u_n^2] + V(u_n)$. After including the potential energy from the coupling between the first two oscillators, the total energy of the system at any time becomes "'

$$E = \sum_{n=1}^{\infty} H_n + \frac{c^2}{2}(u_1 - u_0)^2,$$

and the fact that u_n tends to 0 as n increases implies that the sequence $J_n = -c^2\dot{u}_n(u_n - u_{n-1})$ converges to zero pointwisely at any fixed time. Simplifying and rearranging terms of the derivative of the Hamiltonian H_n yields the expression

$$\frac{dH_n}{dt} = (J_n - J_{n+1}) + \beta(\dot{u}_{n+1} - 2\dot{u}_n + \dot{u}_{n-1})\dot{u}_n - \gamma(\dot{u}_n)^2.$$

The result follows now from this identity after computing the derivative of the total energy of the system, using the formula for telescoping series and applying our discrete version of Green's First Identity. □

Observe from the proposition that the expression of the rate of change of energy associated with damped system (5.1) is in agreement with the undamped formula derived in [59]. Moreover, it is clear that the external damping coefficient contributes decreasing the total amount of energy in the chain system for β equal to zero.

5.3 Numerical analysis

5.3.1 Finite-difference scheme

From a practical point of view, we will restrict our study to a system consisting of a finite number N of coupled oscillators with constant internal and external damping coefficients, described by the system of ordinary differential equations

$$\frac{d^2u_n}{dt^2} - \left(c^2 + \beta\frac{d}{dt}\right)\Delta_x^2 u_n + \alpha\frac{du_n}{dt} + m^2u_n + V'(u_n) = 0$$

for $1 \leq n \leq N$, where α includes both the effect of external damping and a simulation of an absorbing boundary slowly increasing in magnitude on the last $N - N_0$ oscillators. More concretely, we let $u_{N+1}(t)$ be equal to zero at all time t, and let α be the sum of external damping and the function

$$\gamma'(n) = \begin{cases} \kappa\left[1 + \tanh\left(\dfrac{2n - N_0 + N}{2\sigma}\right)\right], & N_0 < n \leq N, \\ 0, & \text{otherwise.} \end{cases}$$

In practice, we will let $\kappa = 0.5$, $\sigma = 3$, $N_0 = 150$ and $N = 200$.

We proceed now to discretize problem (5.1) using a finite system of N differential equations and a regular partition $0 = t_0 < t_1 < \cdots < t_M = T$ of the time interval $[0, T]$ with time step equal to Δt. For each $k = 0, 1, \ldots, M$, let us represent the approximate solution to our problem on the n-th oscillator at time t_k by u_n^k. If we convey that $\delta_t u_n^k = u_n^{k+1} - u_n^{k-1}$, that $\delta_t^2 u_n^k = u_n^{k+1} - 2u_n^k + u_n^{k-1}$ and that

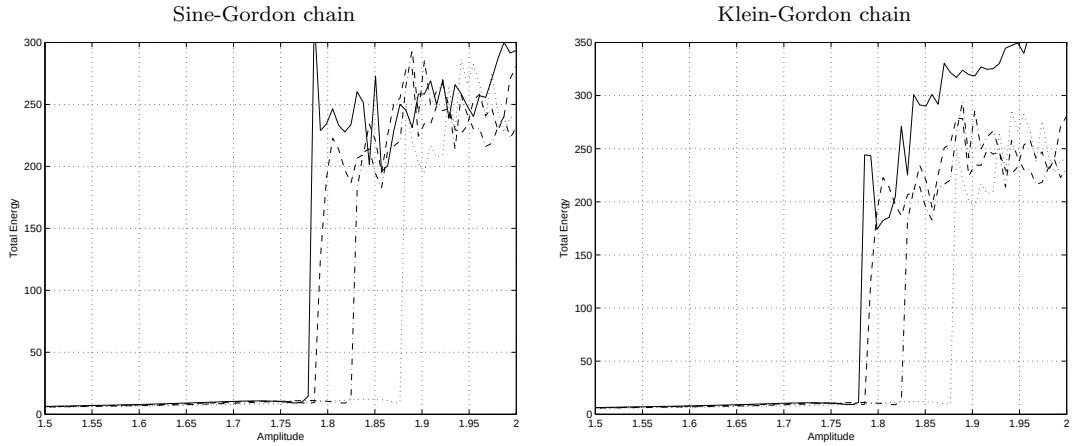

FIGURE 5.4: Graphs of total energy transmitted into the massless sine-Gordon and Klein-Gordon systems vs. driving amplitude for a driving frequency of 0.9, with $\gamma = 0$ and $\beta = 0$ (solid), 0.1 (dashed), 0.2 (dash-dotted), 0.3 (dotted).

$\delta_x^2 u_n^k = u_{n+1}^k - 2u_n^k + u_{n-1}^k$, our problem takes then the discrete form

$$\begin{aligned} &\frac{\delta_t^2 u_n^k}{(\Delta t)^2} - \left(c^2 + \frac{\beta}{2\Delta t}\delta_t\right)\delta_x^2 u_n^k + \frac{\alpha}{2\Delta t}\delta_t u_n^k + \frac{m^2}{2}[u_n^{k+1} + u_n^{k-1}] \\ &\qquad + \frac{V(u_n^{k+1}) - V(u_n^{k-1})}{u_n^{k+1} - u_n^{k-1}} \;=\; 0, \\ &\text{subject to :} \begin{cases} u_n^0 = \phi(n), & 1 \le n \le N, \\ u_n^1 = \phi(n) + \Delta t\varphi(n), & 1 \le n \le N, \\ u_0^k = \psi(k\Delta t), & 1 \le k \le M, \\ u_{N+1}^k = 0, & 1 \le k \le M. \end{cases} \end{aligned} \tag{5.2}$$

Observe that the proposed numerical method is nonlinear and requires an application of Newton's method for systems of equations in order to be implemented. Notice also that if $V'(u_n)$ at the k-th time step is approximated by $V'(u_n^k)$ then the finite-difference scheme becomes linear and an application of Crout's reduction technique for tridiagonal systems suffices to approximate solutions of (5.1). In such case, it is readily seen that the vector equation $A\mathbf{u}^{k+1} = B\mathbf{u}^k + C\mathbf{u}^{k-1} - V'(\mathbf{u}^k) + \mathbf{v}^k$ must be satisfied for every $k \ge 2$, for the three N-dimensional tridiagonal matrices

and the N-dimensional vector

$$A = \begin{pmatrix} b & a & \cdots & 0 \\ a & b & \cdots & 0 \\ \vdots & \vdots & \ddots & \vdots \\ 0 & 0 & \cdots & b \end{pmatrix}, \qquad B = \begin{pmatrix} d & c^2 & \cdots & 0 \\ c^2 & d & \cdots & 0 \\ \vdots & \vdots & \ddots & \vdots \\ 0 & 0 & \cdots & d \end{pmatrix},$$

$$C = \begin{pmatrix} e & a & \cdots & 0 \\ a & e & \cdots & 0 \\ \vdots & \vdots & \ddots & \vdots \\ 0 & 0 & \cdots & e \end{pmatrix}, \qquad \mathbf{v}^k = \begin{pmatrix} c^2 u_0^k - a\delta_t u_0^k \\ 0 \\ 0 \\ \vdots \\ 0 \end{pmatrix},$$

respectively, and constants

$$a = -\frac{\beta}{2\Delta t}, \qquad b = \frac{\alpha + 2\beta}{2\Delta t} + \frac{m^2}{2} + \frac{1}{(\Delta t)^2},$$
$$d = \frac{2}{(\Delta t)^2} - 2c^2 \qquad \text{and} \qquad e = \frac{\alpha + 2\beta}{2\Delta t} - \frac{m^2}{2} - \frac{1}{(\Delta t)^2}.$$

Here $\mathbf{u}^k = (u_1^k, \ldots, u_n^k)^t$ for every $k \in \{0, 1, \ldots, M\}$, and $V(\mathbf{u}^k)$ is the n-th dimensional vector whose i-th component is equal to $V(u_i^k)$. This latter formulation of our problem will be used for validation purposes only, since we will prefer the nonlinear formulation due to the quadratic order of convergence of Newton's method and other reasons that will be presented in the next section.

5.3.2 Discrete energy

The total energy in the system at the k-th time step will be approximated numerically via

$$\begin{aligned} E_k &= \frac{1}{2}\sum_{n=1}^{M}\left(\frac{u_n^{k+1} - u_n^k}{\Delta t}\right)^2 + \frac{c^2}{2}\sum_{n=1}^{M}(u_{n+1}^{k+1} - u_n^{k+1})(u_{n+1}^k - u_n^k) \\ &\quad + \frac{m^2}{2}\sum_{n=1}^{M}\frac{(u_n^{k+1})^2 + (u_n^k)^2}{2} + \sum_{n=1}^{M}\frac{V(u_n^{k+1}) + V(u_n^k)}{2} \\ &\quad + \frac{c^2}{2}(u_1^{k+1} - u_0^{k+1})(u_1^k - u_0^k). \end{aligned}$$

Proposition 3. *The following identity holds for every sequence (u_n^k) satisfying (5.2) and every positive index k:*

$$\begin{aligned} \frac{E_k - E_{k-1}}{\Delta t} &= c^2(u_0^k - u_1^k)\frac{\delta_t u_0^k}{2\Delta t} - \gamma\sum_{n=1}^{N}\left(\frac{\delta_t u_n^k}{2\Delta t}\right)^2 \\ &\quad -\beta\left[\sum_{n=1}^{\infty}\left(\frac{\delta_t u_n^k - \delta_t u_{n-1}^k}{2\Delta t}\right)^2 + \left(\frac{\delta_t u_1^k - \delta_t u_0^k}{2\Delta t}\right)\frac{\delta_t u_0^k}{2\Delta t}\right]. \end{aligned}$$

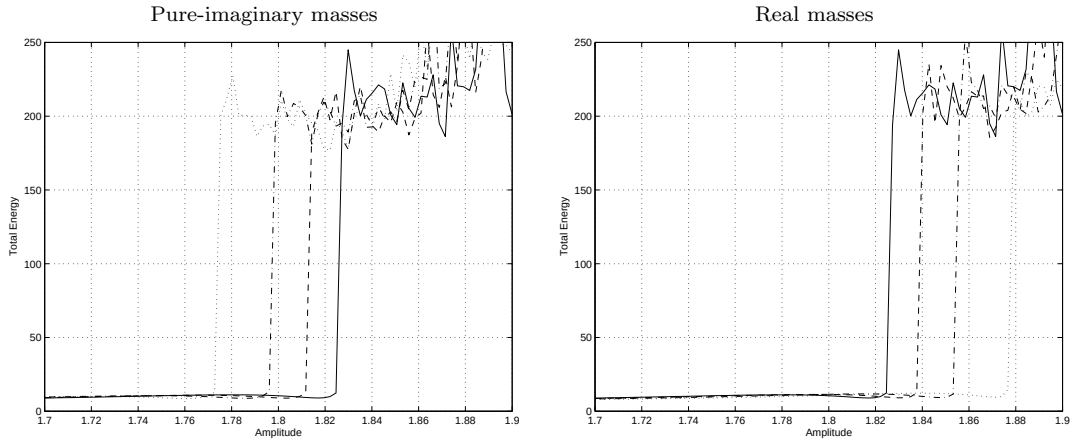

FIGURE 5.5: Total energy transmitted into the sine-Gordon system vs. driving amplitude for a driving frequency of 0.9, with $\beta = 0.2$, $\gamma = 0$, and pure-imaginary and real masses of magnitude 0 (solid), 0.05 (dashed), 0.075 (dash-dotted) and 0.1 (dotted).

Proof. The proof of this result is merely an algebraic task. We need only say that an application of the discrete Green's First Identity with $a_n = (u_n^{k+1} - 2u_n^{k-1})/2\Delta t$ is indispensable in order to reach the correct expression of the term with coefficient β. □

We conclude that the discrete energy associated with scheme (5.2) is a consistent approximation of order $\mathcal{O}(\Delta t)$ of the total energy of system (5.1), whereas the discrete rate of change of energy is consistent order $\mathcal{O}(\Delta t)^2$ with the instantaneous rate of change.

5.3.3 Stability analysis

The following result summarizes the numerical properties of our method.

PROPOSITION 4. *Scheme* (5.2) *is consistent order* $\mathcal{O}(\Delta t)^2$ *with the linear contribution of* (5.1) *for a potential equal to zero. Moreover, a necessary condition for the scheme to be stable order* n *is that*

$$\left(c^2 - \frac{m^2}{4}\right)(\Delta t)^2 < 1 + \left(\frac{\alpha}{4} + \beta\right)\Delta t.$$

Proof. Following the notation in [42], let $U_{1n}^{k+1} = u_n^{k+1}$ and $U_{2n}^{k+1} = u_n^k$ for each $n = 0, 1, \ldots, M$ and $k = 0, 1, \ldots, N-1$. For every $n = 0, 1, \ldots, M$ and $k = 1, 2, \ldots, N$ let $\bar{U}_n^k$ be the column vector whose components are U_{1n}^k and U_{2n}^k. Our problem can be written then in matrix form as

$$\begin{pmatrix} g & 0 \\ 0 & 1 \end{pmatrix} \bar{U}_n^{k+1} = \begin{pmatrix} 2 + c^2(\Delta t)^2\delta_x^2 & -h \\ 1 & 0 \end{pmatrix} \bar{U}_n^k,$$

where

$$\begin{aligned} g &= 1+\alpha\frac{\Delta t}{2}-\beta\frac{\Delta t}{2}\delta_x^2+m^2\frac{(\Delta t)^2}{2} \qquad \text{and} \\ h &= 1-\alpha\frac{\Delta t}{2}+\beta\frac{\Delta t}{2}\delta_x^2+m^2\frac{(\Delta t)^2}{2}. \end{aligned}$$

Applying Fourier transform to the vector equation we obtain

$$\hat{U}_n^{k+1}=\begin{pmatrix} \frac{2}{\hat{g}(\xi)}\left(1-2c^2(\Delta t)^2\sin^2\frac{\xi}{2}\right) & -\frac{\hat{h}(\xi)}{\hat{g}(\xi)} \\ 1 & 0 \end{pmatrix}\hat{U}_n^k.$$

The matrix $A(\xi)$ multiplying $\hat{U}_n^k$ in this equation is the amplification matrix of the problem. It is easy to check that the eigenvalues of A for $\xi=\pi$ are given by

$$\lambda_\pm=\frac{1-2c^2(\Delta t)^2\pm\sqrt{(1-2c^2(\Delta t)^2)^2-\hat{h}(\pi)\hat{g}(\pi)}}{\hat{g}(\pi)}.$$

Suppose for a moment that $1-2c^2(\Delta t)^2<-\hat{g}(\pi)$. If the radical in the expression for the eigenvalues of $A(\pi)$ is a pure real number then $|\lambda_-|>1$. So for every $n\in\mathbb{N}$, $||A^n||\geq|\lambda_-|^n$ grows faster than K_1+nK_2 for any constants K_1 and K_2. A similar situation happens when the radical is a pure imaginary number, except that in this case $|\cdot|$ represents the usual Euclidean norm in the field of complex numbers. Therefore in order for our numeric method to be stable order n it is necessary that $1-2c^2(\Delta t)^2>-\hat{g}(\pi)$, which is what we wished to establish. □

It is worth mentioning that our stability region is in agreement with the stability condition proposed in [61] when $c=1$ for a similar nonlinear continuous problem.

5.4 Numerical results

In this section we study the effects of the internal and external damping coefficients on the behavior of solutions to mixed-value problem (5.1). Particularly, we wish to establish the effect of weak damping on the minimum amplitude value necessary for the phenomenon of supratransmission to take place at a fixed driving frequency. Throughout we validate our code against [59] and against an implementation of our finite-difference scheme using the Runge-Kutta method of order four.

5.4.1 External Damping

For the remainder of this work we consider a semi-infinite coupled chain of oscillators initially at rest in their equilibrium positions, subject to harmonic forcing at the end described by $\psi(t)=A\sin(\Omega t)$ at any time t. The functions ϕ and φ are both identically equal to zero and, in order to avoid the shock wave produced by the vanishing initial velocity in the boundary, we let the driving amplitude linearly increase from 0 to A in a finite period of time before we start to compute the total energy. In the present section we will let β be equal to zero and consider a discrete

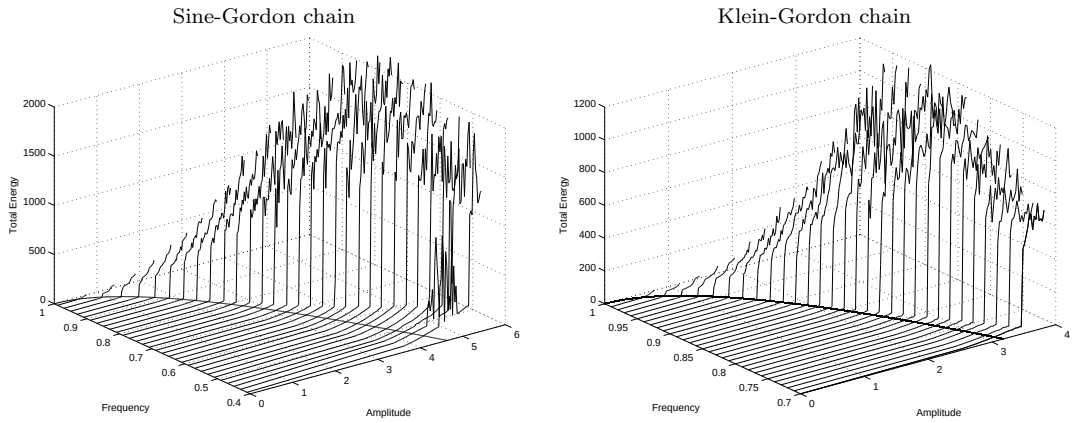

FIGURE 5.6: Graphs of total energy vs. driving frequency and amplitude for massless and undamped sine-Gordon and Klein-Gordon chains of coupled oscillators.

system of 200 coupled oscillators described by (5.1) over a typical time period of 200, with a time step of 0.05 and a coupling coefficient equal to 4.

Let us first examine the massless case when no damping is present at all and $\Omega = 0.9$. In order to verify that our mixed-value problem produces a bifurcation it is necessary to study the qualitative behavior of solutions near the predicted threshold value A_s which, in this case, reads approximately 1.80. The first row of Figure 5.1 shows the function $u_{60}(t)$ in the solution of a sine-Gordon system for two different values of the amplitude of the driving end, while the second row presents the corresponding graphs in the solution of a Klein-Gordon chain. The graphs evidence the presence of a bifurcation in the behavior of solutions around the amplitude value 1.79 for both chains.

Naturally, the next step in our investigation will be to determine the behavior of the total energy flow injected by the periodic forcing at the end of the undamped discrete chain of oscillators as a function of the amplitude. The solid lines of Figure 5.2 represent the graphs of total energy transmitted into the system vs. amplitude for a forcing frequency of 0.9 and external damping coefficient equal to zero, for a sine-Gordon system in the first column and a Klein-Gordon system in the second. It is worthwhile noticing the abrupt increase in the total energy administered to the system for some amplitude value between 1.77 and 1.79. This feature of the graphs evidences the existence of a bifurcation value around the predicted amplitude A_s, after which the phenomenon of nonlinear supratransmission takes place.

Figure 5.2 also presents graphs of total energy vs. forcing amplitude for weak constant damping coefficients $\gamma = 0.01$, 0.02 and 0.03 in a sine-Gordon system of oscillators. The graphs show a tendency of the bifurcation value to increase linearly as the external damping coefficient is increased. Another interesting feature of this figure is the decrease of total energy for increasing values of γ, at least for fixed amplitudes greater than the undamped bifurcation threshold. Needless to point out that similar conclusions are obtained for Klein-Gordon chains of oscillators.

The qualitative effect of m in a sine-Gordon system is also of interest in the analysis of solutions of this chain and is numerically carried out in Figure 5.3 for a chain with external damping equal to 0.01 and pure-imaginary and real masses, using

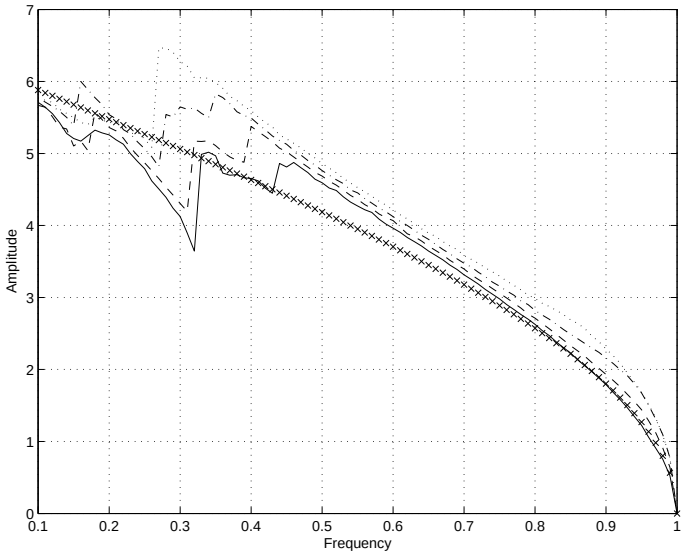

FIGURE 5.7: Diagram of smallest driving amplitude value at which supratransmission begins vs. driving frequency for a massless system with $\beta = 0$ and values of γ equal to 0 (solid), 0.1 (dashed), 0.2 (dash-dotted) and 0.3 (dotted). The theoretical threshold A_s in the undamped is shown as a sequence of $\times$-marks.

graphs of total energy administered into the system through the boundary vs. driving amplitude. A horizontal shift in the occurrence of the bifurcation value is readily noticed in these graphs. Indeed, the displacement of the bifurcation amplitude for the system (5.1) of mass m with respect to the bifurcation amplitude of the massless system is a monotone increasing function of m^2. Analogous computational results (not included here) were obtained for a similar Klein-Gordon chain.

5.4.2 Internal damping

Consider again a system of 200 oscillators ruled by mixed-value problem (5.1) over a time period of 200, with time step 0.05, coupling coefficient equal to 4 and constant external damping equal to zero. In this context, Figure 5.4 shows graphs of total energy vs. forcing amplitude for internal damping coefficients $\beta = 0$, 0.1, 0.2 and 0.3, for sine-Gordon and Klein-Gordon systems. As in the case of external damping, we observe that the threshold value at which supratransmission starts tends to increase as the value of β is increased. Opposite to the case of external damping, though, the minimum value for which supratransmission starts varies with β in a nonlinear way.

Next we verify our conclusions on the effect of the mass m on the qualitative behavior of solutions of the sine-Gordon system. Figure 5.5 shows graphs of total energy vs. driving amplitude for a system with no external damping, $\beta = 0.2$ and driving frequency of 0.9, for different pure-imaginary and real masses. As observed before, the graphs evidence a shift on the bifurcation amplitude with respect to the massless bifurcation value which is an increasing function of m^2.

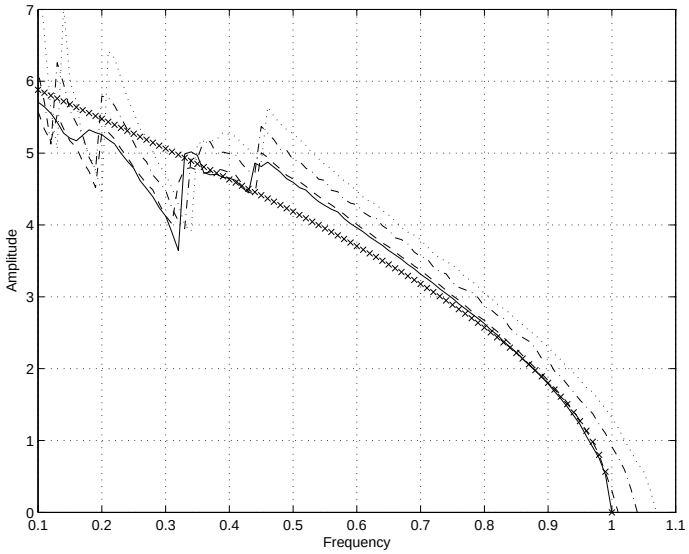

FIGURE 5.8: Diagram of smallest driving amplitude value at which supratransmission begins vs. driving frequency for a massless system with $\gamma = 0$ and values of β equal to 0 (solid), 0.1 (dashed), 0.4 (dash-dotted) and 0.7 (dotted). The theoretical threshold A_s in the undamped case is shown as a sequence of $\times$-marks.

5.4.3 Bifurcation analysis

Both the chain of coupled sine-Gordon equations and the chain of Klein-Gordon equations have numerically proved to undergo nonlinear supratransmission for a driving frequency equal to 0.9 and different values of the external and internal damping coefficients, thus establishing that the results obtained in this work do not depend on integrability. Naturally we are interested in determining that the process of nonlinear supratransmission happens for any frequency value in the forbidden band gap. With that purpose in mind, we obtained graphs of total energy vs. driving frequency and various amplitude values for undamped discrete systems of 200 coupled oscillators with coupling coefficient 4, time period of 200 and time step 0.05. The 3-dimensional results for both chains of oscillators are shown in Figure 5.6 together with a graph of the continuous-limit threshold amplitude As vs. driving frequency on the amplitude-frequency plane for comparison purposes.

Several observations may be immediately drawn from Figure 5.6. First of all, the predicted bifurcation values As display an excellent concordance to the corresponding values obtained using the finite difference-schemes associated with the sine-Gordon and the Klein-Gordon chains. Second, the process of supratransmission ceases to appear in the Klein-Gordon case for driving frequencies below 0.7. Third, for driving frequencies close to the band gap limit, the bifurcation threshold is not clearly determined from the energy vs. driving amplitude graph of the sine-Gordon chain, as prescribed by [59]. For those frequencies, it is indispensable to increase the time period of approximation at least up to 500. Fourth, strong numerical proof of the existence of the occurrence of the supratransmission process is at hand and we have now reasons to believe that there exists a bifurcation function $A(\Omega; \beta, \gamma, m^2)$ for driving amplitude associated with (5.1).

We proceed then to obtain graphs of amplitude values for which nonlinear

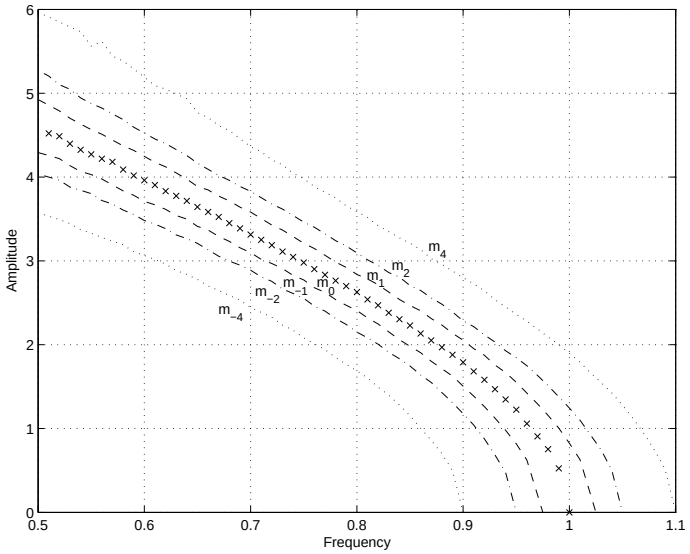

FIGURE 5.9: Diagram of smallest driving amplitude value at which supratransmission begins vs. driving frequency for an undamped sine-Gordon system with $\sqrt{m_\ell^2+1} = 1+\frac{\ell}{40}$ for $\ell = -4,\ -2,\ -1,\ 0,\ 1,\ 2,\ 4$.

supratrasmission starts vs. driving frequency for a massless sine-Gordon chain of coupled oscillators with internal damping coefficient equal to zero and different values of γ. The numerical results are summarized in Figure 5.7 together with the plot of the prescribed continuous-limit bifurcation amplitudes As. It is worth noticing that the bifurcation threshold increases with γ for fixed frequencies above 0.35, as previously evidenced for a frequency equal to 0.9. We must notice also that the discrepancies that appear for frequencies below 0.35 when $\gamma = 0$, also appear for greater values of γ, each time bounded in smaller intervals. In fact, we have checked that the discrepancy region — an effect of the phenomenon of harmonic phonon quenching — tends to vanish for higher values of external damping (results not included). In this state of matters, we wish to point out that better numerical approximations to the bifurcation threshold are obtained for larger systems of oscillators at the expense of superior needs in terms of computational time. Likewise, we have confirmed that larger values of the coupling coefficient lead to better approximations to the bifurcation threshold, as prescribed by [59].

Figure 5.8 shows bifurcation diagrams for a massless sine-Gordon system of oscillators with no external damping and different constant internal damping coefficients. As expected, the bifurcation threshold tends to increase with β for a fixed driving frequency. The effects of harmonic phonon quenching are present again in all the bifurcation diagrams, but contrary to the case of external damping, in the case of internal damping the range over which discrepancies occur slightly widens as β increases. Also, it is worth observing that the length of the forbidden band gap increases with the parameter β apparently in a linear fashion. Moreover, the graphs of bifurcation diagrams for nonzero values of β are approximately obtained by shifting horizontally the corresponding graph of the undamped diagram a number of β units to the right. More concretely, $A(\Omega; 0, 0, 0)$ is a good approximation for $A(\Omega - \beta; \beta, 0, 0)$.

Finally, we compute bifurcation diagrams for an undamped sine-Gordon system with different real and pure-imaginary masses in order to establish the effect of m on the occurrence of the bifurcation threshold. The numerical results are summarized in Figure 5.9 for some real and pure-imaginary masses, and driving frequencies starting at 0.5. Our results lead us to conclude that the bifurcation diagram of the sine-Gordon system of oscillators with mass m is approximately equal to the graph of the corresponding massless graph shifted $\sqrt{1+m^2}-1$ horizontal units, for $|m| \ll 1$. In order to test our claim numerically, we obtained graphs of absolute differences between the massless undamped bifurcation diagram, and shifted undamped bifurcation diagrams for several mass values (results not included). We observed that the differences tend to attenuate for high frequency values and that smaller differences are obtained for smaller values of m in magnitude.

5.5 Conclusions

In this paper we have developed a numerical method to approximate solutions of a semi-infinite nonlinear chain of coupled oscillators ruled by modified sine-Gordon equations harmonically driven at its end. The proposed finite-difference scheme is consistent order $\mathcal{O}(\Delta t)^2$ and we provided a necessary condition in order for the method to be stable order n. The process of nonlinear supratransmission for a coupled system of oscillators described by sine-Gordon equations was studied numerically under the scope of this numerical technique, and the dependence of supratransmission on damping was analyzed.

Several conclusions can be drawn from our computational experiments on the sine-Gordon system of coupled oscillators (5.1). First of all, we have shown that the phenomenon of harmonic phonon quenching still appears in the presence of external and internal damping and that the discrepancy region due to phonon quenching is shortened as the external damping coefficient is increased, while it slightly widens as the internal damping coefficient increases. Second, the threshold value at which supratransmission first occurs for fixed frequencies outside the discrepancy region is seen to increase for both external and internal damping as the damping coefficient increases; both conclusions are clearly consequences of the dispersive and dissipative natures of the parameters β and γ, respectively.

Finally, the bifurcation diagram for a value of the parameter β is approximately equal to the corresponding diagram for the undamped system shifted β horizontal units to the right. Likewise, a horizontal shift of $\sqrt{1+m^2}-1$ units in the bifurcation diagram of a sine-Gordon system of mass m with respect to the corresponding massless system is observed for small masses and frequencies outside the discrepancy region.

5.6 Acknowledgment

It is our duty to express our deepest gratitude to Dr. Álvarez Rodríguez, dean of the Centro de Ciencias Básicas of the Universidad Autónoma de Aguascalientes, and to Dr. Avelar González, head of the Dirección General de Investigación y Posgrado of the same university, for uninterestedly providing us with computational

resources to produce this article. The present work represents a set of partial results under project PIM07-2 at this university.

Chapter 6

An application of nonlinear supratransmission to the propagation of binary signals in weakly damped, mechanical systems of coupled oscillators

In the present article, we simulate the propagation of binary signals in semi-infinite, mechanical chains of coupled oscillators harmonically driven at the end, by making use of the recently discovered process of nonlinear supratransmission. Our numerical results — which are based on a brand-new computational technique with energy-invariant properties — show an efficient and reliable transmission of information.

6.1 Introduction

The process of nonlinear supratransmission consists of a sudden increase in the amplitude of wave signals transmitted into a nonlinear chain by a harmonic disturbance at the end, irradiating at a frequency in the forbidden band gap. The phenomenon was first discovered in mechanical chains of oscillators described by coupled sine-Gordon and Klein-Gordon equations [59], and it was quickly studied in other nonlinear models [60, 62, 63, 64]. Several applications of nonlinear supratransmission have been realized so far [65, 66], and more physical applications have been given a mathematical foundation to its realization [67, 68] have been suggested.

In this paper, we develop an application of nonlinear supratransmission to the propagation of binary signals in weakly damped semi-infinite mechanical chains of coupled oscillators, by modulating the amplitude of the driving signal at the end. The first section introduces the mathematical model under study and the energy expressions to be used. A numerical study of the idealized problem is carried out in the following section; here we provide a numerical analysis of the breather propagation, based on the method proposed in [69], which in turn is based on a numerical scheme to approximate radially symmetric solutions of modified Klein-Godon equations [61]. The next section presents a simulation of the propagation of a binary signal in a

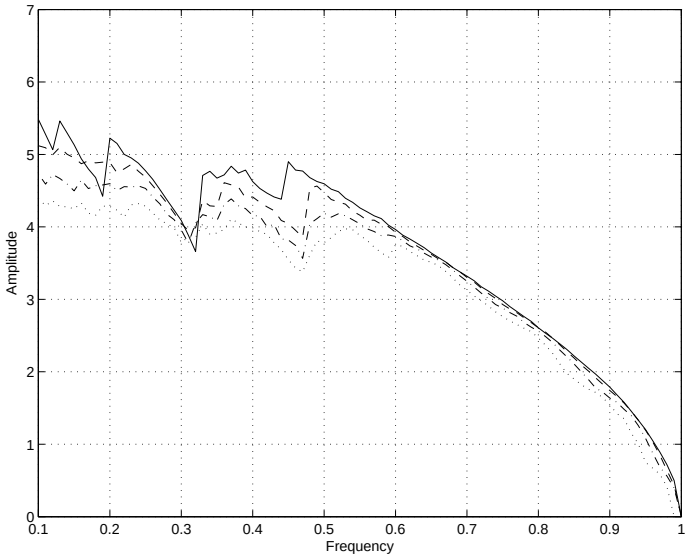

FIGURE 6.1: Bifurcation diagram of critical amplitude vs. driving frequency for system (6.1) for various values of γ: 0 (solid), 0.1 (dashed), 0.2 (dash-dotted), 0.3 (dotted).

weakly damped system. Finally, we present a section of concluding remarks and propose complementary directions of research.

6.2 Preliminaries

6.2.1 Mathematical model

Throughout this paper, we assume that α, β and γ are nonnegative real numbers, and that $c \gg 1$ (see [59]). Likewise, we consider a system $(u_n)_{n=1}^{\infty}$ of oscillators satisfying the mixed-value problem studied in [69], namely,

$$\begin{aligned} &\frac{d^2u_n}{dt^2} - \left(c^2 + \alpha\frac{d}{dt}\right)\Delta_x^2 u_n + \beta\frac{du_n}{dt} + V'(u_n) = 0, \\ &\text{subject to :} \quad \begin{cases} u_n(0) = 0, & n \in \mathbb{Z}^+, \\ \dfrac{du_n}{dt}(0) = 0, & n \in \mathbb{Z}^+, \\ u_0(t) = \psi(t), & t \geq 0, \end{cases} \end{aligned} \tag{6.1}$$

where c is the coupling coefficient, and α and β evidently play the roles of internal and external damping coefficients, respectively. Here, $\Delta_x^2 u_n$ is used to denote the spatial second-difference $u_{n+1} - 2u_n + u_{n-1}$ for every $n \in \mathbb{Z}^+$, the boundary-driving function is given by $\psi(t) = A(t)\sin(\Omega t)$ for every $t \in (0, +\infty)$, and $V(u_n) = 1 - \cos(u_n) - \gamma u_n$ where, due to the analogy with the Josephson model [70], γ will be called here the *normalized current*. Notice that the Hamiltonian of the n-th lattice site is given by

$$H_n = \frac{1}{2}\left[\dot{u}_n^2 + c^2(u_{n+1} - u_n)^2\right] + V(u_n),$$

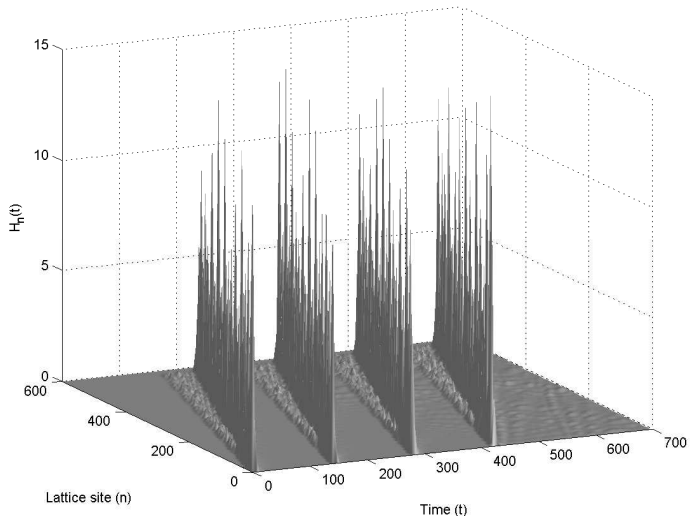

FIGURE 6.2: Local energies $H_n(t)$ of (6.1) vs. lattice site n and time t, corresponding to the transmission of binary signal '1111'.

for any differentiable function V. After including the potential energy from the coupling between the first two oscillators, the total energy of the system becomes

$$E = \sum_{n=1}^{\infty} H_n + \frac{c^2}{2}(u_1 - u_0)^2.$$

6.2.2 Numerical schemes

We consider a finite system of N differential equations satisfying (6.1), and a regular partition $0 = t_0 < t_1 < \cdots < t_M = T$ of the time interval $[0, T]$ with time step equal to Δt. For each $k = 0, 1, \ldots, M$, let us represent the approximate solution to our problem on the n-th lattice site at time t_k by u_n^k. If we convey that $\delta_t u_n^k = u_n^{k+1} - u_n^{k-1}$, that $\delta_t^2 u_n^k = u_n^{k+1} - 2u_n^k + u_n^{k-1}$ and that $\delta_x^2 u_n^k = u_{n+1}^k - 2u_n^k + u_{n-1}^k$, the differential equations in our problem take then the discrete form

$$\frac{\delta_t^2 u_n^k}{(\Delta t)^2} - \left(c^2 + \frac{\alpha}{2\Delta t}\delta_t\right)\delta_x^2 u_n^k + \frac{\beta'}{2\Delta t}\delta_t u_n^k + \frac{V(u_n^{k+1}) - V(u_n^{k-1})}{u_n^{k+1} - u_n^{k-1}} = 0, \qquad (6.2)$$

where β' includes both the effect of external damping and a simulation of an absorbing boundary slowly increasing in magnitude on the last $N - N_0$ oscillators. More concretely, we let $u_{N+1}(t)$ be equal to zero at all time t, and let β' be the sum of external damping and the function

$$\beta''(n) = 0.5\left[1 + \tanh\left(\frac{2n - N_0 + N}{6}\right)\right],$$

where usually $N_0 = 50$ and $N \geq 200$.

Finite-difference scheme (6.2) (which is a modified version of the one proposed

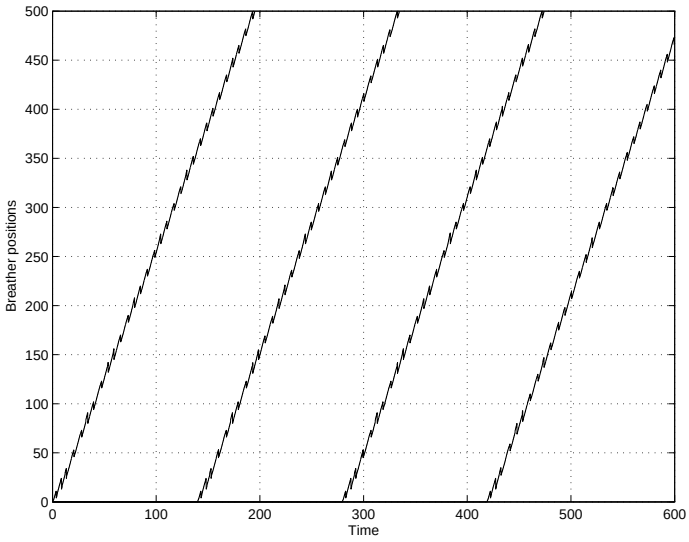

FIGURE 6.3: Time-dependent graphs of the position of the breathers generated in (6.1) by the binary signal '1111'.

in [61]) is consistent with our mixed-value problem and conditionally stable, having the inequality $(c\Delta t)^2 < 1 + (\alpha + \beta'/4)\,\Delta t$ as a necessary condition for stability when β' is assumed constant [69]. Moreover, if the energy of the system at the k-th time step is computed using the expression

$$\begin{aligned} E_k &= \frac{1}{2}\sum_{n=1}^{M}\left(\frac{u_n^{k+1}-u_n^k}{\Delta t}\right)^2 + \frac{c^2}{2}\sum_{n=1}^{M}(u_{n+1}^{k+1}-u_n^{k+1})(u_{n+1}^k-u_n^k) \\ &\quad + \sum_{n=1}^{M}\frac{V(u_n^{k+1})+V(u_n^k)}{2} + \frac{c^2}{2}(u_1^{k+1}-u_0^{k+1})(u_1^k-u_0^k), \end{aligned}$$

then the discrete rate of change of energy turns out to be a consistent approximation of order $\mathcal{O}(\Delta t)^2$ for the corresponding instantaneous rate of change.

6.3 Numerical study

6.3.1 Bifurcation analysis

The existence of a bifurcation threshold of the energy administered into a semi-infinite chain of damped coupled oscillators described by (6.1) has been established and numerically predicted in [69] for a potential $V(u) = 1 - \cos u$. Numerical experiments on undamped mechanical chains with nonzero normalized bias currents have shown that the process of nonlinear supratransmission is likewise present in these models. In fact, Fig. 6.1 provides bifurcation diagrams of driving amplitude at which supratransmission first occurs vs. driving frequency Ω for a system of 200 undamped oscillators with coupling coefficient equal to 4 and several values of γ, over a time interval $[0, T(\Omega)]$ where $T(\Omega)$ is equal to 200 for all frequencies except for those satisfying $\Omega > 0.95$, in which case $T(\Omega)$ had to be increased up to 500.

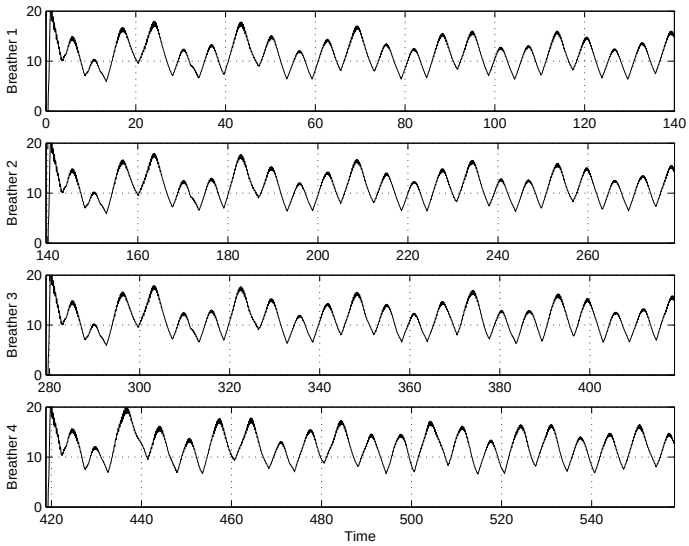

FIGURE 6.4: Time-dependent graphs of the maximum energy of the breathers generated in (6.1) by the binary signal '1111'.

6.3.2 Moving breather solutions

For the sake of simplification, let $\gamma = 0$ and consider a discrete system described by (6.1), harmonically driven at the boundary by a frequency Ω. A binary bit b will be transmitted into the medium during a fixed and sufficiently long period of signal generation P equal to an integer multiple of the driving period, by defining

$$A(t) = \frac{8}{5} bCA_s \left(e^{-\Omega t/4.5} - e^{-\Omega t/0.45} \right)$$

for every $t \in [0, P]$, where A_s represents the critical amplitude at which nonlinear supratransmission starts and $C > 0$ is an *adjusting constant*.

Fig. 6.2 shows the time evolution of the local energies H_n corresponding to solutions of the undamped problem (6.1) with coupling coefficient equal to 4, driving frequency 0.9 (in which case A_s is approximately equal to 1.79) and $C = A_s$. The period of signal generation is equal to 20 driving periods, and the binary code transmitted at the boundary is '1111'. The results show that a single moving breather is generated per period, and that the phase velocity v_p through the medium is approximately constant. To verify this claim, we include in Fig. 6.3 the graphs of the positions of the four breathers generated by the binary signal vs. time. The fact that the breathers are transmitted at a constant velocity is now obvious, the common phase velocity being approximately 2.549.

In order to determine the strength of the emitted signals at sites located far away from the source, it is important to determine the time behavior of the maximum local energy attained by a discrete breather. Fig. 6.4 presents this behavior for the breather solutions obtained under the conditions above. Notice that the maximum local energy is well above a cutoff limit of 2.

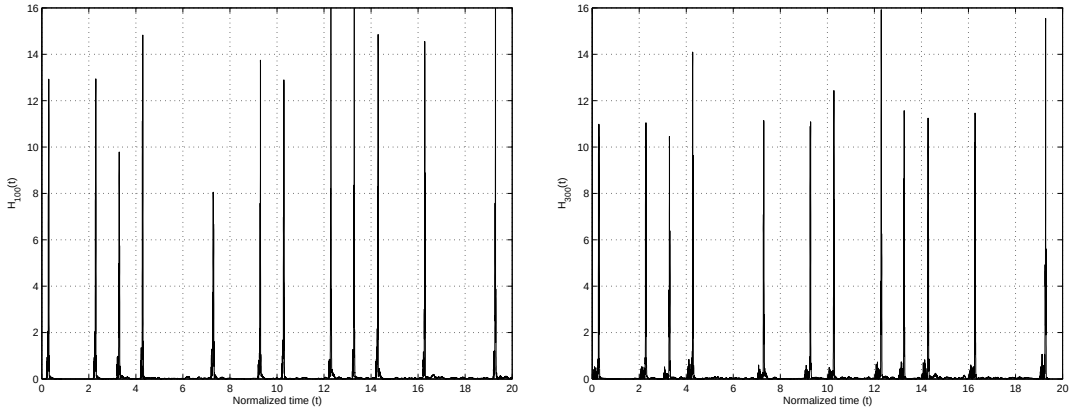

FIGURE 6.5: Local energy of the 100-th (left) and 300-th (right) sites in (6.1) vs. normalized time, as a response to the transmission of the binary signal '10111001011011101001'.

6.4 Application

The discrete medium described by (6.1) with $\alpha = \beta = \gamma = 1 \times 10^{-3}$, and the rest of the parameters as in the previous section, will be our object of study in this section. Local energy-based reception devices will be placed on the 100-th and 300-th lattice sites, and the signal to be transmitted through the chain system is '10111001011011101001'. Our system will consist of 600 sites, and a time step of 0.05 will be employed.

Assuming the general convention that site $n_0 \geq 100$ will start signal reception at time $t = (n_0 - 100)/v_p$, Fig. 6.5 shows the evolution of the local energy in the 100-th and 300-th sites in terms of the time normalized with respect to the period of signal generation. In either case, it is clear that the transmission of a bit equal to 1 in the n-th period is completely characterized in the graph by peak(s) of height greater than the cutoff limit 2 on the interval $[n-1, n]$.

6.5 Conclusions and perspectives

In this letter, we have proposed a simple mathematical model to transmit binary information in discrete, semi-infinite chains of couped oscillators using the process of nonlinear supratransmission. In the absence of dispersive and dissipative effects, our model (which is based on the modulation of amplitudes of source signals with constant frequency) has shown to be highly reliable for sufficiently long periods of single-bit generation, independently of the distance between the source of transmission and the point of reception.

When weak damping is present the general picture does not change much. Stronger damping, however, manifests itself through a substantial decrease in the amplitude of the maximum local energy of the moving breathers with respect to the lattice site. In a forthcoming work, we will examine the possibility to overcome this problem via the concatenation of chain systems, where the driving at the beginning of each lattice will irradiate with an amplitude equal to a value just below its critical point multiplied by the amplitude of the last site in the previous lattice.

Finally, we wish to point out that the problem of determining whether it is possible to design a propagation system of binary signals in Josephson junction arrays still remains an open topic of research. Moreover, in view of the recently discovered phenomenon of nonlinear infratransmission (or lower-transmission, as named by the authors [62]), the problem of finding more efficient pathways to achieve signal transmission in other models is still an open question of general interest.

6.6 Acknowledgments

One of us (J. E. M. D.) wishes to express his most sincere gratitude to Dr. Álvarez Rodríguez, dean of the Centro de Ciencias Básicas of the Universidad Autónoma de Aguascalientes, and to Dr. Avelar González, head of the Dirección General de Investigación y Posgrado of the same university, for providing him with the physical means to produce this article. He also wishes to acknowledge enlightening conversations with Prof. F. Rizo Díaz in the Departamento de Sistemas Electrónicos. The present work represents a set of partial results under project PIM07-2 at this university.

Chapter 7

On the propagation of binary signals in damped mechanical systems of oscillators

In the present work, we explore efficient ways to transmit binary information in discrete, semi-infinite chains of coupled oscillators using the process of nonlinear supratransmission. A previous work showed that such transmission is possible and, indeed, reliable under the idealistic condition when weak or no damping is present. In this paper, we study a more realistic case and propose the design of mechanical devices in order to avoid the loss of information, consisting on the linear concatenation of several such mechanical systems. Our results demonstrate that the loss of information can be minimized or avoided using such physical structures.

7.1 Introduction

The recently discovered process of energy transmission in the forbidden band gap of nonlinear chains [71] has opened a wide variety of new physical applications. This phenomenon consists in the sudden increase in the amplitude of wave signals that propagate in a semi-infinite, discrete, nonlinear chain driven at its end by a harmonic disturbance irradiating at a frequency in the forbidden band gap, and it has been studied in sine-Gordon and Klein-Gordon systems [59], double sine-Gordon systems [60], Fermi-Pasta-Ulam systems [62], Bragg media in the nonlinear Kerr regime [63], and even in continuous, nonlinear, bounded media described by undamped sine-Gordon equations driven at one end [64].

From a mathematical point of view, the theory that describes the mechanism sustaining the phenomenon of nonlinear supratransmission has not been entirely unveiled in general. In fact, most of the analytical results on undamped, discrete systems that we posses nowadays rely on the use of approximation techniques such as the rotating wave approximation [62], or the study of the continuous limiting case [59]. Meanwhile, the study of the damped case has relied on the development of new perturbation methods for the weakly damped scenario [72], and the use of conventional or sofisticated computational techniques [69].

From an experimental perspective, the phenomenon of supratransmission in nonlinear media described by sine-Gordon equations was first observed in mechanical systems of coupled pendula [60], and applications to the design of digital amplifiers of ultra weak signals [65] and light detectors sensitive to very weak excitations [66] have been realized recently. Further applications to optical waveguide arrays using the discrete nonlinear Schrödinger equation [67], the realization of light filters [68], and the propagation of binary signals in undamped or weakly damped mechanical chains of oscillators [73] have been proposed.

In this article, we tackle the problem of propagating binary signals in damped, discrete sine-Gordon systems through amplitude modulation (a rather interesting physical problem not studied hitherto), with future studies of signal transmission in Josephson-junction arrays in mind. We make use of analytical approximations and perturbation methods derived from the continuous limiting situation (equivalently, the strongly coupled case) in order to propose the design of a propagation device for binary signals in damped mechanical systems. Our numerical study will be based on a novel computational technique with energy-invariance properties [69], and the proposed designs will be based on the serial concatenation of such systems.

Section 7.2 of this work is devoted to introduce the model under study, analytical results on the exact solution of the classical sine-Gordon equation, and the perturbation technique used; the presentation of the computational method to be employed, the finite-difference scheme to estimate the continuous energy and the numerical prediction of the supratransmission occurrence will be the topic of study in Section 7.3. Section 7.4 presents the mathematical procedure to generate binary signals, and analyzes characteristics of the propagating signals in the discrete system with respect to the value of the damping coefficients and the normalized bias current. In Section 7.5, we propose an alternative for the efficient propagation of binary signals in discrete sine-Gordon systems based on the linear concatenation of semi-infinite chain either bound mechanically of energetically. The results of the simulations for both models are presented in this section, and we summarize our conclusions and propose new directions of future research in a final stage.

7.2 Analysis

7.2.1 Mathematical model

Throughout this paper, we assume that α, β, γ and c are nonnegative real numbers. Likewise, we consider a system $(u_n)_{n=1}^{\infty}$ of particles satisfying the mixed-value problem studied in [69], namely,

$$\begin{aligned} &\frac{d^2u_n}{dt^2} - \left(c^2 + \alpha\frac{d}{dt}\right)\Delta_x^2 u_n + \beta\frac{du_n}{dt} + V'(u_n) = 0, \\ &\text{subject to :} \quad \begin{cases} u_n(0) = 0, & n \in \mathbb{Z}^+, \\ \dfrac{du_n}{dt}(0) = 0, & n \in \mathbb{Z}^+, \\ u_0(t) = \psi(t), & t \geq 0, \end{cases} \end{aligned} \tag{7.1}$$

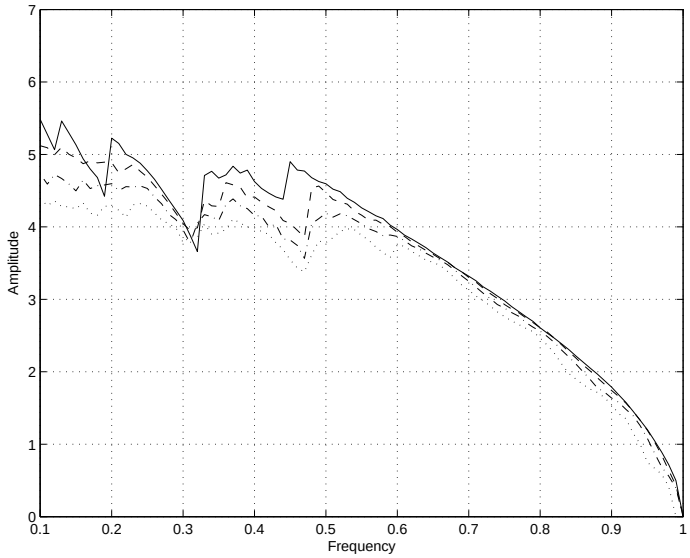

FIGURE 7.1: Bifurcation diagram of occurrence of critical amplitude versus driving frequency for problem (7.1) with $c = 4$ (solid line). The limiting solution to (7.2) is depicted as a sequence of crosses.

where α and β evidently function as the internal and external damping coefficients, respectively. Here, $\Delta_x^2 u_n$ is used to denote the spatial second-difference $u_{n+1} - 2u_n + u_{n-1}$ for every $n \in \mathbb{Z}^+$, the boundary-driving function is given by $\psi(t) = A(t)\cos(\Omega t)$ for every $t \in (0, +\infty)$, and $V(u_n) = 1 - \cos(u_n) - \gamma u_n$ where, due to its analogy with the model describing long Josephson junctions, the parameter γ will be denominated the *normalized bias current*. Notice that the Hamiltonian of the n-th site is

$$H_n = \frac{1}{2}\left[\dot{u}_n^2 + c^2(u_{n+1} - u_n)^2\right] + V(u_n),$$

for any differentiable function V. After including the potential energy from the coupling between the first two oscillators, the total energy of the system becomes

$$E = \sum_{n=1}^{\infty} H_n + \frac{c^2}{2}(u_1 - u_0)^2.$$

The next result provides us with a convenient way to compute the instantaneous rate of change of the energy for solutions of (7.1) with *square-summable* derivatives in time, that is, solutions $(u_n(t))_{n=0}^{\infty}$ for which $\sum \dot{u}_n^2(t)$ is convergent for every $t \geq 0$.

THEOREM 1 (Macías-Díaz and Puri [69]). *Let $(u_n(t))_{n=0}^{\infty}$ be a solution of system (7.1) such that $(\dot{u}_n(t))_{n=0}^{\infty}$ is square-summable at any fixed time t. The instantaneous rate of change of the total energy in the system is given by*

$$\frac{dE}{dt} = c^2(u_0 - u_1)\dot{u}_0 - \gamma\sum_{n=1}^{\infty}(\dot{u}_n)^2 - \beta\left[\sum_{n=1}^{\infty}(\dot{u}_n - \dot{u}_{n-1})^2 + (\dot{u}_1 - \dot{u}_0)\dot{u}_0\right].$$

□

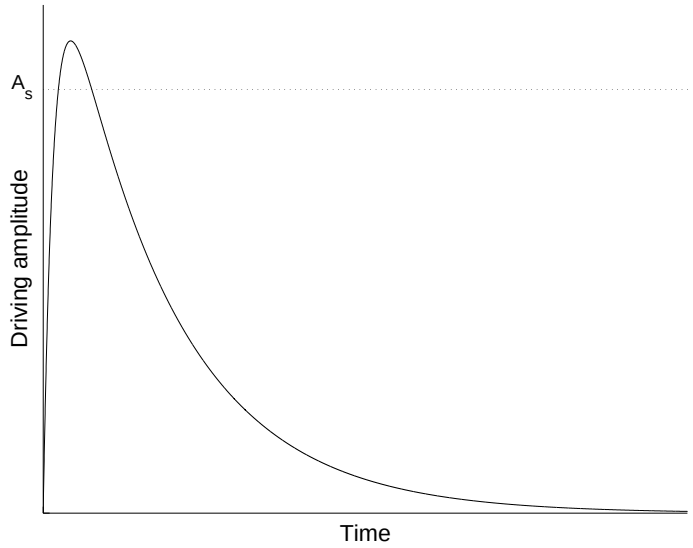

FIGURE 7.2: Time-dependent graph of the amplitude function used to generate a bit of '1' in a semi-infinite, discrete, mechanical array, with unitary amplification coefficient.

COROLLARY 2 (Geniet and Leon [60]). *Let* $(u_n(t))_{n=0}^{\infty}$ *be a solution of undamped system* (7.1) *with* $\gamma = 0$, *such that* $(\dot{u}_n(t))_{n=0}^{\infty}$ *is square-summable at any time* t. *Then*

$$E(t) = -c^2 \int_0^t \dot{u}_0(s)(u_1(s) - u_0(s))\, ds$$

□

We wish to mention that qualitative results similar to those presented here were obtained using the expressions of the individual energies provided by [74]. These formulas were used for validation purposes only.

7.2.2 The continuous approximation

For theoretical purposes, we will provisionally assume that $\alpha = \beta = 0$, and will consider a long, linear array consisting of N coupled oscillators described by the system of differential equations in (7.1), with a coupling coefficient $1 \ll c \ll , N$. Under these conditions, the problem under study can be approximated by the continuous, mixed-value problem

$$\begin{aligned} &\frac{\partial^2 u}{\partial t^2} - \frac{\partial^2 u}{\partial x^2} + V'(u) = 0, \\ \text{subject to :} \quad &\begin{cases} u(x,0) = 0, & 0 \le x \le L, \\ \dfrac{\partial u}{\partial t}(x,0) = 0, & 0 \le x \le L, \\ u(0,t) = \psi(t), & t \ge 0, \end{cases} \end{aligned} \tag{7.2}$$

where $L = N/c$, which in turn can be simplified to the study of a sine-Gordon model when the normalized bias current is equal to zero. For a sufficiently long linear chain, a sufficiently short interval of time $[0, T]$, and a driving function $\psi(t) = A_0 \cos(\Omega t)$, it is reasonable to impose the boundary condition $u_x(L, t) = 0$.

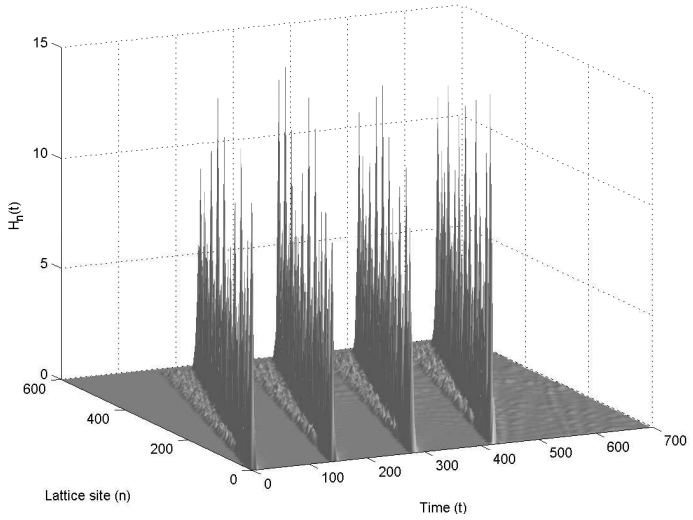

FIGURE 7.3: Local energies $H_n(t)$ of unperturbed system (7.1) vs. site n and time t, corresponding to the transmission of binary signal '1111', with $\Omega = 0.9$.

Following [64] now, there exist solutions to problem (7.2) in the form

$$u(x,t) = 4\arctan[X(x)T(t)],$$

with $X(L) = A_L$ and normalized time scale T satisfying $T(t_0) = 1$ for some time t_0. We assume that the solutions are periodic in time with period equal to the driving period, and that the solutions adapt to the driving amplitude, that is, $A_0 = 4\arctan(a)$, which yields $X(0) = a$. These solutions are seen to depend on a free parameter λ and the parameter

$$\Gamma = A_L^{-2} + \frac{1}{\lambda(1+A_L^2)}.$$

The relations between a, A_L and λ are summarized in the following result. Here $\mathbb{K}(m)$, $\mathrm{sn}(\cdot,m)$, $\mathrm{cn}(\cdot,m)$ and $\mathrm{dn}(\cdot,m)$ are the complete elliptic integral of the first kind, the sine-amplitude and the cosine-amplitude Jacobi elliptic function of modulus m, and the identity-amplitude Jacobi elliptic function of modulus m, respectively.

THEOREM 3 (Khomeriki and Leon [64]).

(1) *If $\lambda > 0$ then $X = A_L\,\mathrm{cn}(k(x-L),\mu)$ and $T = \mathrm{cn}(\omega(t-t_0),\nu)$, with equations $\Omega\mathbb{K}(\nu) = \frac{\pi}{2}\omega$ and $a = A_L\,\mathrm{cn}(kL,\mu)$ being satisfied for*

$$\begin{aligned} \omega^2 &= \lambda(1+\Gamma), & \nu^2 &= \frac{1}{1+\Gamma}, \\ k^2 &= \lambda\Gamma\left(A_L^2 + \frac{1}{\Gamma A_L^2}\right), & \mu^2 &= \frac{\Gamma A_L^2}{1+\Gamma A_L^4}. \end{aligned}$$

(2) *If $\lambda < 0$ and $\Gamma A_L^4 < -1$ then $X = A_L\,\mathrm{dn}(k(x-L),\mu)$ and $T = \mathrm{sn}(\omega(t-$*

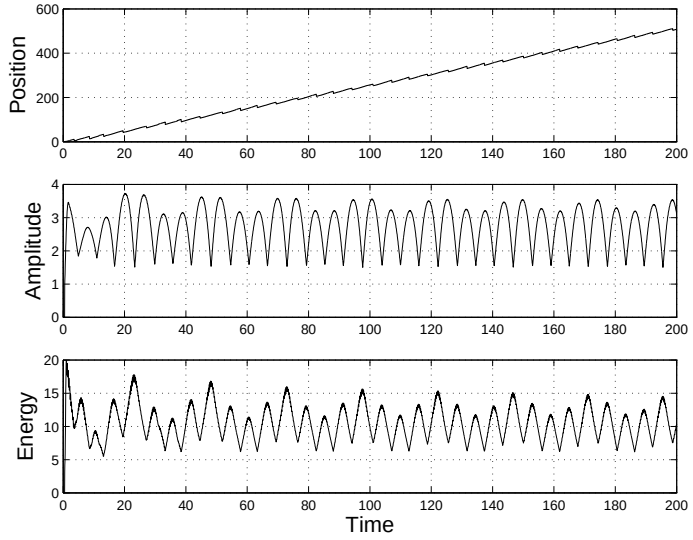

FIGURE 7.4: Time-dependent graphs of the position and maximum energy amplitude of the breather generated in unperturbed system (7.1) by bit '1', with $\Omega = 0.9$.

$t_1), \mu)$, *with equations* $\Omega\mathbb{K}(\nu) = \frac{\pi}{2}\omega$ *and* $a = A_L \,\mathrm{dn}(kL, \mu)$ *satisfied for*

$$\begin{aligned} \omega^2 &= \lambda\Gamma, & \nu^2 &= -\frac{1}{\Gamma}, \\ k^2 &= \lambda\Gamma A_L^2, & \mu^2 &= 1 + \frac{1}{\Gamma A_L^4}, \\ t_1 &= t_0 + \frac{\mathbb{K}(\nu)}{\omega}. \end{aligned}$$

(3) *If* $\lambda < 0$ *and* $\Gamma A_L^4 > -1$ *then* $X = A_L \,\mathrm{dn}^{-1}(k(x-L), \mu)$ *and* $T = \mathrm{sn}(\omega(t - t_1), \mu)$, *where* $\Omega\mathbb{K}(\nu) = \frac{\pi}{2}\omega$ *and* $a = A_L \,\mathrm{dn}^{-1}(kL, \mu)$ *are satisfied for*

$$k^2 = -\frac{\lambda}{A_L^2}, \qquad \mu^2 = 1 + \Gamma A_L^4,$$

and for ω^2, ν^2 *and* t_1 *as in* (2). □

COROLLARY 4 (Khomeriki and Leon [64]). *The limiting solution of mixed-value problem* (7.2) *as* $L \to \infty$ *is given by*

$$u(x,t) = 4 \arctan\left(a_s \frac{\sin(\omega(t - t_0))}{\cosh(kx)}\right),$$

when $\psi(t) = A_0 \sin(\Omega t)$. *Here* $a_s^2 = A^2(1-\mu^2)^{-1}$ *and the rest of the parameters are as in* (3) *of Theorem* 3. □

7.2.3 Perturbation analysis

In this section, we will assume that $u(x,t)$ represents an exact solution of the unperturbed sine-Gordon equation in (7.2) with $-\infty < x < \infty$, and that β and γ are

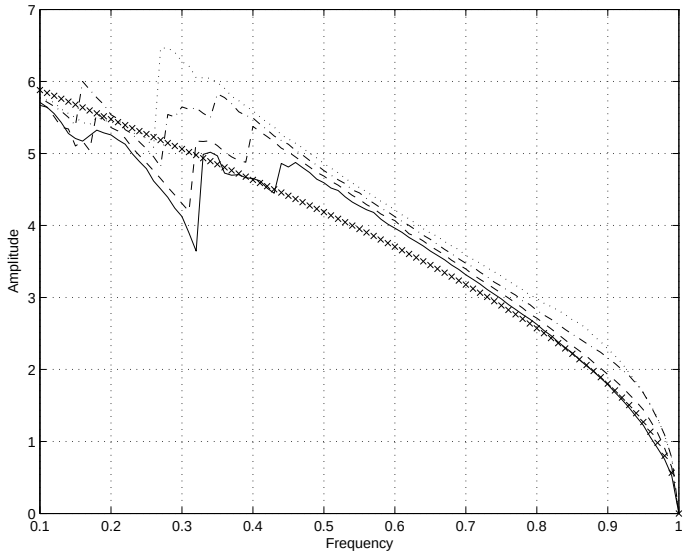

FIGURE 7.5: Bifurcation diagram of occurrence of critical amplitude versus driving frequency for problem (7.1) with $c = 4$, for $\beta = 0$ (solid), 0.1 (dashed), 0.2 (dashed-dotted), 0.3 (dotted). The limiting solution to unperturbed system (7.2) is depicted as a sequence of crosses.

small, nonnegative real numbers. We will consider the perturbed sine-Gordon model

$$\frac{\partial^2 v}{\partial t^2} - \frac{\partial^2 v}{\partial x^2} + \beta \frac{dv}{dt} + \sin v - \gamma = 0, \qquad -\infty < x < \infty.$$

Following [72], we assume the existence of a solution of the perturbed sine-Gordon equation of the form $u(g(\phi(t))x, T(t), \phi(t))$ with

$$T(t) = \int_0^t g(\phi(s))\phi(s)ds \qquad \text{and} \qquad g(\phi) = (1 \pm \phi^2)^{-1/2},$$

for some suitable function ϕ. If we let u be a localized intrinsic mode (static breather) solution of the unperturbed model confined in some region $|x| < \delta$, then

$$\frac{\partial u}{\partial t} \approx \frac{\partial u}{\partial T} g(\phi)\phi,$$

and it follows that the Hamiltonian of the unperturbed sine-Gordon equation can be approximated through the expression

$$H^*(\phi(t)) = \int_{-\infty}^{\infty} \left[\frac{1}{2} \left(\frac{\partial u}{\partial T} g(\phi)\phi \right)^2 + \frac{1}{2} \left(\frac{\partial u}{\partial x} \right)^2 + 1 - \cos u \right] dx.$$

It can be shown then that the relation between the variables ϕ, t and T is described

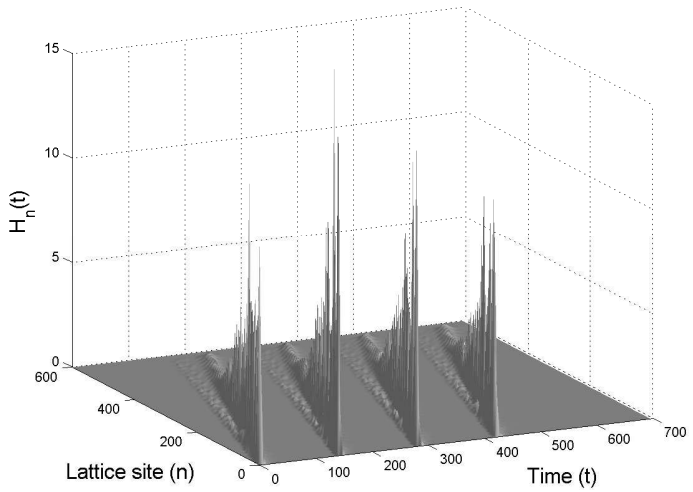

FIGURE 7.6: Local energies $H_n(t)$ of perturbed system (7.1) with $\beta = 0.01$ vs. lattice site n and time t, corresponding to the transmission of binary signal '1111', with $\Omega = 0.9$.

through the system

$$\begin{cases} \dfrac{d\phi}{dT} &= -\dfrac{1}{\phi g(\phi)\dfrac{dH^*}{d\phi}} \displaystyle\int_{-\infty}^{\infty} \left[\beta \left(\frac{du}{dt}\right)^2 + \gamma \frac{du}{dt}\right] dx, \\ \dfrac{dt}{dT} &= \dfrac{1}{\phi g(\phi)}. \end{cases}$$

7.3 Computational approach

7.3.1 Finite-difference schemes

We consider a finite system of N differential equations satisfying (7.1), and a regular partition $0 = t_0 < t_1 < \cdots < t_M = T$ of the time interval $[0, T]$ with time step equal to Δt. For each $k = 0, 1, \ldots, M$, let us represent the approximate solution to our problem on the n-th lattice site at time t_k by u_n^k. If we convey that $\delta_t u_n^k = u_n^{k+1} - u_n^{k-1}$, that $\delta_t^2 u_n^k = u_n^{k+1} - 2u_n^k + u_n^{k-1}$ and that $\delta_x^2 u_n^k = u_{n+1}^k - 2u_n^k + u_{n-1}^k$, the N differential equations in our problem take then the discrete form

$$\frac{\delta_t^2 u_n^k}{(\Delta t)^2} - \left(c^2 + \frac{\alpha}{2\Delta t}\delta_t\right)\delta_x^2 u_n^k + \frac{\beta'}{2\Delta t}\delta_t u_n^k + \frac{V(u_n^{k+1}) - V(u_n^{k-1})}{u_n^{k+1} - u_n^{k-1}} = 0, \qquad (7.3)$$

where β' includes both the effect of external damping and a simulation of an absorbing boundary slowly increasing in magnitude on the last $N - N_0$ oscillators. More concretely, we let $u_{N+1} = u_N$ at all time, and let β' be the sum of external damping and the function

$$\beta''(n) = 0.5\left[1 + \tanh\left(\frac{2n - N_0 + N}{6}\right)\right],$$

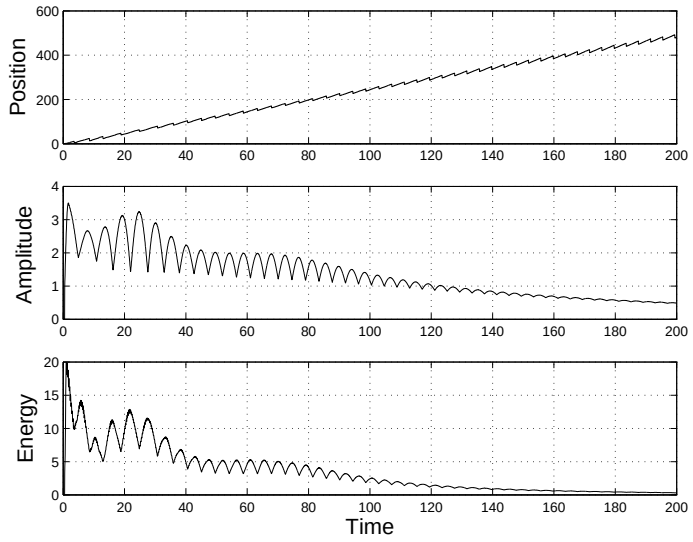

FIGURE 7.7: Time-dependent graphs of the position and maximum energy amplitude of the breather generated by bit '1' in (7.1) with $\beta = 0.01$ and $\Omega = 0.9$.

where usually $N_0 = 50$ and $N \geq 200$.

Finite-difference scheme (7.3) (which is a modified version of the one developed in [61] to compute radially symmetric solutions of modified Klein-Gordon equations) is consistent with our mixed-value problem and conditionally stable, having the inequality $(c\Delta t)^2 < 1 + (\alpha + \beta'/4)\,\Delta t$ as a necessary condition for stability when β' is assumed constant [69]. Moreover, if the energy of the system at the k-th time step is computed using the expression

$$E_k = \sum_{n=1}^{M} H_n^k + \frac{c^2}{2}(u_1^{k+1} - u_0^{k+1})(u_1^k - u_0^k),$$

where the individual energy of the n-th lattice site is computed by

$$H_n^k = \frac{1}{2}\left(\frac{u_n^{k+1} - u_n^k}{\Delta t}\right)^2 + \frac{c^2}{2}(u_{n+1}^{k+1} - u_n^{k+1})(u_{n+1}^k - u_n^k) + \frac{V(u_n^{k+1}) + V(u_n^k)}{2},$$

then the discrete rate of change of energy turns out to be a consistent approximation of order $\mathcal{O}(\Delta t)^2$ for the corresponding instantaneous rate of change, while the approximations of the individual and the total energies are consistent estimates order $\mathcal{O}(\Delta t)$ of their continuous counterparts.

7.3.2 Supratransmission threshold

It has been proved that a discrete or continuous medium described by damped problem (7.1) or undamped problem (7.2), respectively, can undergo nonlinear energy transmission when the driving amplitude is increased above a critical threshold that depends on the driving frequency, and which has been numerically predicted in [69, 64]. In the discrete case particularly, the numerical results obtained using the computational technique described in the previous section have produced bifurcation

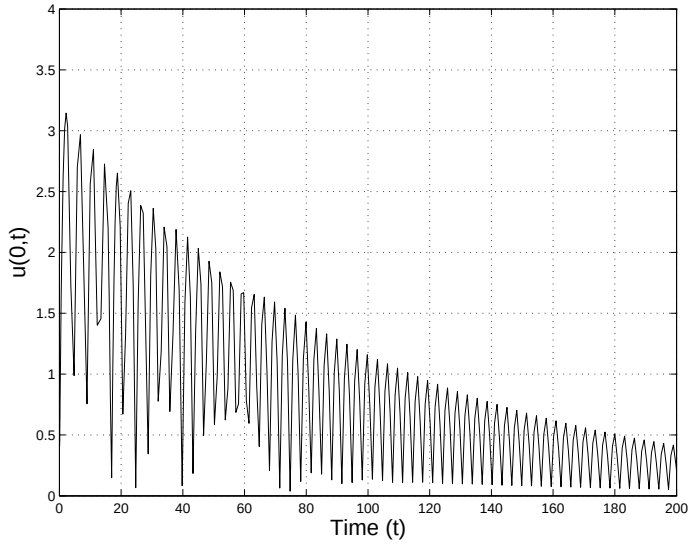

FIGURE 7.8: Time-dependent graph of decay of a static breather in infinite system (7.2), for constant damping $\beta = 0.01$.

diagrams for various values of α, β and γ, which are in excellent agreement with the undamped, unbiased formulation of the problem for large coupling coefficients. In this case the bifurcation threshold can be approximated via the continuous approximation provided by Corollary 4, which in turn can be approximated through

$$A_s = 4 \arctan\left(\frac{\sqrt{1-\Omega^2}}{\Omega}\right). \tag{7.4}$$

For the sake of convenience, we have included a bifurcation diagram in Figure 7.1, which shows the numerical (solid line) and theoretical (sequence of crosses) critical amplitude at which supratransmission starts for each frequency Ω in the forbidden band gap. The theoretical approximation was realized using (7.4).

In the continuous limit, the mechanism of the bifurcation is explained by the fact that the medium starts to transmit energy in the form of moving breathers once the driving amplitude reaches its critical value [64], and the medium continues transmitting energy well until a vanishing driving amplitude is reached. In the discrete case, it has been checked numerically that this phenomenon still occurs [59], and that the expression of the moving breathers is given by

$$u_n(t) = 4 \arctan\left[\frac{r \sin\left(\frac{1}{\sqrt{1+r^2}} \frac{t-vn/c}{\sqrt{1-v^2}}\right)}{\cosh\left(\frac{r}{\sqrt{1+r^2}} \frac{n/c-vt}{\sqrt{1-v^2}}\right)}\right],$$

where r and v represent, respectively, the group amplitude and the group velocity of the breather. Numerical experiments have shown that r and v are variables that linearly depend on A_s, for values of $0.87 < \Omega < 1$ (see [60]). Moreover, we have verified numerically that the amplitude of the emitted breathers tend to decrease as the driving amplitude is decreased from A_s toward zero.

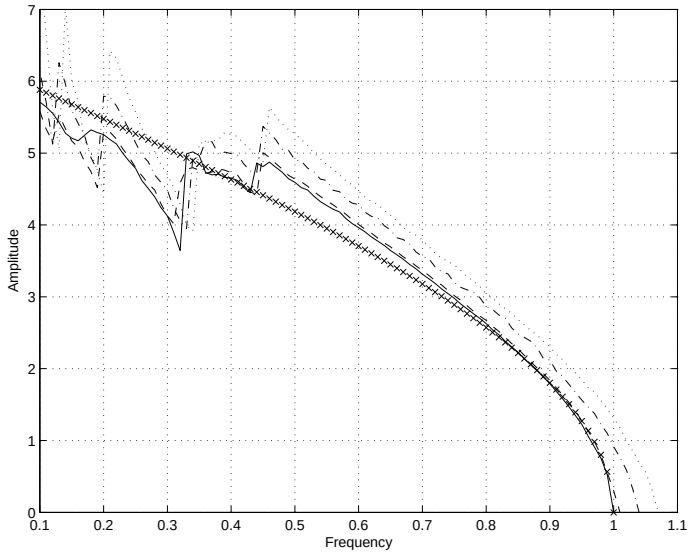

FIGURE 7.9: Bifurcation diagram of occurrence of critical amplitude versus driving frequency for problem (7.1) with $c = 4$, for $\alpha = 0$ (solid), 0.1 (dashed), 0.4 (dashed-dotted), 0.7 (dotted). The limiting solution to unperturbed system (7.2) is depicted as a sequence of crosses.

7.4 Numerical results

Following [73], in this section we consider a semi-infinite, mechanical system described by (7.1). A single binary bit b will be transmitted into the medium during a fixed and sufficiently long period of time P equal to an integer multiple of the driving period, by letting

$$A(t) = \frac{8}{5} b C A_s \left(e^{-\Omega t/4.5} - e^{-\Omega t/0.45} \right), \tag{7.5}$$

for every $t \in [0, P]$, where A_s represents the amplitude threshold at which nonlinear supratransmission begins, and C is an *amplification constant* that depends of Ω. It is worth noticing that A is identically equal to zero for a bit b equal to zero; when b is equal to one, the qualitative behavior of A over a period equal to several times the driving period is presented in Figure 7.2.

Before we study the effects of damping and the normalized current in the moving breathers generated by the amplitude function above, it is highly convenient to introduce some terminology. Thus, for a breather moving away from the irradiating source at a constant velocity v, we assume the existence of constants $\delta > 0$ and $n_0 \in \mathbb{Z}$ with the property that the breather is approximately equal to zero outside of the region A defined by $|n - (n_0 + vt)| \leq \delta$. In such case, we say that the *position of the breather* at time t is equal to $n_0 + vt$, and that its *amplitude* and *energy* are, respectively,

$$A_b(t) = \max_{n \in A} |u_n(t)| \qquad \text{and} \qquad E_b(t) = \max_{n \in A} H_n(t).$$

Of course, this definition of position of a breather is rather subjective. A bit more formally, if we know that the breather is located in a region R at time t, its position

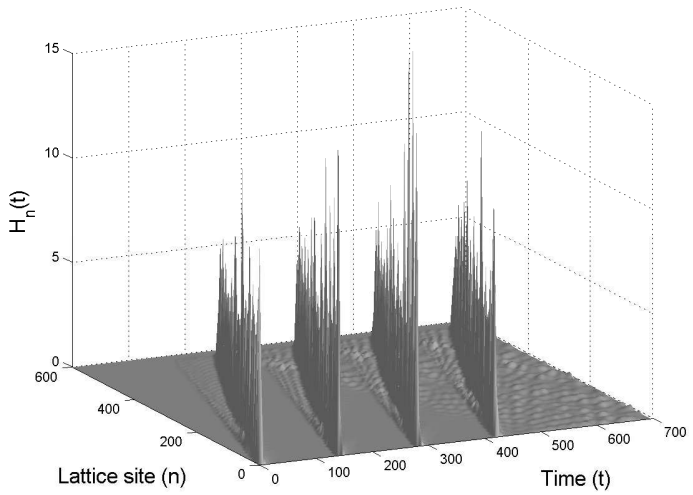

FIGURE 7.10: Local energies $H_n(t)$ of (7.1) with $\alpha = 0.05$ vs. lattice site n and time t, corresponding to the transmission of binary signal '1111', with $\Omega = 0.9$.

may be defined as the integer $n_1 \in R$ such that $H_{n_1}(t) = \max_{n \in R} H_n(t)$.

7.4.1 The ideal case

Let us consider an undamped, mixed-value problem (7.1) for which the normalized bias current is equal to zero, the coupling coefficient is equal to 4 and the period of bit generation equals 20 driving periods. Numerically, we consider a finite chain system of length $N = 600$, a time step of 0.05, and use the computational scheme sketched in Section 7.3.1. A bifurcation diagram similar to the one found in [69] is readily obtained, and the critical amplitudes A_s are used in the determination of the velocities for single moving breathers. Under this situation, a binary signal of '1111' is transmitted into chain (7.1) driven at a frequency equal to 0.9, with an amplification constant equal to A_s.

Figure 7.3 shows the development of the local energy in this system with respect to time and lattice site. The fact that moving breathers are generated in the chain is clear from the graph. The fact that the first of the breathers moves at approximately a constant speed is shown by the upper graph in Figure 7.4, while its maximum local energy is analyzed in the bottom portion of the same figure. Clearly, this maximum is above a positive cutoff limit, say, equal to 5.

In order to find a more reliable estimate of the lower cutoff limit for the maximum local energy carried by a breather generated using (7.5), we have transmitted a single bit '1' into a chain consisting of 6000 lattice sites during a period of time equal to 2000, with all other parameters as in the previous paragraph. As a result, we obtain that the absolute minimum and maximum values of the maximum local energy in a single breather are equal to 5.6965 and 17.9835, respectively, whence it particularly follows that a lower cutoff limit of 5 would actually prove to be adequate.

7.4.2 External damping

The next step in our investigation will be to describe the effects of internal and external damping, and the normalized bias current on the behavior of propagat-

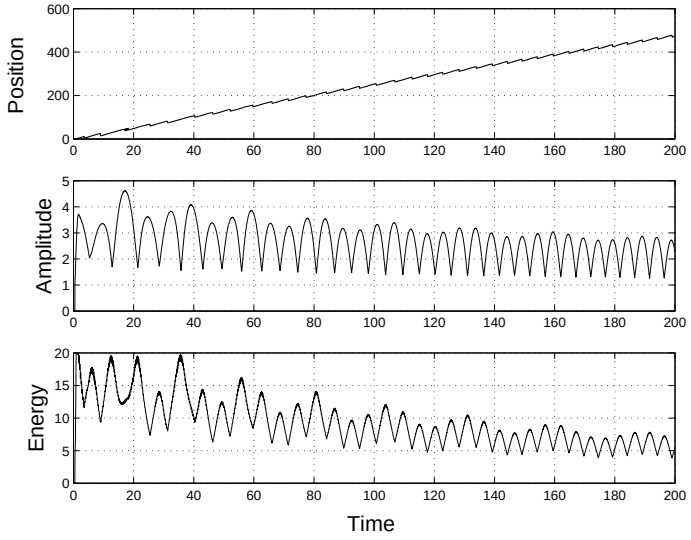

FIGURE 7.11: Time-dependent graphs of the position and maximum energy amplitude of the breather generated by bit '1' in (7.1) with $\alpha = 0.05$.

ing signals in (7.1). More concretely, we wish to establish the qualitative effects of these parameters on the local energy amplitude and speed evolution of the breather solutions with respect to lattice site. To that effect, we consider the same mixed-value problem studied in the previous section with similar choices of parameters, and provide a bifurcation diagram for several values of β in Figure 7.5.

The binary signal '1111' will be propagated again using the driving amplitude function (7.5) assuming that the medium is externally damped with a coefficient of 0.01. In this context, Figure 7.6 shows the time and lattice site evolution of the local energy carried by the breathers generated by the transmitted signals. These results evidence a drastic decay in the amplitudes of the local energies of a breather as it moves in the chain, a claim that is confirmed by Figure 7.7, in which we have tracked the position and the development of the maximum local energy of the moving breather generated by a single bit '1'.

Two conclusions are now evident from the graphs in Figure 7.7: first, the breathers generated using our transmission process move away from the source at a constant speed; second, a decrease of the maximum local energy amplitude carried by the breather with respect to time (and, hence, with respect to lattice site) is now apparent.

From Section 7.2.2, the solution to problem (7.2) in the continuous limit case is given by

$$u(x,t) = 4\arctan\left(\frac{\lambda c\sin(\Omega t)}{\Omega\cosh(\lambda x)}\right), \tag{7.6}$$

where $\lambda = \operatorname{arccosh}\left(1 + (1-\Omega^2)/2c^2\right)$. Using this solution and applying the perturbation method of Section 7.2.3 with $g(\phi) = 1/\sqrt{1+\phi^2}$, we obtain the time evolution of the amplitude at the origin of a static breather initially described by (7.6), with an external damping coefficient equal to 0.01. The results, which are presented in Figure 7.8, evidence a good agreement with the time evolution of the amplitude decay of the breather presented in Figure 7.6.

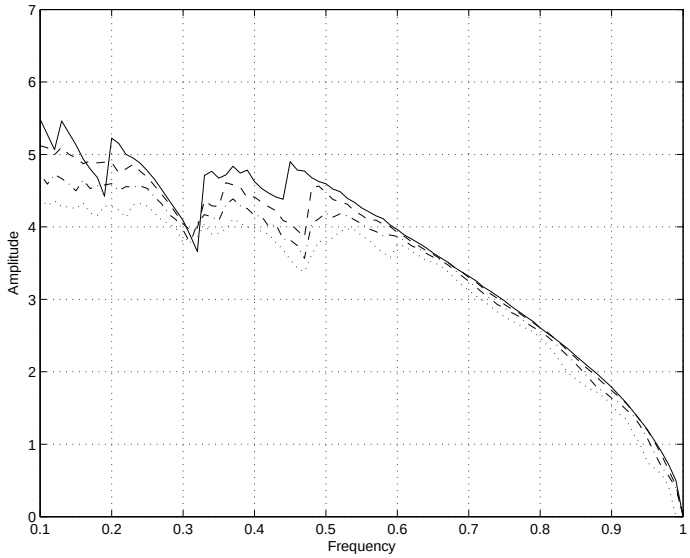

FIGURE 7.12: Bifurcation diagram of occurrence of critical amplitude versus driving frequency for problem (7.1) with $c = 4$, for $\gamma = 0$ (solid), 0.01 (dashed), 0.02 (dashed-dotted), 0.03 (dotted).

7.4.3 Internal damping

Consider again problem (7.1) with the same parameters as in Section 7.4.2 and similar numerical setting, describing a medium with no external damping and internal damping coefficient equal to 0.05. Again, the binary signal '1111' will be propagated into the medium using driving amplitude function (7.5). For convenience, Figure 7.9 provides a bifurcation diagram of energy transmission for several values of α.

Under this state of matters, Figure 7.10 presents the dependence of the local energy amplitude of each lattice site with respect to time. The graphs shows a decrease in time of the local energy amplitude of the generated breathers. To verify this claim, Figure 7.11 presents the time development of the position and maximum local energy attained by the first breather produced. This last figure also suggests that the breathers generated in this case move away from the driving boundary with approximately a constant speed, a fact that was corroborated using linear regression analysis.

We must remark that, like in the case of external damping, higher values of internal damping produce graphs of amplitude and local energy that decrease faster toward zero in time, as it is expected. In any case, we have verified that the phase velocity of the emitted breathers remains constant.

7.4.4 Normalized bias current

Finally, we carry out a similar analysis for the normalized bias current.

Figure 7.12 shows the effect of several values of the parameter γ in the occurrence of the supratransmission threshold. As before, the binary signal '1111' is generated by the driving boundary of a mechanical chain with parameters as in the previous section, and $\gamma = 0.1$. Figure 7.13 shows then the motion of the generated breathers in our mechanical system, while Figure 7.14 provides time-dependent

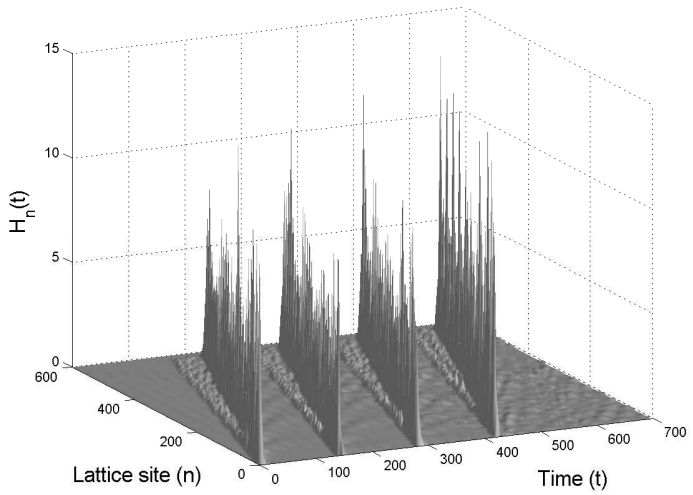

FIGURE 7.13: Local energies $H_n(t)$ of (7.1) with $\gamma = 0.1$ vs. lattice site n and time t, corresponding to the transmission of binary signal '1111', with $\Omega = 0.9$.

graphs of velocity, amplitude and local energy of the breather generated by the first bit. For this choice of γ, a slight decrease in the amplitude and the local energy of the breathers is shown.

7.5 Application

7.5.1 Concatenated mechanical chains

Let ℓ be a positive integer, and for every $j = 0, 1, \ldots \ell$, assume that Ω_j and c_j are positive numbers, that α_j, β_j and γ_j are nonnegative real numbers, and that L_j is a positive integer. Suppose that the sequence $(\mathbf{u}_n)_{n=1}^{\infty}$ of vectors $\mathbf{u}_n = (u_{jn})_{j=1}^{\ell}$ satisfies the system of concatenated equations

$$\left\{\begin{array}{l} \dfrac{d^2u_{jn}}{dt^2} - \left(c_j^2 + \alpha_j \dfrac{d}{dt}\right)\Delta_x^2 u_{jn} + \beta_j \dfrac{du_{jn}}{dt} + V'(u_{jn}) \;=\; 0, \\ \qquad \text{subject to :} \qquad \left\{\begin{array}{ll} u_{jn}(0) = 0, & n \in \mathbb{Z}^+, \\ \dfrac{du_{jn}}{dt}(0) = 0, & n \in \mathbb{Z}^+, \\ u_{j0}(t) = \psi_j(t), & t \geq 0, \end{array}\right. \\ \qquad \text{for } j = 0, 1, \ldots, \ell, \end{array}\right. \tag{7.7}$$

with potential functions given by $V_j(u) = 1 - \cos(u) - \gamma_j u$, and boundary-driving functions $\psi_j(t) = A_j(t)\cos(\Omega_j t)$ for every $t \in (0, +\infty)$ and $j = 0, 1, \ldots, \ell$, where each frequency Ω_j is assumed to be in the forbidden band gap of the j-th discrete array. The number ℓ will be called the *length of the system* of concatenated arrays.

Let P_0 be equal to a multiple of the period of the harmonic driving in the zeroth mechanical array. As in Section 6.3, a single bit of information b will be transmitted during a period of time equal to P_0 by modulating the amplitude of the

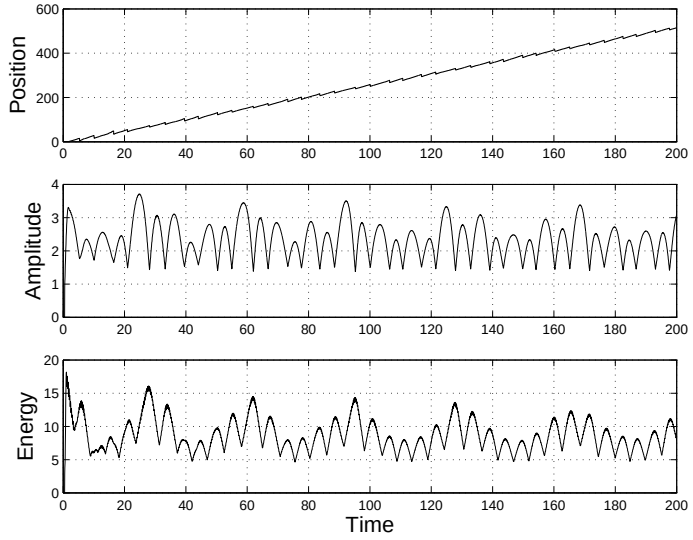

FIGURE 7.14: Time-dependent graphs of the position and maximum energy amplitude of the breather generated by bit '1' in (7.1) with $\gamma = 0.1$ and $\Omega = 0.9$.

driving oscillator in the zeroth array through

$$A_0(t) = \begin{cases} \dfrac{8}{5} bCA_s \left(e^{-\Omega_0 t/4.5} - e^{-\Omega_0 t/0.45} \right), & \text{if } b = 1. \\ \\ 0, & \text{if } b = 0. \end{cases}$$

The reception device of the first mechanical array will be initialized then at time L_0/v, where v represents the phase velocity of the generated breathers in the zeroth array. After initialization, a time equal to a period of the driving oscillator in the first array will be spent in order to determine if a bit equal to '0' or '1' passes by site L_0. This determination is done by comparing the local-energy amplitude of site L_0 with respect to a predetermined cutoff limit. Next, a driving amplitude in the first array defined by (7.5.1) will be used for a period of time equal to P_1, and the process continues inductively.

Following the conventions of Section 7.3.1, the j-th system of differential equations in model (7.7) will be approximated numerically by a finite number of equations $N_j \gg L_j$ via the set of finite-difference schemes

$$\frac{\delta_t^2 u_{jn}^k}{(\Delta t)^2} - \left(c_j^2 + \frac{\alpha_j}{2\Delta t} \delta_t \right) \delta_x^2 u_{jn}^k + \frac{\beta_j'}{2\Delta t} \delta_t u_{jn}^k + \frac{V(u_{jn}^{k+1}) - V(u_{jn}^{k-1})}{u_{jn}^{k+1} - u_{jn}^{k-1}} = 0,$$

where β_j' is the sum of the external damping coefficient in the j-th mechanical array and the effect of an absorbing boundary in the last few lattice sites. We mimic now the rest of Section 7.3.1 in order to define computational schemes to approximate the total energy and the individual energies in each mechanical array.

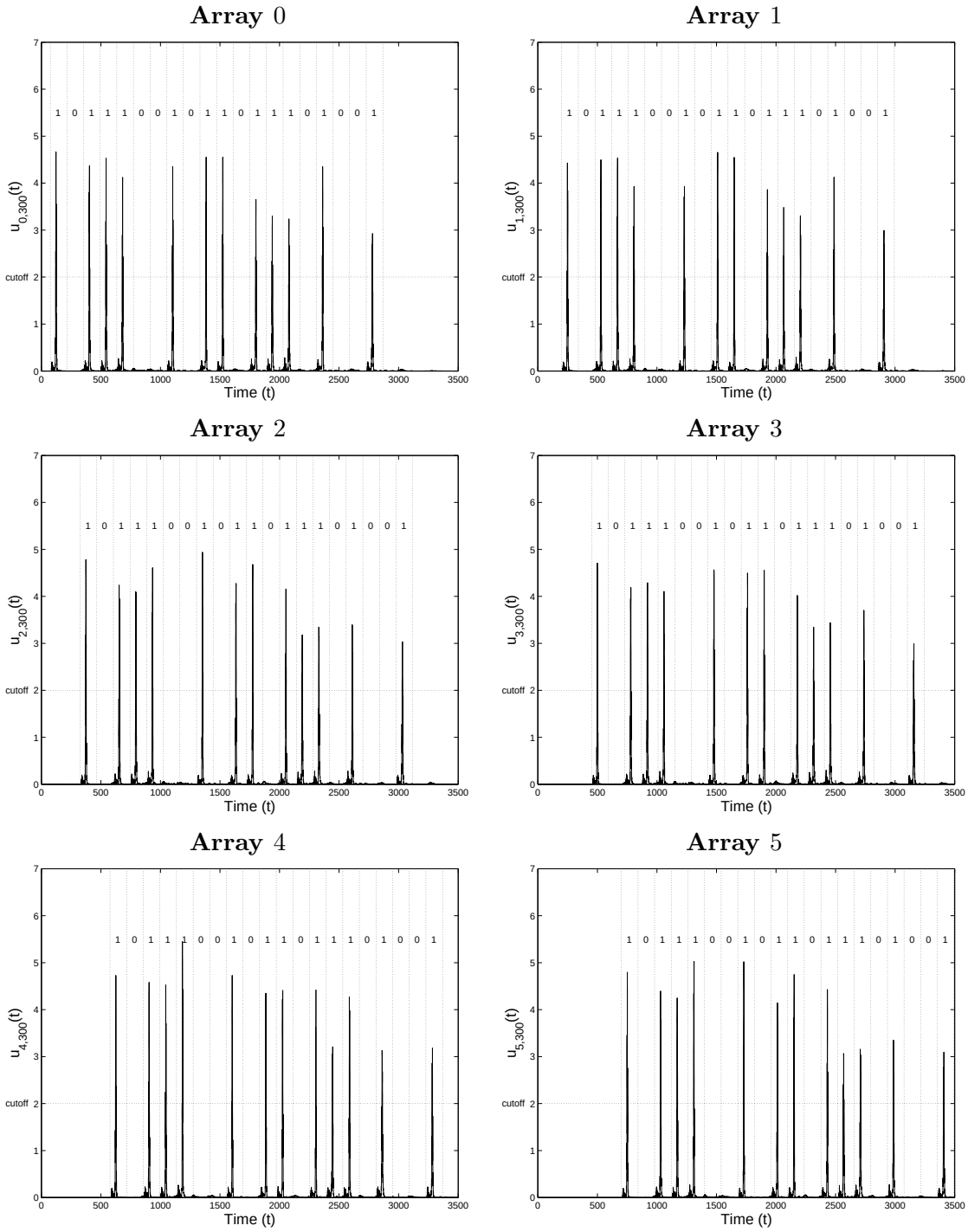

FIGURE 7.15: Time-dependent local energies at sites 300 in a linear concatenation of mechanical arrays of length 5, as a result of the transmission of signal '10111001011011101001' and using a cutoff limit equal to 2. The decoding of the transmitted message is shown in each array at the top of the reception periods.

7.5.2 Simulation

As an application, assume that the binary signal '10111001011011101001' will be transmitted in a linearly concatenated, mechanical system (7.7) of length 5, in which a period of single-bit generation equal to 20 driving periods will be used. For the sake of simplicity, we will assume that $\alpha_j = 0.02$, $\beta_j = 0.003$, $\gamma_j = 0.01$ and $\Omega_j = 0.9$ for every $j = 0, 1, \ldots, 5$, for which numerical simulations yield a common critical amplitude $A_s = 1.778$ and a phase velocity equal to 2.395.

Computationally, we consider arrays consisting of $N = 600$ sites each, and assume that the link between two consecutive arrays is invariably placed on site $L = 300$. An analysis similar to that done in Section 6.3 reflects that the estimate for the minimal value of the energy carried by a breather at site L is above the value of A_s when an amplification coefficient $C = A_s$ is used.

In this state of matters, Figure 7.15 presents the time-dependent local energy of the 300-th site in each of the 6 mechanical arrays in our system, as a consequence of the transmission of signal '10111001011011101001'. For the sake of convenience, each graph shows approximate periods of reception and, the value of the transmitted bit on top of each period. Our numerical results establish that a rather reliable transmission can be achieved using model (7.7) under suitable parametric conditions.

7.6 Conclusions and Discussion

In this work, we have presented a simple, mathematical model to efficiently transmit binary signals in certain semi-infinite, discrete mechanical systems using the process of nonlinear supratransmission, which is physically described as a concatenation of a finite sequence of n such arrays, in such a way that the amplitude of the driving oscillator at the end of the k-th lattice for $2 \leq k \leq n$, is equal to the local energy amplitude of some fixed oscillator in the $(k-1)$-st lattice, located relatively far away from its driving oscillator. Of course, this energy-bound series of arrays requires that the local energy of the linking site in the $(k-1)$-st lattice induced by the moving breather be at least equal to the critical amplitude of the driving disturbance in the k-th lattice, and simulations of this type of structures have shown that perfect transmission may be achieved under suitable choices of parameters.

7.7 Acknowledgment

One of us (JEMD) wishes to thank Dr. Álvarez Rodríguez, dean of the Centro de Ciencias Básicas of the Universidad Autónoma de Aguascalientes, and Dr. Avelar González, head of the Dirección General de Investigación y Posgrado of the same university, for uninterestedly providing him with the means to produce this paper. The present work represents a set of partial results under project PIM07-2 at this university.

Chapter 8

An application of nonlinear supratransmission to the propagation of binary signals in discrete Josephson-junction arrays

The phenomena of supratransmission and infratransmission (or lower transmission) in certain discrete, nonlinear systems have opened a whole new range of potential physical applications. These processes have been predicted numerically in some instances, and sometimes approximated in continuous-limit scenarios, yet the mathematical apparatus of the fully discrete case is not completely understood. In this paper, we make use of a recently developed, non standard, energy-based method in order to predict numerically the occurrence of these processes in discrete Josephson-junction arrays submitted to external damping and nonzero normalized bias current, where the underlying model is a Neumann boundary-value problem involving a system of coupled, dissipative sine-Gordon equations. We use supratransmission and infratransmission in the mathematical modeling of the propagation of digital signals in weakly damped, discrete Josephson-junction arrays, using an energy-based detection criterion for which our results show an efficient and reliable transmission of binary information.

8.1 Introduction

The process of nonlinear supratransmission consists of a sudden increase in the amplitude of wave signals transmitted into a nonlinear chain by a harmonic disturbance at the end, irradiating at a frequency in the forbidden band gap. The phenomenon was first discovered in mechanical chains of oscillators described by coupled sine-Gordon and Klein-Gordon equations [59], and it was quickly studied in many in chains of coupled double sine-Gordon equations [75], in Fermi-Pasta-Ulam nonlinear chains [62], Bragg media in the nonlinear Kerr regime [63] and, recently, in continuous nonlinear bounded media described by sine-Gordon equations [64].

The study of the process of nonlinear supratransmission in undamped sine-Gordon systems has been analytically has been carried out via the study of coherent structures, and the results have proved to yield good predictions for the occurrence

of the process when compared to numerical results. In the weakly damped case, though, the investigation relies on analytical techniques for the ideal case and numerical methods. Here the use of methods of quadratic convergence as well as methods that satisfy energy-invariance properties have shown to produce more than satisfactory results [69].

On the other hand, the process of nonlinear infratransmission or lower transmission, as opposed to supratransmission, consists in a sudden decrease in the amplitude of wave signals in a chain harmonically driven at its end. A system possessing both supratransmission and infratransmission exhibits a bistable behavior that makes it an outstanding source of physical applications. The Fermi-Pasta-Ulam model has been found to posses both processes [62], and analytical proof for the existence of infratransmission has been provided in discrete Josephson-junction arrays [76]; however, the literature still lacks a numerical prediction in this case.

From an experimental perspective, the phenomenon of supratransmission in nonlinear media described by sine-Gordon equations was first observed in mechanical systems of coupled pendula [75], and applications to the design of digital amplifiers of ultra weak signals [65] and light detectors sensitive to very weak excitations [66] have been realized recently. Further applications to optical waveguide arrays using the discrete nonlinear Schrödinger equation [67], the realization of light filters [68] and the propagation of binary signals in semi-infinite mechanical systems of coupled oscillators [73, 77] have been suggested. In this paper, we develop an application of nonlinear supratransmission and infratransmission to the propagation of binary information in weakly damped, discrete, finite Josephson-junction arrays, by modulating the amplitudes of the driving signal at one end. The task has been motivated by previous numerical work on semi-infinite mechanical systems of coupled oscillators [73, 77], where the model involved a Dirichlet boundary-initial-value problem.

Historically, the numerical study of wave transmission in long Josephson structures submitted to harmonic driving was initiated in the middle 1980's by Olsen and Samuelsen [78], and the investigation was immediately extended to coupled arrays of short superconducting tunnel junctions [79]. The study of the nonlinear bistability in Josephson junctions was the central topic of research in these works, a study that was continued later on via perturbation analysis with partially satisfactory results [80] until, finally, the whole analytical apparatus for the undamped, continuous-limit case was recently unveiled [76, 64].

The first section of this letter introduces the mathematical model under study and the energy expressions associated with the problem, while the next section briefly presents the finite-difference scheme employed to approximate the model, and states its numerical properties. A bifurcation analysis to predict the occurrence of nonlinear supratransmission under the presence of external damping and normalized bias currents is carried out in the next section. Next, we study briefly the characteristics of emitted kinks in the arrays. The following section describes the technique employed in order to transmit binary information in discrete Josephson junction arrays, and presents a simulation of transmission. Finally, we provide a section of concluding remarks, discussion of results, and perspectives of future work.

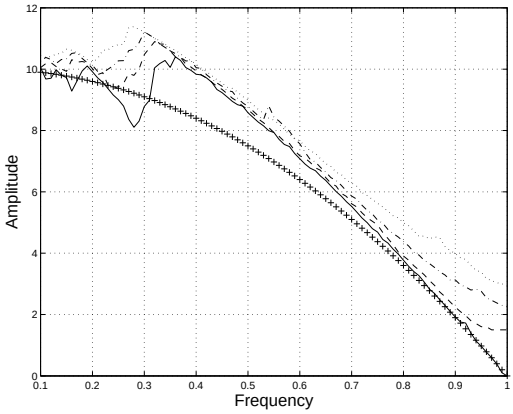

FIGURE 8.1: Bifurcation diagram of occurrence of critical amplitude versus driving frequency for problem (8.2) with $c = 5$, for $\gamma = 0$ (solid), 0.1 (dashed), 0.2 (dash-dotted), 0.3 (dotted). The continuous-limit prediction (8.3) of the bifurcation threshold is represented by a sequence of plus signs.

8.2 Mathematical model

Throughout this paper, we assume that γ and c are nonnegative real numbers. Likewise, we consider a system $(u_n)_{n=1}^N$ of N Josephson junctions coupled through superconducting wires, satisfying the discrete, initial-value problem

$$\begin{array}{rcl} \ddot{u}_1 - c^2\Delta_x u_1 + \gamma\dot{u}_1 + \sin u_1 &=& \mu + \phi(t), \\ \ddot{u}_n - c^2\Delta_x^2 u_n + \gamma\dot{u}_n + \sin u_n &=& \mu \quad (1 < n < N), \\ \ddot{u}_N + c^2\Delta_x u_{N-1} + \gamma\dot{u}_N + \sin u_N &=& \mu - I, \\ \text{subject to :} \quad \left\{ \begin{array}{l} u_n(0) = 0, \quad 1 \le n \le N, \\ \dfrac{du_n}{dt}(0) = 0, \quad 1 \le n \le N, \end{array} \right. \end{array} \tag{8.1}$$

where c will be called the *coupling coefficient*, γ evidently plays the role of an external damping coefficient, and μ is the *Josephson current* of the system.

Notationally, $\dot{u}$ and $\ddot{u}$ denote the first- and the second-order derivatives of u with respect to time, respectively, I is the *output current intensity* of the system, $\Delta_x u_n$ represents the spatial first-difference $u_{n+1} - u_n$ while $\Delta_x^2 u_n$ is used to denote the second-difference $u_{n+1} - 2u_n + u_{n-1}$ for every $n \in \mathbb{Z}^+$, and the function ϕ—called the *input intensity function*—is may be assumed to be continuously differentiable over $(0, +\infty)$ in general. The particular case when ϕ is a sinusoidal function will be particularly interesting. More concretely, we will study the case when the driving is given by the function $\phi(t) = A\sin(\Omega t)$.

It is easy to check that the introduction of the time-dependent functions u_0 and u_{N+1} defined by the relations $u_0 - u_1 = \phi(t)/c^2$ and $u_{N+1} - u_N = 0$, respectively,

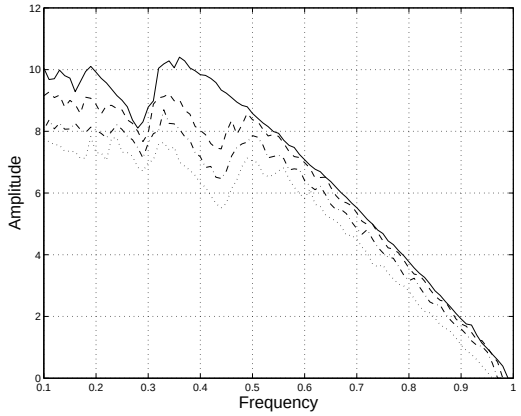

FIGURE 8.2: Bifurcation diagram of occurrence of critical amplitude versus driving frequency for undamped problem (8.2) with $c = 5$, for $\mu = 0$ (solid), 0.1 (dashed), 0.2 (dash-dotted), 0.3 (dotted).

transforms problem (8.1) into the discrete, boundary-initial-value problem

$$\begin{aligned} &\ddot{u}_n - c^2\Delta_x^2 u_n + \gamma_n \dot{u}_n + \sin u_n = \mu \quad (1 \le n \le N), \\ &\text{subject to :} \quad \begin{cases} u_n(0) = 0, & 1 \le n \le N, \\ \dfrac{du_n}{dt}(0) = 0, & 1 \le n \le N, \\ u_0 - u_1 = \dfrac{\phi(t)}{c^2}, & t \in (0, +\infty), \\ u_{N+1} - u_N = 0, & t \in (0, +\infty), \end{cases} \end{aligned} \tag{8.2}$$

where $\gamma_n = \gamma$ for every $n < N$, and $\gamma_N = \gamma + 1/R$. The number R is called the *output reading resistance* of the system, and it is related to the output current intensity through Ohm's law: $I = \dot{u}_N/R$.

It is worth noticing that our mixed-value problem may be approximated via a continuous, Neumann boundary-value problem involving a perturbed sine-Gordon model for strong coupling. Also, notice that if $\gamma = 0$, then the Hamiltonian of the n-th lattice site is given by

$$H_n = \frac{1}{2}\left[\dot{u}_n^2 + c^2(u_{n+1} - u_n)^2\right] + 1 - \cos u_n,$$

After including the potential energy from the coupling between the first two sites, the total energy of the system becomes

$$E = \sum_{n=1}^{N} H_n + \frac{c^2}{2}(u_1 - u_0)^2.$$

A simple integration of this formula over a finite interval of time gives the total energy injected into the system over such interval.

The limiting case consisting of the discrete Josephson-junction array with an infinite number of junctions is of particular interest. In this situation, it is easy to verify [69] that the rate of change of the energy of the system with respect to time is

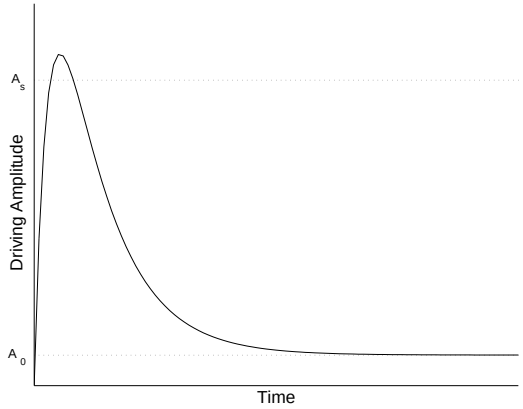

FIGURE 8.3: Graph of the driving amplitude function $A(t)$ given by (8.4). The figure depicts a situation when the driving amplitude A_0 has surpassed the infratransmission threshold.

provided by the formula

$$\frac{dE}{dt} = \phi(t)\dot{u}_0 - \gamma \sum_{n=1}^{\infty} (\dot{u}_n)^2.$$

8.3 Numerical scheme

We consider the system of differential equations (8.2), and a regular partition $0 = t_0 < t_1 < \cdots < t_M = T$ of the time interval $[0, T]$ with time step equal to Δt. For each $k = 0, 1, \ldots, M$, let us represent the approximate solution to our problem on the n-th lattice site at time t_k by u_n^k, and let us convey that $\delta_t u_n^k = u_n^{k+1} - u_n^{k-1}$, that $\delta_t^2 u_n^k = u_n^{k+1} - 2u_n^k + u_n^{k-1}$ and that $\delta_x^2 u_n^k = u_{n+1}^k - 2u_n^k + u_{n-1}^k$. In order to posses discrete energy expressions that consistently approximate their continuous counterparts [69], the continuous-time equations will be approximated by the discrete expressions

$$\frac{\delta_t^2 u_n^k}{(\Delta t)^2} - c^2 \delta_x^2 u_n^k + \frac{\gamma_n}{2\Delta t} \delta_t u_n^k + \frac{V(u_n^{k+1}) - V(u_n^{k-1})}{u_n^{k+1} - u_n^{k-1}} = 0,$$

for every $n = 1, \ldots, N$. Here, $V(u) = 1 - \cos u$ at any time.

We must declare that our finite-difference scheme (which is a modified version of the one proposed in [61]) is consistent with our mixed-value problem, conditionally stable, and possesses energy-invariant properties [69].

In order to simulate a discrete array of Josephson junctions of infinite length, we consider a finite system (8.2) of relatively large length N, in which each γ_n includes both the effect of external damping described above and a simulation of an absorbing boundary slowly increasing in magnitude on the last $N - N_0$ oscillators. Specifically, we let

$$\gamma_n = \kappa \left[1 + \tanh\left(\frac{2n - N_0 + N}{2\sigma} \right) \right] + \gamma + \frac{1}{R} \delta_N(n),$$

where $\delta_N(n)$ is equal to 1 if $n = N$, and zero otherwise. In practice, we will let $\kappa = 0.5$, $\sigma = 3$, $N = 60$, and $N_0 = 50$.

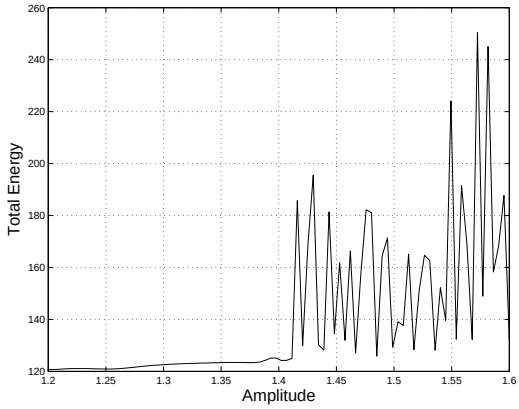

FIGURE 8.4: Graph of total energy vs. driving amplitude in an undamped, semi-infinite, discrete Josephson-junction array, driven at a frequency of $\Omega = 0.9$ via expression (8.4) during a period of time equal to 6000, with a coupling coefficient of 5.

8.4 Bifurcation analysis

The existence of a nonlinear supratransmission threshold of the energy administered into a finite array of Josephson junctions satisfying (8.2) for a harmonic function ϕ and driving frequency in the forbidden band gap region $\Omega < 1$, has been established in the continuous-limit case [76] and numerically predicted [76, 75] for a discrete system. Using our numerical scheme, a prediction of the occurrence of nonlinear supratransmission can be approximated for every driving frequency in the forbidden band gap of the system of equations (8.2), by estimating the value of the driving amplitude at which a drastic increase in the total energy of the system is detected. In the continuous-limit case, the driving amplitude A_s at which supratransmission first starts is related to Ω through the relation

$$A_s = 2c(1 - \Omega^2). \tag{8.3}$$

In a first stage, we proceed to compute the total energy associated with system (8.2) of length $N = 60$ with coupling coefficient 5 and no Josephson current, for driving frequencies in the interval $[0.1, 1]$ contained in the forbidden band gap region, during a finite period of time. Several values of the damping coefficient are chosen. The results of our numerical computations are shown in Figure 8.1. The bifurcation diagram representing the undamped scenario exhibits a good agreement with the continuous prediction for high frequencies, and damping clearly delays the appearance of the bifurcation threshold for frequencies $\Omega > 0.35$.

Next we wish to check the role of the Josephson current in the occurrence of the bifurcation threshold. Figure 8.2 shows bifurcation diagrams at which supratransmission first starts, for driving frequencies in the interval $[0.1, 1]$ and various values of the Josephson current. It is clear that the effect of a positive μ is to decrease the value of the threshold at which supratransmission first starts.

As mentioned previously, the existence of a nonlinear infratransmission threshold under which there is a drastic decrease in the energy injected into the system was established in [76] in the continuous-limit case. As a matter of fact, the infratrans-

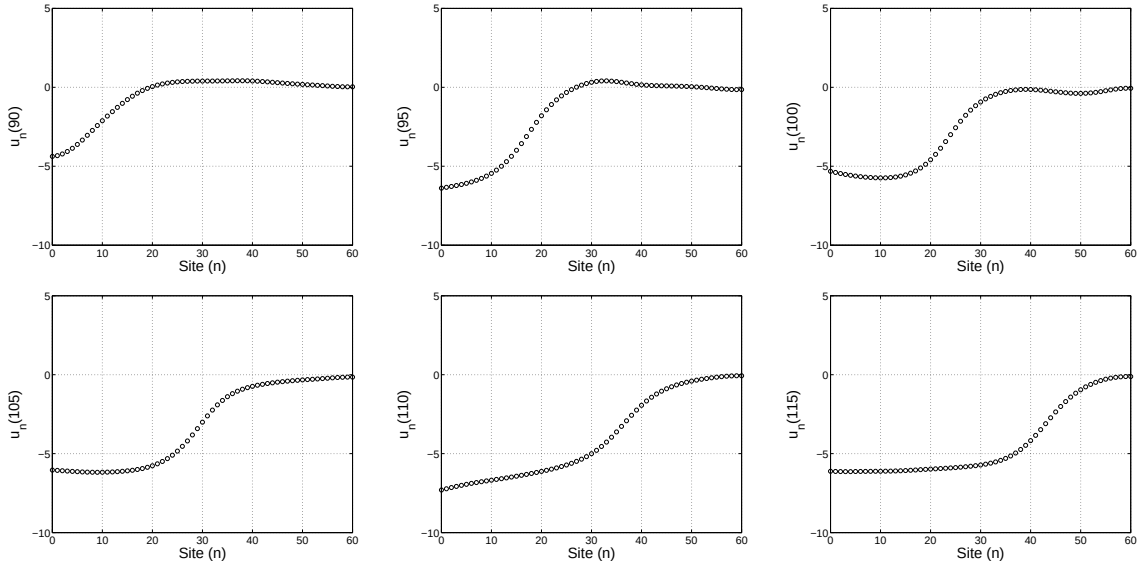

FIGURE 8.5: Development of a kink solution of (8.2) for discrete array of 60 Josephson junctions, with $\gamma = \mu = 0$ and $c = 5$, driving at the end with by a frequency $\Omega = 0.9$ and an amplitude $A = 2$ slightly above the supratransmission threshold. The snapshots were taken at 6 times equally spaced between 90 and 115, employing a step size of 0.2 and an absorbing boundary in the last 10 junctions.

mission threshold A_i is less than the supratransmission threshold A_s, and between the amplitudes A_i and A_s lies a region of bistability.In order to approximate numerically the value of A_i for a given driving frequency in the forbidden band gap with associated supratransmission threshold A_s, we chose a driving amplitude function

$$A(t) = B_s(1 - e^{-t/\tau_1}) + (A_0 - A_s)(1 - e^{-t/\tau_2}), \tag{8.4}$$

where $\tau_2 \gg \tau_1$. A typical graph of $A(t)$ is presented in Figure 8.4 for a constant A_0 just above the infratrasmission value.

A finite time period of relatively large length is chosen, and a finite, undamped system consisting of 60 Josephson junctions with no Josephson current, a coupling coefficient of 5, and a driving frequency of 0.9 is fixed, for which the nonlinear supratransmission threshold equals 1.945. Several driving amplitudes A_0 are employed, and the total energy of the system is computed for each amplitude. The results of driving the system with an amplitude function equal to (8.4) with $\tau_1 = 10$ and $\tau_2 = 100$ are shown in Figure 8.4, in which a drastic change in the behavior of the total energy with respect to A_0 is detected around the value 1.41. This value is identified as the nonlinear infratransmission threshold of the system for $\Omega = 0.9$.

8.5 Signal propagation

8.5.1 Character of solutions

Consider a system of 60 coupled oscillators described by (8.2) with coupling coefficient equal to 5, driven at a frequency of 0.9 in the forbidden band gap, and an amplitude of 2, just above the approximate supratransmission threshold. Figure

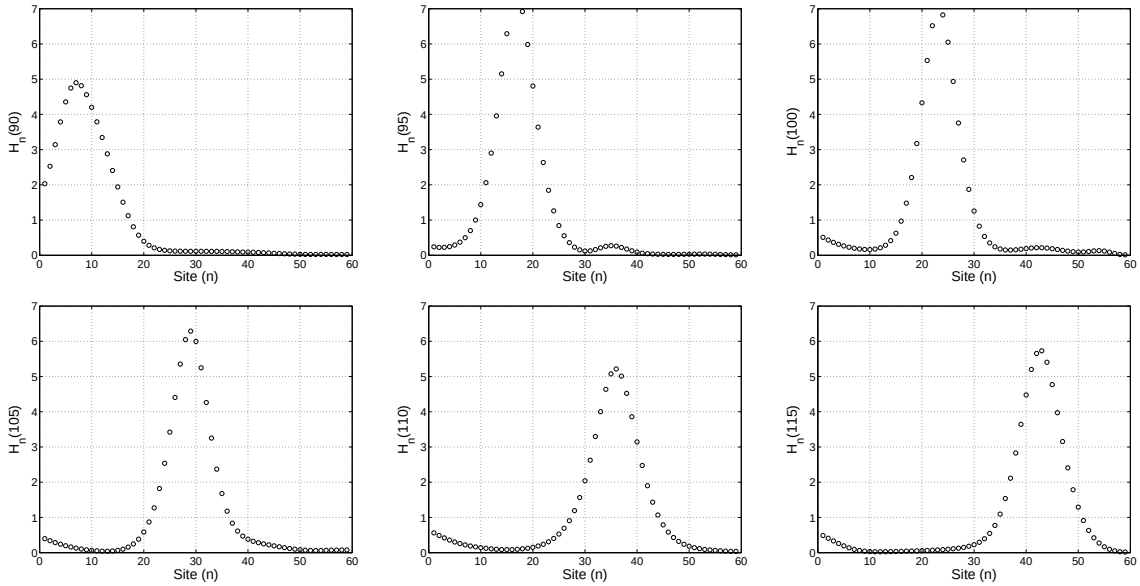

FIGURE 8.6: Development of the local energies in a kink solution of (8.2) for discrete array of 60 Josephson junctions, with $\gamma = \mu = 0$ and $c = 5$, driving at the end with by a frequency $\Omega = 0.9$ and an amplitude $A = 2$ slightly above the supratransmission threshold. The snapshots were taken at 6 times equally spaced between 90 and 115, employing a step size of 0.2 and an absorbing boundary in the last 10 junctions.

8.5 shows the time evolution of a kink moving away from the driving boundary. The exact location of the kink can be better determined by studying the time evolution of the local energies of the 60 sites at the corresponding times.

With that purpose in mind, Figure 8.6 presents the evolution of the local energies of the six snapshots in the previous figures. The location of the kinks is accurately identified, at each individual time, as the absolute maximum of the local energies. Moreover, a constant phase velocity of approximately 1.44 sites per unit of time is observed.

8.5.2 Simulation

Let Ω be a frequency in the forbidden band gap of our problem, and assume that B_i and B_s are, respectively, nonnegative values that are just a bit smaller than the infratransmission and supratransmission thresholds associated with a driving harmonic function ϕ with driving frequency equal to Ω. We define the *seed* of the system as the function

$$I_s(t) = \frac{1}{2}\left[(B_s - B_i)\sin(\Omega t) + B_i + B_s\right], \tag{8.5}$$

for every $t > 0$. A typical graph of this function is depicted in Figure 8.7.

Next, we define the *period of signal generation* P as an integer multiple of the driving period. In our case, P will be equal to 20 times the period of driving.

Let α be a positive number with the property that $I_s(t) + \alpha$ overcomes the nonlinear supratransmission threshold for some values of t. With these conventions in mind, a single binary message $(b_1, b_2, \ldots, b_l)$ consisting of l binary bits will be transmitted into system (8.1). In general, for every $m = 1, 2, \ldots, l$, we define the

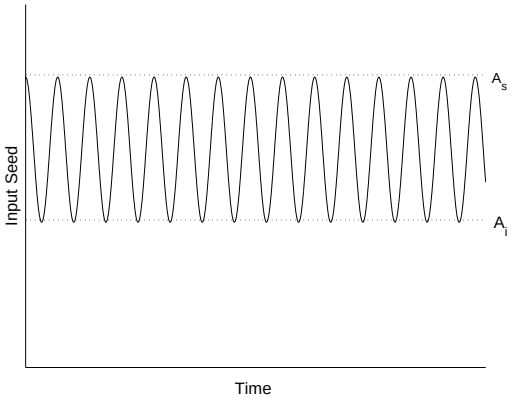

FIGURE 8.7: Graph of a typical seed function (8.5). The maxima and the minima of the seed are just below the supratransmission and infratransmission threshold, respectively.

signal function S_m by

$$S_m(t) = \begin{cases} \alpha b_m \sin(\Omega t), & \text{if } mP < t < (m+1)P, \\ 0, & \text{otherwise.} \end{cases}$$

The input intensity function will be defined then by

$$\phi(t) = I_s(t) + \sum_{m=1}^{l} S_m(t). \tag{8.6}$$

Consider a discrete Josephson junction arrays consisting of 8 junctions with coupling coefficient equal to 2. A driving frequency $\Omega = 0.9$ will be employed, for which the values $B_i = 0.23$, $B_s = 0.41$, $\alpha = 0.05$ and $R = 10$ will be used. The binary sequence '10111001011011101001' is to be transmitted into system (8.1) by modulating the input current intensity and read by the corresponding output current. The resulting outcome of our simulations is summarized in Figure 8.8 for a normalized time.

Nonzero bits are clearly identified with output intensities of absolute values higher than the corresponding intensities associated with bits equal to zero. More accurately, nonzero bits are completely characterized by the fact that, at some time in the corresponding period of reception, the value of the intensity of the output signal is higher than a cutoff limit (in this case equal to 0.01).

8.6 Conclusions, discussion, and perspectives

In this letter, we have proved, using numerical computations, that it is possible to transmit binary information in discrete Josephson junction arrays using the processes of nonlinear supratransmission and infratransmission. In the absence of dissipative effects, our model (which is based on the modulation of amplitudes of source signals with constant frequency) has shown to be highly reliable for sufficiently long periods of single-bit generation. Moreover, our computations show that the general picture does not change much when weak damping is present.

It is worth noticing the similarities and differences of our results with respect

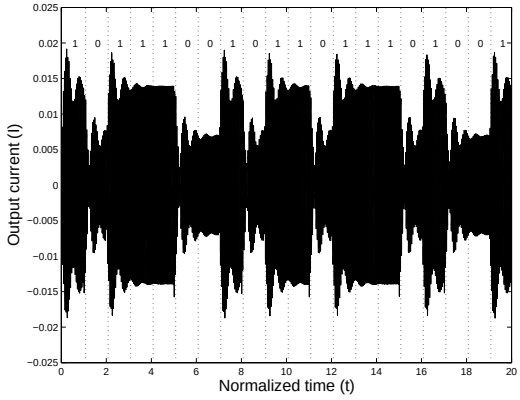

FIGURE 8.8: Graph of output current intensity vs. normalized time of system (8.1) consisting of 8 coupled junctions with $c = 2$, as a response of the input current function (8.6) for the binary message '10111001011011101001'. The parameters $\Omega = 0.9$ and $R = 10$ are employed.

to the corresponding Dirichlet boundary-value problem. The results derived in this paper in the bifurcation analysis for the external damping and the Josephson current are qualitatively similar to those presented in [69] and [73]. On the other hand, the fundamental structures for transmission of wave signals in the Dirichlet scenario involved the propagation of moving breathers; meanwhile, kinks and anti-kinks have been generated in the Neumann boundary-value problem.

We must remark that no bifurcation analysis for the occurrence of the process of nonlinear infratransmission has been presented in this work. The task has been left out as the main topic for some future letter.

8.7 Acknowledgment

JEMD wishes to express his gratitude to Dr. Álvarez Rodríguez, dean of the Faculty of Sciences of the Universidad Autónoma de Aguascalientes, and to Dr. Avelar González, head of the Office for Research and Graduate Studies of the same university, for providing him with the means to produce this article. The present work represents a set of partial results under project PIM07-2 at this university.

Chapter 9

Conclusions

In this paper, we have presented a brand-new, energy-based, finite-difference scheme to approximate solutions of certain class of systems of discrete-space, ordinary differential equations involving modified, coupled Klein-Gordon equations. Moreover, we have shown that the proposed finite-difference scheme is consistent to the second order, and conditionally stable.

We have established energy relations for systems of mechanical oscillators with damping, and we have proved that the finite-difference schemes we use to approximate the total energy of the system are in perfect agreement with the energy of the model. More concretely, the energy estimators derived in the dissertation are consistent approximations to the second order. Further more, our numerical method is able to detect the occurrence of the process of nonlinear supratransmission of energy in the proposed model. Bifurcation diagrams predicting the occurrence of this process for several values of the considered parameters evidence the fact that our method is likewise in perfect agreement with the theory.

From a practical point of view, our results have established that the moving breathers generated by driving the boundary of a semi-infinite chain of coupled oscillators above the supratransmission threshold, have certain invariant characteristics. Thus, for instance, the moving breathers move away from the source at a constant speed, which is basically independent of the damping coefficients. Also, from a 'probabilistic' perspective, the moving breathers conserve their amplitude and their energy in undamped systems.

Likewise, we have shown that, under suitable conditions, the transmission of binary information is possible in mechanical systems of coupled oscillators as well as in discrete Josephson junction arrays.

Interesting as our results may appear, there are still many open questions that we plan to answer in the future as part of an agenda of research projects:

- To start with, a deeper analysis of the occurrence of the process of nonlinear infratransmission in discrete Josephson junction arrays appears indispensable. As stated before, the process has been given a solid background in the continuous-limit case. However, no analysis of the occurrence of this phenomenon has been given for the weakly coupled case, and no relationship with the values of the parameters of our model is known so far.

- A better way to control the switching between supratransmission and infratransmission in discrete Josephson junction arrays seems necessary, in

order to achieve a better-defined output signal. Empirically, our results suggest that the closer the values of A_i and A_s to the nonlinear infratransmission and supratransmission threshold, respectively, and the larger the value of the parameter α, the better defined the output signals.

- Apparently, the process of nonlinear supratransmission as well as the process of nonlinear infratransmission seem to be natural phenomena appearing in discrete systems of nonlinear, coupled differential equations submitted to harmonic driving. It is of interest to investigate the possibility to generate these processes in other systems with practical applications.

- The process of nonlinear supratransmission has been studied for some linear (1-dimensional) systems in this dissertation. Question arises as whether it is possible to induce supratransmission in 2-dimensional systems. More interestingly, we ask whether nonlinear supratransmission can be reached in radially symmetric, 3-dimensional systems (discrete or continuous) consisting of Klein-Gordon-like equations.

- The search for interesting applications of the nonlinear supratransmission and infratransmission is still a priority in our investigation.

Appendix A

Numerical subroutine functions

The numerical results were obtained using programs we wrote for Matlab 6.1. We give here the computational routines employed without the subroutines of graphical display. In particular, the following routines were used to approximate radially symmetric solutions to the nonlinear Klein-Gordon equation with external damping and no internal damping. The method is implicit and makes use of Newton's method in each iteration to approximate the roots of a nonlinear equation.

```
     function u = KleinGordon(p,Tol,Delta,k,m,N,damp);
%    To approximate radial solutions of the nonlinear Klein-Gordon
%    equation with constant external damping coefficient c=damp,
%
%              2     2
%             d u   d u     du
%             --- - --- + c -- + u + G'(u) = 0
%               2     2     dt
%             dt    dr
%
%    with
%                                 p-1
%                      G'(u) = |u|   u,
%
%    using N time steps of length equal to k and a regular partition
%    of the interval [0,0.4] consisting of m subintervals.
%    Tol indicates the tolerance to be used in the applications of
%    Newton's method, and Delta is used in the determination of the
%    initial approximation in every iteration.
          clear;       %   Clear all variables
          h = 0.4/m;       %   Define the radial step
          x = 0:h:0.4;     %   Create radial partition
          u1(1) = 0 ; u1(m+1) = 0;    %
          u2(1) = 0 ; u2(m+1) = 0;    %   Apply boundary conditions
          u3(1) = 0 ; u3(m+1) = 0;    %
          for i = 2:m;                          %   Apply first
               u1(i) = InitFunc((i-1)*h);       %     initial
          end                                   %    condition
          for i = 2:m;                             %   Apply second
```

```
            u2(i) = u1(i)+k*InitDeriv((i-1)*h);  %     initial
        end                                      %    condition
        for j = 2:N;   %  Compute the next N-1 approximations
            for i = 2:m;  %  Use Newton's method to approximate
                          %  the solution in the j-th time step
                u3(i) = Newton(u2(i-1),u2(i),u2(i+1),u1(i),...
                        p,h,k,i-1,Tol,Delta,damp);
            end
            E = CalcEnergy(u2,u3,h,k,p,m);  %  Calculate Energy
            u1(:) = u2(:);      %  Update information vectors
            u2(:) = u3(:);      %    for the next time step
        end
        u = u2./x;

    function x = Newton(a,b,c,d,p,h,k,j,Tol,Delta,damp);
%   Newton's method to approximate the solutions to the nonlinear
%   equation
%           x-2b+d     x-d   c-2b+a   x+d     G(x) - G(d)
%   f (x) = ------ + f --- - ------ + --- + -------------- ,
%            2        2k      2      2              p-1
%           k                h            (jh(x - d))
%   where f = damp.
        Gd = FuncG(d,p,j,h);
        Diff = 1.0;            %   Initialize difference
        n = 1;                 %   Initialize iterations
        x = b+Delta;           %   Initialize approximation
        while (Diff > Tol) & (n < 25)
            Gx = FuncG(x,p,j,h);
            DGx = FuncDG(x,p,j,h);
            Fx = FuncF(x,a,b,c,d,p,h,k,j,Gx,Gd,damp); %  Newton's
            DFx = FuncDF(x,d,p,h,k,j,DGx,Gx,Gd,damp); %   method
            x1 = x-Fx/DFx;      %  Compute new approximation
            n = n+1;            %  Update counter
            Diff = abs(x1-x);   %  Compute difference
            x = x1;
        end

    function y = InitFunc(r);
        if r < 0.2
            y = 5*r*exp(100*(1-1/(1-(10*r-1)^2)));
        else
            y = 0;
        end

    function y=InitDeriv(r);
        if r < 0.195
```

```
            y = 5*r*exp(100-5/(r-5*r^2))*(5-49*r-...
                 10*r^2+25*r^3)/(r^2*(1-5*r)^2);
       else
            y = 0;
       end

  function y = CalcEnergy(u2,u3,h,k,p,m);
       y = .5*((u3(1)-u2(1))/k)^2+.5*(u3(2)-u3(1))...
            *(u2(2)-u2(1))/h^2+.25*((u3(1))^2+(u2(1))^2);
       for j = 2:m;
            G2 = FuncG(u3(j),p,j-1,h);
            G1 = FuncG(u2(j),p,j-1,h);
            y = y+.5*((u3(j)-u2(j))/k)^2+.5*(u3(j+1)-u3(j))...
                 *(u2(j+1)-u2(j))/h^2+.25*((u3(j))^2...
                 +(u2(j))^2)+.5*(G2+G1)/((j-1)*h)^(p-1);
       end
       y = y*h;

  function y = FuncG(x,p,j,h);
       y = (abs(x)^(p+1))/(p+1);

  function y = FuncDG(x,p,j,h);
       y = x*(abs(x)^(p-1));

  function y = FuncF(x,a,b,c,d,p,h,k,j,Gx,Gd,damp);
       y = (x-2*b+d)/(k^2)+damp*(x-d)/(2*k)-(c-2*b+a)/(h^2)...
            +(x+d)/2+(Gx-Gd)/((x-d)*(j*h)^(p-1));

  function y = FuncDF(x,d,p,h,k,j,DGx,Gx,Gd,damp);
       y = 1/(k^2)+damp/(2*k)+1/2+((x-d)*DGx+Gd-Gx)...
            /((j*h)^(p-1)*(x-d)^2);
```

The following procedures were used to approximate radially symmetric solutions to the dissipative nonlinear Klein-Gordon equation. Our method is implicit and makes use of Newton's method with tolerance `Tol` to approximate the roots of a nonlinear system of equations in each iteration. In turn, each iteration of Newton's method makes use of Crout's reduction method for tridiagonal linear systems. All the routines used by `KleinGordonMult` which are not explicitly written below are assumed to be the same as those of `KleinGordon`.

```
  function u2 = KleinGordonMult(p,Tol,Delta,k,m,N,damp,idamp);
%    To approximate radial solutions of the nonlinear Klein-Gordon
%    equation with constant external damping coefficient c=damp
%    and constant internal damping coefficient i=d=idamp, %
%                2     2               3
%               d u   d u     du      d  u
```

```
%              --- - --- + c -- - i ------ + u + G'(u) = 0
%                2     2     dt         2
%              dt    dr             dt d r
%
%    with
%                                  p-1
%                       G'(u) = |u|   u,
%
%    using N time steps of length equal to k and a regular partition
%    of the interval [0,0.4] consisting of m subintervals.
%    Tol indicates the tolerance to be used in the applications of
%    Newton's method, and Delta is used in the determination of the
%    initial approximation in every iteration.
         clear;       %   Clear all variables
         h = 0.4/m;       %   Define the radial step
         x = 0:h:0.4;     %   Create radial partition
         u1(1) = 0 ; u1(m+1) = 0;    %
         u2(1) = 0 ; u2(m+1) = 0;    %   Apply boundary conditions
         u3(1) = 0 ; u3(m+1) = 0;    %
         for i = 2:m;                          %   Apply first
              u1(i) = InitFunc((i-1)*h);       %     initial
         end                                   %    condition
         for i = 2:m;                            %   Apply second
              u2(i) = u1(i)+k*InitDeriv((i-1)*h); %     initial
         end                                     %    condition
         for j = 2:N;   %  Compute the next N-1 approximations
              for i = 2:m;  %  Use Newton's method to approximate
                            %  the solution in the j-th time step
                   u3(i) = NewtonMult(u1,u2,p,h,k,Tol,Delta,c,d,m);
              end
              E = CalcEnergy(u2,u3,h,k,p,m);  %  Calculate Energy
              u1(:) = u2(:);      %  Update information vectors
              u2(:) = u3(:);      %    for the next time step
         end
         u = u2./x;

    function x = NewtonMult(u1,u2,p,h,k,Tol,Delta,c,d,m);
         Diff = 10.0;
         n = 1;
         x = u2+Delta;
         numa = c/(2*k*h^2);
         numb = d/(2*k)+1/k^2+1/2+c/(k*h^2);
         while (Diff > Tol) & (n < 15)
              y = LUsolver(x,u1,u2,h,k,p,numa,numb,c,d,m);
              n = n+1;
              Diff = sqrt(y*transpose(y));
```

```
          x = x+y;
     end
     x(1) = 0;
     x(m+1) = 0;

function y = LUsolver(x,u1,u2,h,k,p,numa,numb,c,d,m);
     lu(1) = Diagonal(1,x,u1,u2,h,p,numb);
     u(1) = -numa/lu(1);
     for i = 2:m-2;
          ll(i-1) = -numa;
          lu(i) = Diagonal(i,x,u1,u2,h,p,numb)-ll(i-1)*u(i-1);
          u(i) = -numa/lu(i);
     end
     ll(m-2) = -numa;
     lu(m-1) = Diagonal(m-1,x,u1,u2,h,p,numb)-ll(m-2)*u(m-2);
     z(1) = Constants(1,x,u1,u2,h,k,p,c,d)/lu(1);
     for i = 2:m-1;
          z(i) = (Constants(i,x,u1,u2,h,k,p,c,d)-ll(i-1)*...
               z(i-1))/lu(i);
     end
     y(m) = z(m-1);
     for i = m-2:-1:1;
          y(i+1) = z(i)-u(i)*y(i+2);
     end
     y(1) = 0;
     y(m+1) = 0;

function y = Diagonal(i,x,u1,u2,h,p,numb);
     y = numb+i*h*((x(i+1)-u1(i+1))*Gprime(x(i+1)/(i*h),p)...
          -i*h*(Gfunc(x(i+1)/(i*h),p)-Gfunc(u1(i+1)/...
          (i*h),p)))/(x(i+1)-u1(i+1))^2;

function y = Constants(i,x,u1,u2,h,k,p,c,d);
     y = (x(i+1)-2*u2(i+1)+u1(i+1))/(k^2)-(u2(i+2)-2*u2(i+1)+...
          u2(i))/(h^2)+d*(x(i+1)-u1(i+1))/(2*k)-c*((x(i+2)-...
          2*x(i+1)+x(i))-(u1(i+2)-2*u1(i+1)+u1(i)))/(2*k*h^2)...
          +(x(i+1)+u1(i+1))/2;
     y = -(y+((i*h)^2)*(Gfunc(x(i+1)/(i*h),p)-...
          Gfunc(u1(i+1)/(i*h),p))/(x(i+1)-u1(i+1)));

function y = Gfunc(x,p);
     y = (abs(x)^(p+1))/(p+1);

function y = Gprime(x,p);
     y = x*(abs(x)^(p-1));
```

References

[1] Remoissenet, M., *Waves Called Solitons*, third ed., Springer-Verlag, New York, 1999.

[2] Lomdahl, P. S.; Soerensen, O. H.; Christiansen, P. L., "Soliton Excitations in Josephson Tunnel Junctions", *Phys. Rev. B* **25** (1982), no. 9, 5737–5748.

[3] Makhankov, V. G.; Bishop, A. R.; Holm, D. D. (ed.), *Nonlinear Evolution Equations and Dynamical Systems Needs '94; Los Alamos, NM, USA 11-18 September '94: 10th International Workshop*, first ed., World Scientific Pub. Co. Inc., Singapore, 1995.

[4] Polyanin, A. D.; Zaitsev, V. F., *Handbook of Nonlinear Partial Differential Equations*, first ed., Chapman & Hall CRC Press, Boca Raton, Fla., 2004.

[5] Glassey, R. M., "Blow-up theorems for nonlinear wave equations", *Math. Zeit.* **132** (1973), 183–203.

[6] Jörgens, K, "Das Anfangswertproblem im Grossen für eine Klasse nichtlinearer Wellengleichungen", *Math. Zeit.* **77** (1961), 295–308.

[7] Barone, A.; Esposito, F.; Magee, C. J.; Scott, A. C., "Theory and Applications of the Sine-Gordon Equation", *Riv. Nuovo Cim.* **1** (1971), 227–267.

[8] Strauss, W. A.; Vázquez, L., "Numerical Solution of a Nonlinear Klein-Gordon Equation", *J. Comput. Phys.* **28** (1978), 271–278.

[9] Alexander, F. J.; Habib, S., "Statistical Mechanics of Kinks in $1 + 1$ Dimensions", *Phys. Rev. Lett.* **71** (1993), 955–958.

[10] Zwillinger, D., *Handbook of Differential Equations*, third ed., Academic Press, Boston, MA, 1997.

[11] Perring, K. K.; Skyrme, T. H., "A Model Uniform Field Equation", *Nucl. Phys.* **31** (1962), 550–555.

[12] Tabor, M., *Chaos and Integrability in Nonlinear Dynamics: An Introduction*, John Wiley and Sons, New York, 1989.

[13] Gibbon, J. D.; James, I. N.; Moroz, I. N., "The Sine-Gordon Equation as a Model for a Rapidly Rotating Baroclinic Fluid", *Phys. Script.* **20** (1979), 402–408.

[14] Bishop, A. R.; Schneider, T. (ed.), *Solitons and Condensed Matter Physics*, Springer-Verlag, New York, 1981.

[15] Fisher, R. A., "The Wave of Advance of Advantageous Genes", *Annals of Eugenics* **7** (1937), 355–369.

[16] Kolmogorov, A.; Petrovsky, I.; Piscounoff, N., "Étude de l'équations de la diffusion avec croissance de la quantité de matière et son application a un problème biologique", *Bull. Univ. Moskou, Ser. Internat.* **1A** (1937), 1–25.

[17] Sherratt, J. A.; Murray, J. D., "Models of Epidermal Wound Healing", *Proc. Biol. Sci.* **241** (1990), no. 1300, 29–36.

[18] Wallace, P. R., *Mathematical Analysis of Physical Problems*, first ed., Dover, New York, 1984.

[19] Rashba, E. I. and Sturge, M. D. (ed.), *Excitons*, North Holland, Amsterdam, 1982.

[20] Doering, C. R.; Mueller, C.; Smereka, P., "Interacting Particles, the Fisher-Kolmogorov-Petrovsky-Piscounov Equation, and Duality", *Physica A* **325** (2003), 243–259.

[21] McGee, H.; McInerney, J.; and Harrus, A., "The Virtual Cook: Modeling Heat Transfer in the Kitchen", *Physics Today* **52** (1999), 30–36.

[22] Fourier, J. B. J. (ed.), *Théorie Analytique de la Chaleur*, Firmin Didot, Paris, 1822.

[23] Cattaneo, M. C., "Sulla Conduzione de Calor", *Atti Sem. Matem. e Fis. Della U. Modena* **3** (1948), 3.

[24] Lieberstein, H. M., *Theory of Differential Equations*, first ed., Academic Press, New York, 1972.

[25] Nayfeh, A. H., *Perturbation Methods*, first ed., Wiley and Sons, New York, NY, 1993.

[26] Segal, I. E., "The Global Cauchy problem for a relativistic scalar field with power interaction", *Bull. Soc. Math. Fr.* **91** (1963), 129–135.

[27] Morawetz, C. S.; Strauss, W. A., "Decay and scattering of solutions of a nonlinear relativistic wave equation", *Comm. Pure and Appl. Math.* **25** (1972), 1–31.

[28] Josephson, B. D., Ph.D. thesis, Cambridge University, Cambridge, England, 1964.

[29] Mason, W. P. (ed.), *Physical Acoustics, Vol. III*, first ed., Academic Press, New York, 1966.

[30] Krumhansl, J. A.; Schrieffer, J. R., "Dynamics and Statistical Mechanics of a One-Dimensional Model Hamiltonian for Structural Phase Transitions", *Phys. Rev. B* **11** (1975), 3535–3545.

[31] Currie, J. F.; Krumhansl, J. A.; Bishop, A. R.; Trullinger, S. E., "Statistical Mechanics of One-Dimensional Solitary-Wave-Bearing Scalar Fields: Exact Results and Ideal-Gas Phenomenology", *Phys. Rev. B* **22** (1980), 477–496.

[32] Zabusky, N. J.; Kruskal, M. D., "Interaction of Solitons in a Collisionless Plasma and the Recurrence of the Initial State", *Phys. Rev. Lett.* **15** (1965), 240–243.

[33] Drazin, P. G.; Johnson, R. S. (ed.), *Solitons: An Introduction*, first ed., Cambridge University Press, Cambridge, 1989.

[34] Hochstadt, H. (ed.), *The Functions of Mathematical Physics*, Dover Publications, Inc., New York, 1986.

[35] Lamb Jr., G. L., "Analytical Descriptions of Ultrashort Optical Pulse Propagation in a Resonant Medium", *Rev. Mod. Phys.* **49** (1971), 99–124.

[36] Skyrme, T. H. R., "A Nonlinear Theory of Strong Interactions", *Proc. Roy. Soc. London* **A247** (1958), 260–278.

[37] ———, "Particle States of a Quantized Meson Field", *Proc. Roy. Soc. London* **A262** (1961), 237–245.

[38] Enz, U., "Discrete Mass, Elementary Length, and a Topological Invariant as a Consequence of a Relativistic Invariant Variational Principle", *Phys. Rev.* **131** (1963), 1392–1394.

[39] Josephson, B. D., "Supercurrents Through Barriers", *Adv. Phys.* **14** (1965), 419–451.

[40] Vvedensky, D., *Partial Differential Equations with Mathematica*, first ed., University Press, Cambridge, Great Britain, 1993.

[41] Royden, H., *Real Analysis*, third ed., Prentice Hall, New York, 1988.

[42] Thomas, J. W., *Numerical Partial Differential Equations*, first ed., Springer-Verlag, New York, 1995.

[43] Gelfand, I. M.; Fomin, S. V., *Calculus of Variations*, first ed., Dover Publications, Inc., Mineola, New York, 2000.

[44] Bradbury, T. C., *Theoretical Mechanics*, first ed., John Wiley & Sons, Inc., New York, 1968.

[45] Benzi, R.; Sutera, A.; Vulpiani, A., "Stochastic Resonance in the Landau-Ginzburg Equation", *J. Phys. A: Math. Gen.* **18** (1985), 2239–2245.

[46] Kudryavtsev, A. E., "Solitonlike Solutions for a Higgs Scalar Field", *JETP Lett.* **22** (1975), no. 3, 82–83.

[47] Winternitz, P.; Grundland, A. M.; Tuszyński, J. A., "Exact Results in the Three-Dimensional Landau-Ginzburg Model of Magnetic Inhomogeneities in Uniaxial Ferromagnets: I. Continuous Transitions", *J. Phys. C: Solid State Phys.* **21** (1988), 4931–4953.

[48] Noest, A. J., "Domains in Neural Networks with Restricted-Range Interactions", *Phys. Rev. Lett.* **63** (1989), no. 16, 1739–1742.

[49] Feynman, R. P., *Feynman Lectures on Physics*, Addison Wesley Longman, New York, NY, 1970.

[50] Swihart, J. C., "Field Solution for a Thin-Film Superconducting Strip Transmission Line", *J. Appl. Phys.* **32** (1961), no. 3, 461–469.

[51] Strauss, W. A., *Partial Differential Equations: An Introduction*, second ed., John Wiley & Sons, Inc., New York, 1992.

[52] Hasegagwa, A.; Tappert, F., "Transmission of stationary nonlinear optical pulses in dispersive dielectric fibers. i. anomalous dispersion", *Appl. Phys. Lett.* **23** (1973), 142–144.

[53] Mollenauer, L. F.; Stolen, R. H.; Gordon, J. P., "Experimental observation of picosecond pulse narrowing and solitons in optical fibers", *Phys. Rev. Lett.* **45** (1980), 1095–1098.

[54] McCall, S. L.; Hahn, E. L., "Self-induced transparency", *Phys. Rev.* **183** (1969), 457–485.

[55] Ablowitz, M. J.; Kaup, D. J.; Newell, A. C., "Coherent pulse propagation, a dispersive, irreversible phenomenon", *J. Math. Phys.* **15** (1974), 1852–1858.

[56] Ustinov, A. V., "Solitons in josephson junctions", *Physica D* **123** (1998), 315–329.

[57] Ustinov, A. V.; Mygind, J.; Oboznov, V. A., "Phase-locked flux-flow josephson oscillator", *J. Appl. Phys.* **72** (1992), 1203–1205.

[58] Ustinov, A. V.; Mygind, J.; Pedersen, N. F.; Oboznov, V. A., "Millimeter-wave-induced fluxon pair creation in flux-flow josephson oscillators", *Phys. Rev. B* **46** (1992), 578–580.

[59] Geniet, F.; Leon, J., "Energy transmission in the forbidden band gap of a nonlinear chain", *Phys. Rev. Lett.* **89** (2002), 134102.

[60] ———, "Nonlinear supratransmission", *J. Phys.: Condens. Matter* **15** (2003), 2933–2949.

[61] Macías-Díaz, J. E.; Puri, A., "A numerical method for computing radially symmetric solutions of a dissipative nonlinear modified klein-gordon equation", *Num. Meth. Part. Diff. Eq.* **21** (2005), 998–1015.

[62] Khomeriki, R.; Lepri, S.; Ruffo, S., "Nonlinear supratransmission and bistability in the fermi-pasta-ulam model", *Phys. Rev. E* **70** (2004), 066626.

[63] Leon, J., Spire, A., "Gap soliton formation by nonlinear supratransmission in bragg media", *Phys. Lett. A* **327** (2004), 474–480.

[64] Khomeriki, R.; Leon, J., "Bistability in sine-gordon: The ideal switch", *Phys. Rev. E* **71** (2005), 056620.

[65] Khomeriki, R.; Leon, J.; Chevriaux, D., "Quantum hall bilayer digital amplifier", *Euro. Phys. J. B* **49** (2006), 213–218.

[66] Chevriaux, D.; Khomeriki, R.; Leon, J., "Bistable transmitting nonlinear directional couplers", *Mod. Phys. Lett. B.* **20** (2006), 515–532.

[67] Khomeriki, R., "Nonlinear band gap transmission in optical waveguide arrays", *Phys. Rev. Lett.* **92** (2004), 063905.

[68] Khomeriki, R.; Ruffo, S., "Nonadiabatic landau-zener tunneling in waveguide arrays with a step in the refracting index", *Phys. Rev. Lett.* **94** (2005), 113904.

[69] Macías-Díaz, J. E.; Puri, A., "An energy-based computational method in the analysis of the transmission of energy in a chain of coupled oscillators", *Appl. Num. Anal. & Comp. Math.* (2006), submitted.

[70] van der Zant, H. S. J.; Barahona, M.; Duwel, A. E., Trias, E.; Orlando, T. P.; Watanabe, S.; Strogatz, S., "Dynamics of one-dimensional josephson-junction arrays", *Physica D* **119** (1998), 219–226.

[71] Caputo, J.-G.; Leon, J.; Spire, A., "Nonlinear energy transmission", *Phys. Lett. A* **283** (2001), 129–135.

[72] Gulevich, D. R.; Kusmartsev, F. V., "Perturbation theory for localized solutions of sine-gordon equation: decay of a breather and pinning by microresistor", *Cond. Matt.* (2006), 0608263.

[73] Macías-Díaz, J. E.; Puri, A., "An application of nonlinear supratransmission to the propagation of binary signals in semi-infinite mechanical systems of coupled oscillators", *Phys. Lett. A* (2006), submitted.

[74] Lepri, S.; Livi, R.; Politi, A., "Thermal conduction in classical low-dimensional lattices", *Phys. Rep.* **377** (2003), 1–80.

[75] Geniet, F.; Leon, J., "Nonlinear Supratransmission", *J. Phys.: Condens. Matter* **15** (2003), 2933–2949.

[76] Chevrieux, D.; Khomeriki, R.; Leon, J., "Theory of a Josephson junction parallel array detector sensitive to very weak signals", *Phys. Rev. B* **73** (2006), 214516.

[77] Macías-Díaz, J. E.; Puri, A., "On the propagation of binary signals in damped mechanical systems of oscillators", *Int. J. Nonlinear Mech.* (2006), submitted.

[78] Olsen, O. H.; Samuelsen, M. R., "Hysteresis in rf-driven large-area Josephson junctions", *Phys. Rev. B* **34** (1986), 3510–3512.

[79] Barday, D.; Remoissenet, M., "Josephson superlattices and low-amplitude gap solitons", *Phys. Rev. B* **41** (1990), 10387–10397.

[80] Kivshar, Y. S.; Olsen, O. H.; Samuelsen, M. R., "Hysteresis loop induced by rf radiation in Josephson junctions: An analytical approach", *Phys. Lett. A* **168** (1992), 391–399.

Vita

Jorge Eduardo Macías Díaz was born in the city of Aguascalientes, of the Mexican state of the same name, on June 19, 1970. He obtained his diploma of bachelor in science in applied mathematics from the Universidad Autónoma de Aguascalientes in the Spring semester of 1994. Mr. Macías Díaz obtained a master of science degree in mathematics from Tulane University in the Spring semester of 1998. He continued his studies in this same institution and was awarded a Ph.D. degree in mathematics in the Spring semester of 2001. Jorge Eduardo obtained a master of science degree in applied physics from the University of New Orleans in Summer of 2004, and expects to obtain a Ph.D. degree in physics on winter 2006.